

Improving The Vibrational Performance of Wood Floor Systems

By


Robert E. Kalkert

Dissertation submitted to the Faculty of the
Virginia Polytechnic Institute and State University
in partial fulfillment of the requirements for the degree of
Doctor of Science

In

Wood Science And Forest Products

Approved


Dieghied Folzer
L. Sheinowitz
Frank Woeste
Thomas M. Murray
D. Earl Klein

July, 1997

Blacksburg, Virginia

c.2

LD

5655

V856

1997

K355

c.2

IMPROVING THE VIBRATIONAL PERFORMANCE OF
WOOD FLOOR SYSTEMS

By

Robert E. Kalkert

James D. Dolan and Frank E. Woeste, Co-Chairman

Wood Science and Forest Products

(ABSTRACT)

A displacement-based Rayleigh-Ritz finite element model is developed to simulate the static and dynamic behavior of stiffened plates. By comparing natural frequency, time-history, and power density predictions with experimental results, it is shown that the model can be used to predict the vibratory behavior of wood floor systems constructed with either solid-sawn joists, I-Joists, or parallel-chord-trusses. Furthermore, using the model, it is shown that appropriate structural modifications can be used to improve the performance of wood floor systems by increasing natural frequency and reducing peak time-history velocity. Using the techniques described, a design example is included that indicates how floor acceptability can be achieved.

Acknowledgement

The author would first like to thank the U.S. Department of Agriculture, the Co-operative State Research Service, and the Food and Agriculture Sciences National Needs Graduate Fellowship Program for their financial support through Fellowship No. 9003012.

Thanks also go to committee members Tom Murray, Seigfried Holzer, Earl Kline, and Leonard Meirovitch. I would especially like to thank committee co-chairman Dan Dolan and Frank Woeste, as well as Geza Ifju. I have learned many valuable lessons from these individuals that I will carry for life.

To my family and friends, your infinite patience has brought many realizations. If I have learned nothing else during my graduate studies, I have learned that you are more important than any personal accomplishment. Salute.

Table of Contents

1	Introduction	1
1.1	Background	1
1.2	Objectives	3
1.3	Significance	3
2	Literature Review	4
2.1	Introduction	4
2.2	Static Performance	4
2.2.1	Experimental/Theory	4
2.2.1.1	Composite Action	5
2.2.1.2	Load Sharing	6
2.2.1.3	Connection Behavior	7
2.2.1.3.1	Nails	7
2.2.1.3.2	Adhesives	8
2.2.1.4	Bridging	9
2.2.2	Numerical Analysis	10
2.2.2.1	FEAFLO	10
2.2.2.1.1	Development Of FEAFLO	10

2.2.2.1.2	Results Of FEAFLO	12
2.2.2.2	NONFLO	13
2.2.2.3	FPL	13
2.2.2.4	FAP	14
2.3	Reliability	15
2.4	Dynamic Performance	16
2.4.1	Experimental/Theory	16
2.4.1.1	Vibration Types	16
2.4.1.2	Defining Human Tolerance Levels	17
2.4.1.3	Characterization Of Transient Wood Floor Vibrations	18
2.4.1.3.1	Frequency	18
2.4.1.3.2	Amplitude	20
2.4.1.3.3	Damping	21
2.4.1.4	Sensitivity	24
2.4.1.4.1	Support Conditions	24
2.4.1.4.2	End Fixity	24
2.4.1.4.3	Applied Dead Load	25
2.4.1.4.4	Bridging	25
2.4.1.4.5	Joist Modulus Of Elasticity	26
2.4.1.4.6	Joist Spacing	26
2.4.1.4.7	Joist-To-Sheathing Connections	26
2.4.1.5	Experimental Design Criteria	27
2.4.2	Numerical Analysis	29
2.4.2.1	Numerical Models	29

2.4.2.2	Numerical Design Criteria	32
2.5	Summary	33
3	Model Overview	35
3.1	Introduction	35
3.2	Modeling Environment	36
3.3	Model Architecture	36
3.4	Application Engine	36
3.4.1	Elements	36
3.4.2	System Construction	37
3.4.3	System Size	37
3.4.4	Frequency Analysis	38
3.4.5	Time-History Analysis	38
4	Model Verification	40
4.1	Introduction	40
4.2	Static Response	41
4.3	Dynamic Response	45
4.4	Summary	52
5	Model Validation	53
5.1	Experimental Floor Background	53
5.2	Experimental Modal Analysis	54
5.3	Model Parameter Specifics	55
5.4	Validation Results	59

5.5 Summary 74

6 Performance Improvement Investigation 75

6.1 Single Span Floors 77

6.1.1 Imposed Mass 77

6.1.2 Double Stiffeners 79

6.1.3 Continuous Blocking 82

6.1.4 Additional Sheathing 85

6.1.5 Summary 87

6.2 Dual Span Floors 87

6.2.1 Beam Supports 88

6.2.2 Rotationally Resistant Supports 91

6.2.3 Summary 95

6.3 Summary 96

7 Tying Research to Practice 97

7.1 Introduction 97

7.2 Design Example 97

8 Conclusions and Recommendations 102

8.1 Conclusions 102

8.2 Recommendations 104

Bibliography 107

A General Theory of Displacement Based Finite Elements 120

A.1	Equation of Motion Generation	120
A.2	Variational Principles	121
A.3	Complexity	123
A.4	Finite Element Formulation	126
A.4.1	Overview	126
A.4.2	Internal Potential Energy	128
A.4.3	External Potential Energy	130
A.4.4	Principle of Stationary Potential Energy	135
A.5	System Construction	136
B	Finite Element Development	137
B.1	Preliminaries	137
B.1.1	Shape Functions	138
B.1.2	Completeness and Continuity	139
B.1.3	Evaluation of Element Matrices	140
B.2	Beam Element Formulation	141
B.2.1	Models and Element Selection	141
B.2.2	Beam Stiffness Matrix	147
B.2.3	Beam Mass Matrix	148
B.3	Basic Plate Element Formulation	149
B.3.1	Models and Element Selection	149
B.3.2	Plate Stiffness Matrix	153
B.3.3	Plate Mass Matrix	154
B.4	Combined Plate-Beam Element Formulation	155

B.5	Summary	158
C	Solution Procedures	159
C.1	Full System	159
C.1.1	Natural Frequencies	159
C.1.2	Time History	162
C.1.3	Summary	166
C.2	Reduced System	167
D	Series Solutions	170
D.1	Static Response	170
D.1.1	Isotropic	170
D.1.2	Orthotropic	171
D.1.3	Isotropic (Transverse Shear Flexible)	172
D.1.4	Isotropic (Equidistant Stiffeners)	173
D.1.5	Isotropic (Dual Span)	174
D.2	Dynamic Response	175
D.2.1	Isotropic	175
E	Quick Reference	178
E.1	Model Validation	178
E.2	Performance Improvement Investigation	191

List of Figures

4.1 Comparison of Predicted and Exact Displacement Time-Histories for an Isotropic, Square Plate	48
4.2 Zoom Comparison of Predicted and Exact Displacement Time-Histories for an Isotropic, Square Plate	48
4.3 Comparison of Predicted and Exact Velocity Time-Histories for an Isotropic, Square Plate	49
4.4 Zoom Comparison of Predicted and Exact Velocity Time-Histories for an Isotropic, Square Plate	49
4.5 Comparison of Predicted and Exact Acceleration Time-Histories for an Isotropic, Square Plate	50
4.6 Zoom Comparison of Predicted and Exact Acceleration Time-Histories for an Isotropic, Square Plate	50
4.7 Zoom Comparison of Predicted and Exact Displacement Time-Histories for an Isotropic, Square Plate, Using the Convolution Sum	51
4.8 Zoom Comparison of Predicted and Exact Velocity Time-Histories for an Isotropic, Square Plate, Using the Convolution Sum	51
4.9 Zoom Comparison of Predicted and Exact Acceleration Time-Histories for an Isotropic, Square Plate, Using the Convolution Sum	52

5.1 Mechanical Dropweight Force Time-History	57
5.2 Typical Floor Configuration	59
5.3 Comparison of Predicted and Experimental Displacements for Floor a (Solid-Sawn Stiffeners)	63
5.4 Comparison of Predicted and Experimental Power Densities for Floor a (Solid-Sawn Stiffeners)	63
5.5 Comparison of Predicted and Experimental Displacements for Floor b (Solid-Sawn Stiffeners)	64
5.6 Comparison of Predicted and Experimental Power Densities for Floor b (Solid-Sawn Stiffeners)	64
5.7 Comparison of Predicted and Experimental Displacements for Floor c (Parallel-Chord-Truss Stiffeners)	65
5.8 Comparison of Predicted and Experimental Power Densities for Floor c (Parallel-Chord-Truss Stiffeners)	65
5.9 Comparison of Predicted and Experimental Displacements for Floor d (Parallel-Chord-Truss Stiffeners)	66
5.10 Comparison of Predicted and Experimental Power Densities for Floor d (Parallel-Chord-Truss Stiffeners)	66
5.11 Comparison of Predicted and Experimental Displacements for Floor e (Parallel-Chord-Truss Stiffeners)	67
5.12 Comparison of Predicted and Experimental Power Densities for Floor e (Parallel-Chord-Truss Stiffeners)	67
5.13 Comparison of Predicted and Experimental Displacements for Floor f (I-Joist Stiffeners)	68

5.14 Comparison of Predicted and Experimental Power Densities for Floor f (I-Joist Stiffeners)	68
5.15 Comparison of Predicted and Experimental Displacements for Floor g (I-Joist Stiffeners)	69
5.16 Comparison of Predicted and Experimental Power Densities for Floor g (I-Joist Stiffeners)	69
5.17 Comparison of Predicted and Experimental Displacements for Floor h (I-Joist Stiffeners)	70
5.18 Comparison of Predicted and Experimental Power Densities for Floor h (I-Joist Stiffeners)	70
5.19 Comparison of Predicted and Experimental Displacements for Floor i (I-Joist Stiffeners)	71
5.20 Comparison of Predicted and Experimental Power Densities for Floor i (I-Joist Stiffeners)	71
5.21 Comparison of Predicted and Experimental Displacements for Floor j (I-Joist Stiffeners)	72
5.22 Comparison of Predicted and Experimental Power Densities for Floor j (I-Joist Stiffeners)	72
5.23 Comparison of Predicted and Experimental Displacements for Floor k (I-Joist Stiffeners)	73
5.24 Comparison of Predicted and Experimental Power Densities for Floor k (I-Joist Stiffeners)	73
6.1 Location of Imposed Mass	78

6.2 Hypothetical Bin Used to Impose Mass	78
6.3 Floor With No Double Stiffeners	80
6.4 Floor With One Double Stiffener	81
6.5 Floor With Three Double Stiffeners	81
6.6 Hypothetical Continuous Blocking System	84
6.7 View of Interior Supporting Beam	89
6.8 Floor D Comparison of Velocity Time-Histories Based on Supporting Beam Section Size	90
6.9 Floor G Comparison of Velocity Time-Histories Based on Supporting Beam Section Size	91
6.10 Floor with Interior Supporting Wall	92
6.11 Floor with Interior Wall/Partition Support	93
6.12 Boundary Condition Equivalent of Figure 6.11	94
6.13 Hypothetical Tie-Rod System Used to Create an Adequate Interior Support Connection	95
A.1 Linear Elastic Stress-Strain Diagram	129
A.2 Linear Elastic Shear Stress-Strain Diagram	129
A.3 Differential Element Rotation	133
B.1 Continuous Beam Model	142
B.2 Beam Deformation Model Excluding Shear and Torsion	143
B.3 Beam Deformation Model Including Shear and Excluding Torsion . . .	143
B.4 Torsion Differential Element and Deformation Model Excluding Warp	146
B.5 Continuous Plate Model	149

B.6 Plate Deformation Model, x-w Plane	150
B.7 Plate Deformation Model, y-w Plane	150
B.8 Model For x-y Plane Shear Deformation	152
B.9 Representation of Typical Floor System	155
B.10 Combined System Model	156
B.11 Combined System Geometry	156
B.12 Combined System Deformation Model	157
D.1 Graphical Representation of Time-Zero Step Function	176
E.1 Actual Stiffener Dimensions Used in Model Validation Chapter	179
E.2a Actual Stiffener Dimensions Used in Performance Improvement Inves- tigation Chapter	191
E.2b Actual Stiffener Dimensions Used in Performance Improvement Inves- tigation Chapter	192

List of Tables

4.1 Plate Properties and Values Used Throughout Chapter 4	42
4.2 Center-Point Displacement Results for Isotropic Plate	43
4.3 Center-Point Displacement Results for Orthotropic Plate	43
4.4 Center-Point Displacement Results for Isotropic, Transverse Shear Flex- ible Plate	44
4.5 Center-Point Displacement Results for Isotropic, Stiffened Plate	44
4.6 Center-Point Displacement Results for Isotropic, Dual Span Plate . . .	45
4.7 Comparison of Predicted and Exact Natural Frequencies for an Isotropic. Square Plate	46
5.1 Stiffener Specifics and Experimental Load Sharing Factors	58
5.2 Stiffener Specifics and Experimental Viscous Damping Factors	60
5.3 Comparison of Predicted and Experimental Natural Frequencies	61
6.1 Floor and Stiffener Dimensions Used Throughout Chapter 6	76
6.2 Comparison of Natural Frequencies and Peak Velocity Based on Imposed Line-Load	80
6.3 Comparison of Natural Frequencies and Peak Velocity Based on Double Stiffener Locations	83

6.4 Comparison of Natural Frequencies and Peak Velocity Based on Rows of Continuous Blocking	84
6.5 Comparison of Natural Frequencies and Peak Velocity Based on Sheath- ing Thickness	86
6.6 Comparison of Natural Frequencies, Right-Span Time-Zero Velocity and Peak Velocity Based on Supporting Beam Section	89
6.7 Comparison of Natural Frequencies and Right-Span Peak Velocity Based on Center-Support Rotational Stiffness	95
6.8 Comparison of Natural Frequencies and Right-Span Peak Velocity Based on Interior Support Type	96
8.1 Approximate Percent Reductions in Peak Velocity Based on Center-Line Imposed Line-Load	105
8.2 Approximate Percent Reductions in Peak Velocity Based on Center-Line Double Stiffener Implementation	105
8.3 Approximate Percent Reductions in Peak Velocity Based on Center-Line Continuous Blocking System Implementation	105
8.4 Approximate Percent Reductions in Peak Velocity Based on Additional Sheathing	106

Chapter 1

Introduction

1.1 Background

Wood floor systems are complex from a structural analysis standpoint. Because of the complexity, researchers in the early 1800's began suggesting stiffness criteria to ensure safety based on personal and group experience. These criteria were based on limiting the live-load deflection of a supporting beam to the span divided by a suggested number (i.e. $L/480$). During the 1930's, an additional reason for prescribing a stiffness criterion was to limit plaster ceiling cracks that were a result of excessive beam deflection. By this time, the now common $L/360$ criterion for floor joists had been adopted. In the 1940's it had become an issue that this rule-of-thumb criterion was not supported by data. By the 1950's, research had suggested that $L/360$ did not ensure sufficient vibrational serviceability¹.

The 1960's saw a beginning to both static and dynamic analyses that would ultimately challenge the legitimacy of the $L/360$ criterion. Research investigating static response was prompted not only by a non-engineered design approach (as previously

¹Based on Percival (1979).

explained), but also by economics. Economics played an instrumental role in the development of static research programs since by better predicting a wood floor's performance, more efficient designs could be implemented to reduce overall housing costs. Also, the preservation movement forced researchers to look at more efficient designs so that the current and future wood resources could be better utilized.

Taken as a whole, static response research found that the $L/360$ criterion and others like it (based on experience rather than data) were overly conservative from a safety standpoint. This led, in many cases, to a suggested reduction in materials, and/or an increase in allowable member strength. At the same time, engineered wood products were being developed, tested, and implemented in design. These products made it possible to span greater distances with a decrease in material, and therefore weight. In essence, these two movements combined to provide a basis for structural design that yielded floors with decreased mass and in many cases, longer spans. As these more "efficient" designs were being implemented, it was found that there was an increase in complaints due to annoying floor vibrations. This is when dynamic response research apparently began to blossom; in response to consumer complaints that were a direct result of less conservative designs.

Currently, wood structures in the United States are still being designed with a static approach that accounts for safety but does not account for vibrational serviceability. Therefore, it is not surprising that annoying vibrations are still common and of great concern to both building designers and building occupants. Rather than propose a design criterion, this dissertation will investigate potential ways of improving floor performance through the use of basic construction techniques. The investigation will be facilitated by the development of a finite element model that simulates the

behavior of wood floor systems.

1.2 Objectives

Regarding the vibrational performance of wood floor systems, the objectives of this research are to:

- Quantify the effects of potential performance improvement techniques.
- Determine the optimal performance improvement technique conditions.
- Show how the optimized performance improvement techniques can be used to design serviceable floors.

1.3 Significance

Accounting for the vibrational response of wood floors is important from a serviceability standpoint in that it can aid the designer in achieving a comfortable structural environment. As the concept of “perceived quality” becomes more dominant in the consumer psyche, it will become increasingly necessary to ensure that products perform at an adequate comfort level. If steps are not taken to address and design for vibrational serviceability, further consumer complaints and lawsuits are likely to result.

Chapter 2

Literature Review

2.1 Introduction

This chapter reviews literature pertinent to the subject matter of wood floor systems. The chapter is divided into static and dynamic performance sections, and each of these sections is divided further based on experimental/theoretical and numerical analysis. In addition, steel and concrete issues that parallel wood systems will be discussed.

2.2 Static Performance

2.2.1 Experimental/Theory

This part of the literature review describes important issues that pertain to the understanding of how wood floor systems behave when subjected to static loads. The important issues that will be described in this section are: composite action, load sharing, connection behavior, and the effect of bridging.

2.2.1.1 Composite Action

Composite action can be considered the interaction between two connected materials as a result of an applied force. In wood floor systems, composite action is most evident between the sheathing and floor joists, and has long been recognized as a phenomenon that must be taken into account to properly predict wood floor performance (Goodman et al., 1974; McCutcheon, 1977). The primary motivation for quantifying composite action has been to account for the phenomenon in numerical models that predict floor performance. In these instances, composite action has either been determined explicitly or accounted for through a slip/spring/stiffness constant.

McCutcheon (1977) explicitly determined composite action through a T-beam analysis using basic material properties and load/slip values for the sheathing-joist connection based on experimentally verified theoretical equations determined by Wilkinson (1972). The analysis also took into account the effects of sheathing gaps along the length of the beam by assuming they were open (discontinuities) and did not transmit any stiffness to the system. Jizba (1978) later developed a way to estimate gap stiffness, and these values were then used in at least two computer numerical models: FEAFL0 (Thompson et al., 1977) and NONFLO (Wheat et al., 1983).

In addition to explicit determination, composite action can be accounted for by a slip/spring/stiffness constant. For example, Sliker (1972) determined empirically from experimental tests that the rotational spring constant was 3370 N-m (29830 lb-in) for nails with diameter 4.0 mm (0.159 in) and shank length of 58 mm (2-5/16 in) spaced at 200 mm (8 in) through a 16 mm (5/8 in) plywood sheathing. Vanderbilt et al. (1974) used a slip modulus of 5.25D6 N/m (3.0D4 lb/in) as a “typical” practical value in

their mathematical model and stated that 1.75D9 N/m (1.0D7 lb/in) represented full composite action whereas 0 N/m (0 lb/in) represented zero composite action. As will be seen later in the numerical analysis section, composite action is shown to be a very important feature of floor performance.

2.2.1.2 Load Sharing

Load sharing (or two-way action) in wood floor systems can be considered the transfer of loads from one joist to the adjacent joist or joists. However, throughout the world, many different interpretations of this basic concept have been formed. For example, whereas the British code defines a load sharing system as “where four or more members can be considered to act together to support a common load”, the Australian Standard specifies “parallel support systems . . . comprised of two or more elements . . . effectively connected so that all the elements are constrained to the same deformation” (Levin, 1975).

In the United States of America, load sharing has been addressed and can be seen in design where an increase of 15% is given to the allowable bending stress, F_b , if there are three or more members spaced a maximum distance of 0.6 m (24 in) apart, assuming adequate sheathing (or load distribution elements) (NDS 1991). Although this is warranted since catastrophic failures in wood systems seldom occur, it may have serious limitations in that it may still yield conservative values for some floors (Bulleit, 1991). For example, Polensek et al. (1972) experimentally tested forty-four wood-joist floor systems and determined that two-thirds of a 1334 N (300 lb) midspan joist load was distributed to primarily six and sometimes eight adjacent joists. These loads decreased as distance from the loaded joist increased. It was also concluded

that an increase of concentrated load from 1334 N to 1868 N (300 lb to 420 lb) did not change the number of joists that deflected. Wheat et al. (1986a) explains that load sharing increases the floor stiffness over bare-joist stiffness due to the presence of the sheathing.

Li (1993) experimentally tested 4.88 m x 4.88 m (16 ft x 16 ft) floors and found that the vast majority of a 2667 N (600 lb) load was carried by joists three or less joist spacings away from the loaded joist. It was also found that a higher coefficient of variation of the joist modulus of elasticity generally caused a higher variation in the load sharing capacity. In comparing a 50 mm x 300 mm (2 in x 12 in) southern pine floor, and a 50 mm x 300 mm (2 in x 12 in) I-Joist floor, the material weight was shown to have no significant effect on the load sharing capacity. The material weight of southern pine was taken as 250 N/m² (5.2 lb/ft²), and the material weight of the I-Joist(s) was taken as 189 N/m² (3.9 lb/ft²).

2.2.1.3 Connection Behavior

It is well known that in the majority of cases, the connections that hold together structural components form the weakest links in a structure. Therefore, knowledge of the connection(s) should provide information about how the structure reacts under load. The two primary types of connections used in wood floor systems to connect the sheathing and joists are nails and adhesives.

2.2.1.3.1 Nails

Foschi (1974) developed a non-linear load-slip analysis that showed good agreement when compared to experimental results. It was concluded that linear approximations were not accurate in predicting ultimate nail loads. Foschi and Bonac (1977) then

extended the analysis to include load-slip characteristics for different connections. Between these two studies, McLain (1975) developed an empirical curvilinear equation accounting for nail non-linearity that was based on experimental results. While each of the before mentioned studies were based on a single type of fastener, Erki (1991) developed a non-linear model that could accept either a glulam rivet, nail, or bolt.

Relating to composite action, Wheat et al. (1986b) used McLain's (1975) equation to compare predicted nail forces based on twelve full scale test floors to NDS allowable values. In addition, slip was measured between the sheathing and joists. An important conclusion was that joist stiffness alone was not considered a good predictor of relative nail slip throughout the floor system.

Studies have shown that total floor deflection responds non-linearly to applied loads due to the non-linear nature of the connections (Wheat et al., 1985a; Foschi, 1985). However, both Wheat et al. and Foschi observed that floor deflection was nearly linear in the range of loading considered for design. Whereas Foschi concluded that a linear analysis would adequately estimate floor response, Wheat et al. remained cautious since joist responses prior to failure were extremely variable. The complications of the linear assumption will be discussed in the numeric analysis section.

2.2.1.3.2 Adhesives

Serious attention to the use of adhesives in wood construction began in the early 1970's. Both Goodman (1969) and McCutcheon (1977) observed that rigid adhesives decreased the deflection of layered beams and floor system joists respectively. Studies by Vick (1971), Zornig and Vick (1974), Dong and Hoyle (1976),

Hoyle and Hsu (1978), and Hsu and Hoyle (1978) looked into the properties of elastomeric construction adhesives and the validity for using them in wood construction. While some adhesives were found to be better than others, there was a definite potential for the outstanding adhesives to be implemented in wood design. For example, McGee and Hoyle (1974) concluded that useful composite action is possible with elastomeric construction adhesives. Hoyle (1976) later went on to suggest that adhesives with a shear modulus of 6.9×10^5 Pa (100 lb/in²) or greater have such potential. In 1988, Hoyle (1988a, 1988b) developed and validated a design method to determine the allowable properties of nail/adhesive joints.

2.2.1.4 Bridging

Bridging has long been thought to be a way to increase the performance of wood floors. The National Association of Home Builders (NAHB) undertook an extensive study of bridging and made numerous conclusions (NAHB, 1961). Important conclusions included: 1) lateral load distribution (load sharing) in cross- and solid- bridging is approximately the same within the 1112 N to 1557 N (250 lb to 350 lb) concentrated load range, 2) lateral load distribution (load sharing) increases as the depth of the joist increased, 3) both forms of bridging when used alone (without subfloor, finish floor, etc...) were effective in transferring lateral load; however, when a subfloor was attached, the effect of the bridging was greatly reduced, and 4) bridging played a minor role in reducing the floor joist deflection subjected to a concentrated load. These conclusions, among others, led to the ultimate conclusion that bridging (cross or solid) did not serve a "useful" purpose in the distribution of concentrated static lateral loads (load sharing) or in the reduction of deflection. In addition to NAHB,

Ohlsson (1988c) also found cross-bridging to be ineffective at increasing the stiffness and thus performance of wood floors.

Stark (1993) experimentally investigated several varieties of bridging mechanisms for wood floors, including: cross-bridging, solid-blocking, post-tensioning, strong-back bracing, steel X-bracing, and bottom-chord-bracing. While the first three mechanisms were considered for solid-sawn floors, the latter three mechanisms were considered for parallel-chord-truss floors. Taken as a whole, it was concluded that the bridging mechanisms were capable of enhancing the load sharing capacity of the floors investigated.

2.2.2 Numerical Analysis

2.2.2.1 FEAFL0

2.2.2.1.1 Development Of FEAFL0

The beginnings of an engineered methodology for static wood floor performance apparently started with Goodman (1968, 1969). In these studies, small deflection theory was utilized to predict the interlayer slip associated with layered beam systems. Theoretical predictions, when compared to experimental interlayer slip results of a flat loaded three-layer 19 mm x 286 mm (1 in x 12 in) beam, showed excellent agreement. It was concluded that the effect of interlayer slip on deflection was significant.

Interlayer slip is generally accounted for through the idea of composite action which is oftentimes denoted in numerical models by a slip modulus. For example, Sliker (1972) utilized a computer program (Beam 3) to simulate joist deflections. In this model, a slip modulus was used that represented 8d nails (4.0 mm (0.159 in) diameter and 58 mm (2-5/16 in) length) at 200 mm (8in) nail spacings. In addi-

tion, the plywood floor was modeled such that horizontal force transmission could be monitored. While some agreement was found in the results when compared to experimental values of joist deflections, it was observed that two-way action was an important part of floor deflection.

Utilizing the ideas of composite and two-way action, Vanderbilt et al. (1974) developed a mathematical model based on a T-beam analysis to predict the performance of wood-joist floor systems at service loads. An important aspect of this research was a parameter study that investigated the effects of varying important input variables. For example, reducing the joist modulus of elasticity (MOE) from 13790 MPa to 6895 MPa (2.0 D6 lb/in² to 1.0 D6 lb/in²) increased midspan deflections by 40%.

Goodman et al. (1974) used the model developed by Vanderbilt et al. (1974) to further the parameter studies dealing specifically with composite and two-way action based on varying material properties. It was shown that approximately 33% of an applied 1334 N (300 lb) load was carried by the loaded joist with the adjacent joists receiving most of the remaining load. It was also shown how an increase in sheathing thickness, 19 mm to 25 mm (0.75 in to 1.0 in), caused an increase in two-way action which resulted in the loaded joist receiving less load and the adjacent joists receiving more load. Two-way action was suggested to be responsible for a “smoothing out” effect that was seen for floor joist deflections (reduces variability).

Dawson and Goodman (1976) also used Vanderbilt’s model, in conjunction with a Monte Carlo simulation method, to evaluate joist deflections based on the variability of materials. Important results from this study included the observation that both the deflection distribution and maximum joist deflection increased in variability as the joist MOE increased in variability. In addition, it was stated that as transverse

sheathing stiffness lessens, there is greater deflection variability since there is less composite action and load sharing present to offset the effects of joist MOE variability (assuming similar MOE variabilities).

Utilizing the work described in this section thus far, Thompson et al. (1976) developed a finite element model to analyze wood floor systems (FEAFLO). The model took into account interlayer slip, orthotropy, gaps at joints, and variability of materials. The connections (nails) were modeled linearly and the joint gaps were given an effective stiffness.

2.2.2.1.2 Results Of FEAFLO

Tremblay et al. (1976) developed a mathematical model based on Goodman's (1968) work and incorporated it into a finite element solution technique based on Thompson et al.'s (1976) FEAFLO work to predict joist deflections at overload conditions. These predictions were made possible by the consideration of non-linear connection slip moduli, variance of properties along the beam length, and the effects of sheathing joints and gaps. Unfortunately, although the results were good, they were only compared and verified against single double T-beam specimens.

Using FEAFLO as a basis, Sazinski and Vanderbilt (1979) developed two design methodologies. The first methodology utilized a dimensionless chart and the second utilized assembly tables. Although it was recognized that the assembly tables would lead to the easiest implementation, certain assumptions built into the tables showed that a designer must have a good understanding of floor behavior in order to interpolate between table values.

Schaefer and Vanderbilt (1983) compared FEAFL0 computed deflections to those found in twenty-two full size floor specimens that were tested during previous studies. It was concluded that while FEAFL0 produced an average error of +10%, a bare-joist design produced an average error of +125%. These differences show the significance of composite and two-way action on floor system deflection.

2.2.2.2 NONFLO

NONFLO was developed by Wheat et al. (1983) on the basis of, and in response to, FEAFL0. FEAFL0 is based on the assumption of linear floor response; however, this assumption is only valid for working load levels since non-linearity in deflections and stresses is small. Above these levels, extending from overload to failure, the true response of the floor is non-linear due mainly to connector deformation. Therefore, it is the main purpose of NONFLO to provide a non-linear analysis of wood floor systems. NONFLO utilizes a curvilinear load-slip equation determined by McLain (1975) to account for this non-linearity. It was concluded that NONFLO was more accurate than FEAFL0 at near failure conditions.

In 1984, Wheat and Moody compared FEAFL0 and NONFLO in order to develop an equation relating the two models. The relation could potentially make it possible to use FEAFL0 for non-linear failure load analysis. The driving force behind this study was that NONFLO was much more complex and expensive than FEAFL0. The identified relation produced excellent results in FEAFL0, as compared to NONFLO.

2.2.2.3 FPL

FPL was developed by McCutcheon (1977) as a mathematical method for predicting floor stiffness and thus floor deflection. The model was based on a T-beam analysis

and composite action was explicitly solved for; however, the model was limited to individual beams since it did not account for two-way action. When computed deflections were compared to experimental mid-joint deflections, very good agreement was found.

McCutcheon et al. (1981) essentially compared FEAFL0 with FPL. Eleven different floor configurations were considered and the computed deflections of both models were compared to each other on the basis of a 1915 Pa (40 psf) uniform load, and given material properties. For the most part, there was good agreement between the two models. However, comparisons carried out to determine how distributions of joist properties affect floor performance were not in agreement. Specifically, joist variability could not be handled accurately by FPL since there was no provision in the model to account for two-way action. As a result of both analyses, it was concluded that composite action was sufficient enough to reduce computed deflections below current design levels; therefore, design that does not account for composite action is conservative from a safety standpoint.

2.2.2.4 FAP

FAP was developed by Foschi (1982) and utilized the finite-strip method to study wood floor behavior. While it was a linear analysis like FEAFL0, the author saw an advantage over FEAFL0 in that while FEAFL0 restricted some degrees-of-freedom (joist torsion and out-of-plane bending), FAP included them. Comparison of computed deflections and experimental deflections were very good. As an application of the model, Foschi looked at the effect of bridging on floor deflection. It was shown that bridging did have an effect on deflection, and that the effect was an excellent

indication that joist torsion and out-of-plane bending can not be neglected. Joist MOE variation was also looked at, and it was concluded that bending stresses were lower, and load was more uniform for floors with higher floor joist MOE uniformity.

Foschi (1985) later used FAP to determine whether initial nail stiffnesses derived from simple compression nail joint tests were representative of those derived from full scale load/slip tests. This investigation was initiated by the author's view that there are experimental difficulties in measuring the small deformations at a nail location and that an approximation may provide sufficient results. The simplification was concluded to produce near optimal results for the 8d (4.0 mm (.159 in) diameter and 63.5 mm (2.5 in) length) nails tested. Other results of the study included: 1) floor behavior was nearly linear up to first joist failure, 2) reliability analysis should be based on first joist failure loads, and 3) first joist failure typically occurred in a joist other than the weakest; this was due to load sharing and the relationship between the MOE and the modulus of rupture (MOR).

2.3 Reliability

"Theoretical reliability analysis is based on the relationship between two idealized distributions...the distributions must be idealized because the computations rely on precise estimates of population density...these precise estimates come from the analysis and study of system behavior such as: two-way action, composite action, finite element analysis (linear), finite element analysis (non-linear), and multiple member failures" (Gromola et al., 1991).

For ultimate reliability analysis, it is necessary to define a failure criterion. For example, while Foschi (1985) suggested that first joist failure loads should be used

for reliability analysis. Bulleit (1987) assumed ultimate load capacity to occur when two adjacent members failed. The issue of whether to use first member failure loads or post-first member failure loads in reliability analysis is open to debate.

An important aspect of system reliability is that analysis must focus on the system as a whole instead of single elements (Folz and Foschi, 1989). DeBonis (1980) stated that simulation or numerical modeling techniques such as those by Vanderbilt et al. (1974) and Goodman et al. (1974) could be used as an intermediate step in attaining reliability-based design.

Folz and Foschi (1989) developed a methodology for determining system modification factors that when applied to a single member, would ensure reliability of the entire system. The system factors accounted for load sharing, and were dependant on the probability distributions of structural members and loading, as well as the differences between single members and complete systems.

Rosowsky and Ellingwood (1991) examined Load Resistance Factor Design (LRFD) concepts as applied to reliability-based wood design in light of duration of load effects (DOL). It was concluded that by not including the DOL effect, "an overly optimistic appraisal" of the system would result.

2.4 Dynamic Performance

2.4.1 Experimental/Theory

2.4.1.1 Vibration Types

Vibrations can essentially be broken down into two categories: 1) steady-state (continuous), and 2) transient (damped). While steady-state vibrations are characterized by frequency and amplitude, transient vibrations are characterized by frequency, am-

plitude and damping. Generally speaking, steady-state vibrations are a result of rotating machinery. It has been found that transient vibrations result from the impact of footfalls during normal walking (Wiss and Parmelle, 1984). Ohlsson (1982, 1988a) has shown that there are two major ranges for footfall forces: a low frequency range (0-6 Hz) and a high frequency range (6-50 Hz). Although the natural frequency for short and medium span wood floors is in the higher range, long span wood floors may exhibit resonance vibrations due to the low frequency component (Ohlsson 1988a). Murray (1991) suggests that a steel and concrete designer must be aware of the low frequency component (below 3 Hz) to avoid resonance vibrations.

2.4.1.2 Defining Human Tolerance Levels

In order for a dynamic design criterion to have validity, it must be linked to some scale of human perception to vibration. After all, perception is what ultimately governs the response of annoying vibrations. Studies in this area have also led to an increase in knowledge concerning the important characteristics of human perception of vibration.

With regard to steel and concrete floors, Reiher and Meister (1931) defined a perception scale with six distinct thresholds based on frequency and peak deflection from steady-state vibrations. Lenzen (1966) later used the Reiher and Meister (1931) results and found that the peak deflection should be reduced by a factor of 10 for transient vibrations lasting 5 cycles or less. Allen (1974) defined a scale with the threshold levels being dependent on the amount of critical damping.

For wood floors, Polensek (1970) reported a five step scale based on peak deflections and frequency as a result of transient vibrations lasting less than 1 second. Wiss and Parmelle (1974) also studied human response to both steady-state and transient

vibrations and defined a five step scale. Atherton et al. (1976) used a scale of 1-5 (larger annoyance to smaller annoyance) to evaluate human response. Last but not least, Ohlsson (1982) defined a three step scale based on velocity response and damping due to walking vibrations.

The qualitative results from these tests combine to show that human response to transient vibration is dependent on frequency, amplitude, and damping. The quantitative results from these tests are difficult to compare and evaluate, primarily because they have different vibration sources, different durations, and different scales. In addition, comparison is difficult because it is well known that human response to vibration is very subjective (Wheeler, 1982; Irwin, 1978; Allen and Rainer, 1985). Lack of sufficient data for studies prior to 1980 led Becker (1980) to suggest that none of the scales had any absolute value.

2.4.1.3 Characterization Of Transient Wood Floor Vibrations

2.4.1.3.1 Frequency

Two important aspects of frequency that should be considered are fundamental frequency and separation of adjacent natural frequencies. Polensek (1970) stated that the fundamental frequency of residential wood floors built with solid wood-joists is between 10 and 25 Hz, a sharp contrast from the common concrete and steel values of 5–8 Hz (Murray, 1991). Experimental laboratory results obtained by Ohlsson (1982), Chui (1987), Hu (1992), and Li (1993) also show the fundamental frequency to be in the 10-25 Hz range. Chui (1990) and Chui and Smith (1991) found that long span I-Joist floors tended to have lower fundamental frequencies than those typically associated with solid-sawn floors.

Methods used in predicting wood floor natural frequencies have included grillage models (Ohlsson, 1982), the Rayleigh-Ritz method (Smith and Chui, 1988), modal synthesis (Hu, 1990), and finite-strip analysis (Filliattrault et al., 1990). For steel and concrete floors, fundamental frequency has been primarily predicted by T-beam models where the corresponding fundamental frequency equation utilizes the transformed moment of inertia of the T-beam (Lenzen, 1966; Allen, 1974; Murray, 1991). Frequency equations have also been developed for special loading situations such as assembly occupancies (Allen et al., 1985).

Determining the fundamental frequency of a floor is important since it has been found that floor performance can be improved by raising the fundamental frequency above a certain threshold level. For wood floors, Ohlsson (1982) and Smith and Chui (1988) found the threshold level to be 8 Hz, and Johnson (1994) and Shue (1995) found the threshold level to be 15 Hz. Raising the fundamental frequency above 8 Hz is beneficial for two reasons: 1) humans are very sensitive to frequencies in the 4-8 Hz range, with the highest annoyance occurring at approximately 5 Hz (Grether, 1971), and 2) at frequencies below 8 Hz there is a possibility of resonance due to human activities (Ellingwood and Tallin, 1984). For steel and concrete floors, there has been little suggestion of threshold levels for frequency, apparently due to the fact that many of the floors are within the highest annoyance frequency range (4-8 Hz). However, for occupancy loading, Allen et al. (1985) have suggested minimum natural frequencies for solid concrete and steel-joist concrete slab floors to be above 7 Hz and 9 Hz respectively for dance floors and gymnasiums, and above 5 Hz and 6 Hz respectively for stadia assuming limited peak accelerations.

Separation of adjacent natural frequencies is also an important way to help en-

sure adequate vibrational serviceability. When joists are spaced too close together, or when the width of a floor is greater than its span, a reduction in the spacing between resonance frequencies may occur (Chui, 1986). This reduction in spacing can become a problem since closely spaced modes of vibration can interact to produce high amplitudes (Ohlsson, 1982; Filliatrault et al., 1990).

Smith and Chui (1988) and Filliatrault et al. (1990) have found that both the introduction of bridging and reduction of orthotropic stiffness of the floor increase the separation of natural frequencies of adjacent modes and therefore improve floor performance. Although a minimum separation has not been determined, the further apart the frequencies, the better the floor performance. Ohlsson (1982) has suggested that the frequencies should be separated by at least 5 Hz.

2.4.1.3.2 Amplitude

Amplitude has been expressed by researchers in three ways: 1) displacement, 2) velocity, and 3) acceleration. It is an important parameter, and it is generally believed that floor performance can be improved by reducing the amplitudes of floor response. Atherton et al. (1976) found that deflection was the best single indicator of both single impact and walking floor vibrations. Atherton et al. (1976) also concluded that the static and geometric characteristics of the floor systems tested were not good indicators of human response.

Velocity has been extensively used by Ohlsson (1982, 1984, 1988a, 1988b, 1991) to account for amplitude. Justification for using velocity has been that it is believed to be the parameter that best describes human disturbance above 8 Hz (Ohlsson, 1988; ISO, 1987). Other evidence by Allen (1974) suggests that from 3-8 Hz, annoyance follows a

constant acceleration criteria, while above 8 Hz, annoyance follows a constant velocity criteria. In other words, the acceleration needed to produce an annoying vibration is the same at 3 Hz as it is at 8 Hz, assuming equal damping (the same follows for velocity).

Acceleration has been used a great deal mainly because it is easily measured, and has been found to correlate well with human tolerance to vibration, especially root mean square acceleration (RMS). Chui (1988) has used RMS acceleration as prescribed by the British Standards Institute (1984). Acceleration has been successfully utilized in accounting for amplitude in steel and concrete structures mainly because the frequency of these floors is in the 3-8 Hz range. For wood floors however, acceleration may not be the best measure since as previously mentioned, it is believed that velocity yields a better description of annoyance to vibration above 8 Hz.

2.4.1.3.3 Damping

Damping is an important parameter since it is responsible for dissipating energy. An increase in damping should improve floor performance by limiting the number of cycles and duration of vibration, as well as reducing peak amplitudes (Polensek, 1988). However, near optimum joint damping may result in loose joints which are unacceptable from a structural standpoint (Ungar, 1973); thus too much damping may be detrimental if the joints are the primary damping source.

Two major sources of damping in wood systems are slip damping (interlayer or hysteretic) and material damping (internal) (Yeh et al. 1971; Polensek, 1988). Since damping in wood systems is predominantly a result of friction, interlayer damping comprises the vast majority of damping while internal damping plays a greatly re-

duced role (Ungar, 1973). Interlayer damping has generally been quantified as an equivalent, percent of critical, viscous damping factor.

Polensek (1975) experimentally tested thirty-four full size wood-joint floors under vertical free vibration, and determined damping factors of 4 to 6% of critical. Polensek (1988) later went on to say that the actual floor system damping factor is probably between 5-10% because of additional damping caused by sheathing gaps.

In contrast, Ohlsson (1982) tested eight small scale floors by hammer impact and determined the damping factor to vary between 0.5 and 1.5%. No significant difference was found in damping values between glued connections and screwed connections. Chui (1987) experimentally tested six wood floors by hammer impact and found the damping factors to be between 0.7 and 3.0%. Ohlsson (1988b) stated that since there was no large volume of experimental damping values available, a reasonable damping factor would be 1%.

The differences in experimentally obtained damping factors has been suggested by Smith and Chui (1988) to be a result of differences in floor loading and data analysis. For example, free vibration analysis requires the release of weight off the floor, while a hammer impact analysis requires the release of weight onto the floor. Also, while time-amplitude traces may be difficult to evaluate, the spectral procedures used by Ohlsson (1982) and Chui (1986, 1987) are straight-forward.

Determining an a-priori value for damping is very difficult and in the vast majority of cases must be prescribed by estimation and experience. For steel and concrete structures, Murray (1991) sets guidelines for estimating damping that are based on observation only. This leads to the realization that damping is not controlled by the design engineer (Ohlsson, 1988a).

Of interest is the role that human bodies play on damping. Polensek (1975) found that damping factors were doubled with the presence of three people on a wooden floor. It appears as though the human body acts similar to a “shock absorber” and has been modelled by Foschi and Gupta (1987) as a single degree-of-freedom spring-dashpot system. Results indicated that this type of model has a substantial effect on damping. However, Ohlsson (1988b) advises against such damping considerations at the design stage because it may not be reasonable to count on the “extra” damping.

Damping is an interesting phenomenon since it may oftentimes be modified after a structure has been erected. Chui (1988) found that higher damping factors resulted from the addition of dead weights on a wooden floor. However, at the same time, an increase in dead weight will result in a decrease in the natural frequencies of the floor. Therefore, more is not necessarily better, and an optimum dead load should be considered.

The main body of knowledge on the idea of “retro-fit” has been researched primarily for steel and concrete structures. Allen (1974) and Allen and Swallow (1975) looked at partitions, damping posts, and tuned dampers and found that all had applications for increasing structural damping.

Tuned dampers appear to be a very interesting and potentially effective treatment to annoying vibrations. Although Allen (1990) suggests that tuned dampers are seldom effective, a recent “real world retro-fit” was accomplished under the leadership of Webster and Levy (1992). Although the analysis and pre-manufacture of the tuned dampers was somewhat extensive, the cost of the system was one-sixth that of a design utilizing damping posts (columns).

2.4.1.4 Sensitivity

This section discusses response sensitivity due to several factors. Unless otherwise specified, the following results were obtained from experimental testing, not simulation.

2.4.1.4.1 Support Conditions

Chui (1987) tested both simple, simple, simple, simple (S-S-S-S) and simple, free, simple, free (S-F-S-F) floors with solid-sawn joists and found that when the edge supports were removed, a reduction in both natural frequencies and damping factors ensued. Hu's (1992) results indicated that neither of Chui's conclusions held for the I-Joist floors she tested. Li (1993) observed that for solid-sawn, I-Joist, and parallel-chord-truss floors, the difference in support conditions affected the natural frequencies above the fundamental, but had no effect on the damping factors.

2.4.1.4.2 End Fixity

Chui (1987) re-tested one floor by increasing the end condition clamp torque to twice its approximate simple support value. Under hammer impact, the change in end fixity increased the natural frequencies by approximately 1%, and the change in damping factors was negligible. It was concluded that in the range of applied loads seen at the end of the floor, the vibrational performance was not sensitive to end fixity. On the other hand, Chui and Smith (1990) found single beams to be sensitive to end fixity (except for beams with low slenderness ratios). It appears that the floor "system" is advantageous in that it reduces the effects of end fixity.

2.4.1.4.3 Applied Dead Load

Chui (1987) placed 100 kg (220 lb) line loads on the free edges of a S-F-S-F floor and excited the floor with a hammer impact. The effects of the line loads were to:

1) lower the fundamental and second natural frequencies, 2) increase the spacing of adjacent natural frequencies, 3) decrease the number of contributing modes, and 4) increase the damping factors. Hu (1992) also found a reduction in the first two natural frequencies, and an increase in damping factors due to an applied dead load. As a specific example, the addition of an 80 kg (176 lb) load to the center of S-F-S-F floor resulted in a 4 Hz reduction in the fundamental frequency and an approximate 1% increase in the modal damping factors. Li (1993) applied uniform loads of 957 N/m^2 (20 lb/ft²), and 1914 N/m^2 (40 lb/ft²) on both S-S-S-S and S-F-S-F floors, and found: 1) a reduction in natural frequencies, 2), a reduction in the spacing between natural frequencies, 3) a reduction in the number of contributing modes, and 4) no effect of applied uniform load on damping factors. These results indicate that while applied dead loads tend to decrease natural frequencies, they do not necessarily tend to influence damping factors.

2.4.1.4.4 Bridging

In terms of dynamic response, Chui (1987) found that solid blocking had very little effect on the first two natural frequencies, and no conclusive evidence was obtained regarding differences in damping factors. The major effect of solid blocking was to increase the separation between natural frequencies. Stark (1993) investigated the effects of X-bracing and blocking on the response of wood floors constructed with solid-sawn joists. Results indicated that neither bridging method significantly

affected the dynamic characteristics of the floors tested. These results and others indicate that conventional bridging can not be relied upon to improve the dynamic response of wood floor systems constructed with solid-sawn joists.

2.4.1.4.5 Joist Modulus Of Elasticity

Li (1993) concluded from testing four floors that the joist MOE coefficient-of-variation (COV) had a statistically significant effect on the floor fundamental frequency. Specifically, changing the joist MOE COV from 9% to 30% resulted in a 0.8 Hz decrease in the fundamental frequency. Incidentally, numerical simulation conducted by Filiatrault et al. (1991) revealed that for the floors simulated, the variability in floor fundamental frequency was five times less than the variability in single-joist stiffness values.

2.4.1.4.6 Joist Spacing

Chui (1987) compared two floors with joist spacings of 400 mm (16 in) and 600 mm (24 in) on-center. It was found that the fundamental frequency of the floor with 400 mm joist spacings was 8% greater than the floor with 600 mm joist spacings. However, the frequencies for mode 3 and higher were lowered resulting in a reduction of natural frequency separation. The overall conclusion from these results is that reducing the joist spacing does not necessarily guarantee an improvement in floor performance.

2.4.1.4.7 Joist-To-Sheathing Connections

By comparing the results of two floors constructed with nails applied at 250 mm (10 in) and 125 mm (5 in) intervals, Chui (1987) found a slight increase in natural frequencies but no conclusive evidence regarding damping factors.

2.4.1.5 Experimental Design Criteria

For wood floors, Onysko (1985) proposed serviceability criteria based on a field study of human response. After one-hundred and seven applicants from around Canada were chosen, in-house testing took place at their residences and questions were asked of the participants as to their evaluation of floor performance. The statistical analysis of the results led Onysko to propose two design criteria, both of which were based on limiting the maximum floor deflection. The first criterion is recommended for living areas, the second for bedroom areas:

$$\delta \leq \frac{6.7}{SPAN^{1.22}} \quad 3.0 \leq SPAN < 6.0 \quad (2.1)$$

$$\leq 1.75 \quad SPAN < 3.0 \quad (2.2)$$

$$\delta \leq \frac{8.9}{SPAN^{1.22}} \quad 3.0 \leq SPAN < 6.0 \quad (2.3)$$

$$\leq 1.75 \quad SPAN < 3.8 \quad (2.4)$$

where: $SPAN$ = clear span (m), and δ = deflection as a result of a concentrated load of 1 kN acting at the midspan of the floor (mm).

In response to the Onysko (1985) study and other research undertaken at Forintek Canada Corp. (Onysko, 1975, 1988), the Canadian Wood Council developed and initiated a design criterion for wood-joist floors. The design criterion is included in *The Span Book* (1990), and the method of establishing this criterion can be found in the National Building Code of Canada (1990), appendix A-9.23.4.1(2).

Recently, Johnson (1994) proposed, and Shue (1995) validated, a criterion based on the results of twelve laboratory and over two-hundred in-situ floors composed of

either solid-sawn joists, parallel-chord-trusses, or I-Joists. The criterion requires the fundamental frequency of the joists and supporting girders to 2 the following relation:

$$f = 1.57 \sqrt{\frac{386EI}{WL^3}} > 15Hz \quad (2.5)$$

where: f = fundamental frequency of the joist or girder (Hz), E = modulus of elasticity, I = Moment of inertia, W = total supported load, and L = joist or girder span. The criterion also requires that the combined frequency of the joists and girders satisfy the following:

$$f = \sqrt{\frac{f_{joist}^2 \times f_{girder}^2}{f_{joist}^2 + f_{girder}^2}} > 15Hz \quad (2.6)$$

Murray (1981) proposed a vibration criterion for steel and concrete floors based on over one-hundred experimentally tested floor systems. The criterion is valid for floors with a natural frequency below 10 Hz and is based on a heel-drop excitation. The criterion is based on the inequality:

$$D > 35A_o f + 2.5 \quad (2.7)$$

where: D = damping in percent of critical, A_o = maximum initial amplitude (in), and f = first natural frequency of the floor system (Hz). If the inequality is satisfied than vibrational problems for office and residential settings should be eliminated.

2.4.2 Numerical Analysis

2.4.2.1 Numerical Models

There are four numerical models specifically designed to predict the dynamic response of wood floor systems. Each will be described in light of major features and findings.

The first numerical model to be discussed was developed by Foschi and Gupta (1987). The model, an extension of FAP (Foschi, 1982), is based on a finite strip representation in the along joist direction and a finite element representation in the perpendicular to joist direction. Sheathing strain energy expressions include both vertical bending and in-plane action, where the orthotropic nature of the sheathing is included. Joist strain energy relations include vertical bending, lateral bending, axial deformation, and torsional deformation. Non-rigid sheathing-to-joist nailed connections are accounted for with respect to lateral deformations by a strain energy representation. This study seeks to calculate the time-history response of wood floors with two humans on the floor, where the humans are represented by single degree-of-freedom mass-spring-damper mechanisms. The mass matrix was obtained in a consistent framework from the kinetic energy contributed by the sheathing and joists. Damping coefficients were prescribed for the sheathing, joists, and connections in quantities that led to an overall viscous damping factor of 15 %. The full damping matrix was constructed and solution of the time-history response was achieved using the Wilson- θ numerical integration procedure. Effects of bridging were investigated by neglecting the torsional deformation in the joists. While a detailed reliability analysis ensued, no mention was given to how the model results compared to experimental results.

The second numerical model, NAFFAP (Filliattrault et al., 1990) was also an extension of the FAP (Foschi, 1982) static analysis Program. Strain energy relations and connection energy relations used in NAFFAP are the same as those used in the Foschi and Gupta (1987) model. From a modeling standpoint, the only addition to the formulation is the inclusion of a rotational sheathing-joist slip energy expression. The mass matrix was consistently derived as in the previous model, with the additional ability to model a uniformly distributed load. With the intent of predicting the natural frequencies of wood floor systems, the subspace iteration method was used to solve the free vibration problem. Effects of bridging were investigated by restricting torsional deformations. Model results were compared to experimental results obtained by Smith and Chui (1988), and good agreement was found between predicted and actual natural frequencies.

Chui (1987) provided a numerical model to predict both the natural frequencies and time-histories of wood floor systems. The analysis was based on the Rayleigh-Ritz method where only vertical bending was included in the strain energy representations for both orthotropic sheathing and joists. Bridging was taken into account by introducing vertical bending strain energy terms where the bridging-joist interface was assumed to be rigid. The mass matrix, obtained from a kinetic energy expression, accounted for only the vertical inertia component of orthotropic sheathing, joists, and bridging. The Jacobi method was used to solve the free vibration problem. Considering solid-sawn floors, comparisons of the predicted and experimental natural frequencies showed the model to generally be within 5 % of the actual values. With regard to the time-history, the Newmark β numerical integration procedure was used where the full damping matrix was calculated based on the fundamental mode.

stiffness proportional damping:

$$\mathbf{C} = \gamma \mathbf{K} \quad (2.8)$$

where:

$$\gamma = \frac{2\zeta_1}{\omega_1} \quad (2.9)$$

where: ζ_1 is the fundamental mode viscous damping factor, and ω_1 is the fundamental mode natural frequency (rad/sec). While model time-histories were not rigorously compared to experimental time-histories, RMS accelerations were. The RMS acceleration, A_r , was calculated according to:

$$A_r = \left[\frac{1}{T} \int_0^T a^2(t) dt \right]^{1/2} \quad (2.10)$$

where: $a(t)$ is the time-history acceleration. Comparisons of predicted and experimental RMS accelerations showed that the predicted values tended to overestimate the actual values by an average of approximately 25 %.

The final numerical model specifically designed to analyze the dynamic response of wood floor systems was constructed by Hu (1992). The model utilizes the free-interface modal synthesis method. Strain energy of the sheathing is due to vertical bending only, where orthotropic plate theory is assumed. Joist strain energy is based on a Timoshenko beam where transverse shear is included in the formulation. No provisions for bridging were included in the formulation. The QZ method was used to solve the free vibration problem. Hu experimentally tested ten I-Joist floors and concluded that in comparison to the models of Chui (1987) and Filiatrault et al. (1990), her model significantly improved the accuracy of natural frequency predic-

tions for light-weight wood floors with relatively deep I-Joists (principally due to the inclusion of joist transverse shear). Time-history analysis was conducted using the Newmark β numerical integration procedure where the full damping matrix was calculated based on the same fundamental mode, stiffness proportional damping as used by Chui (1987). Unfortunately, no comparisons were made comparing the predicted and experimental time-histories due to a point excitation. However, comparisons were made between the predicted and experimental time-histories considering a moving load. The results indicated that while the time-history “trend” was not predicted well, the predictions of peak acceleration were acceptable.

2.4.2.2 Numerical Design Criteria

This section describes design criteria that are evaluated using numerical methods. Foschi and Gupta (1987) extended the previously mentioned static computer program FAP (Fochi, 1982) to include a dynamic analysis. The results of the study yielded a quantitative reliability-based design criterion based on individual joist stiffness and maximum deflection. The criterion proposes that for a concentrated load of 1 kN (225 lb) acting at midspan of a joist with the average modulus of elasticity of the system, the maximum static deflection should be 1 mm (0.04 in), independent of span length.

Ohlsson (1991), also developed a criterion based upon a 1 kN (225 lb) concentrated load. However, instead of only taking into account a bare joist, this criterion includes the effect of joists and sheathing since the load is applied at the center of the floor. The first stipulation of the criterion is that a maximum deflection (determined in this case from a grillage model) should be limited to 1.5 mm (0.06 in). In addition, independent of the previous condition, the floor’s natural frequency should be higher

than 8 Hz. The third stipulation is that the maximum velocity should be less than a value based on the coefficient of damping.

A third criterion has been proposed by Smith and Chui (1988). This criterion, based on a Raleigh-Ritz approach, suggests that the calculated frequency-weighted RMS acceleration for the first one second of vibration should be less than 0.45 m/s^2 (1.48 ft/s^2). The RMS acceleration is frequency weighted since human tolerance is greater at higher frequencies than at lower frequencies. The value of this factor, as given in ISO 2631 (1978) for frequencies between 8 and 80 Hz, is equal to $8/f_n$, where f_n is the fundamental frequency of the floor system. In addition, the fundamental frequency of the floor system should be above 8 Hz.

Allen et al. (1985) have mathematically derived a design criterion for assembly occupancies with regard to the floor constructions of: 1) solid concrete, 2) steel-joint concrete slab, and 3) wood. The criterion limits the floors natural frequency based upon a limiting peak acceleration. For dance floors, limiting natural frequencies of 7 Hz, 9 Hz, and 12 Hz are recommended for solid concrete, steel-joint concrete slab, and wood floors respectively, assuming a limiting peak acceleration of 0.02 g. For stadia arenas, limiting natural frequencies of 5 Hz, 6 Hz, and 8 Hz are recommended assuming a limiting peak acceleration of 0.05 g.

2.5 Summary

Considering the information presented, wood floors are complex from a structural analysis standpoint. If we were to take away three concepts/ideas from each performance condition (static and dynamic), we may observe the following.

Considering the static response, wood floors exhibit composite action. The composite action, or ability of the sheathing and joists to act together, results from the sheathing-joist connection behavior. Additionally, load sharing occurs via the sheathing. What composite action, connection behavior, and load sharing tell us together is that wood floors act as a system, and that a proper representation of the system must include sheathing-joist interaction, not sheathing-joist independence.

Considering the dynamic response, we know that vibration acceptability has been defined by design criteria that generally make use of different human annoyance factors (e.g. frequency, RMS acceleration, unit impulse velocity response, ...). From these results, we can conclude that there is still no established, definitive, quantitative evidence regarding human annoyance to wood floor vibration. Second, an a-priori determination of viscous damping is difficult if not impossible to obtain. Finally, from experimental evidence, we know that wood floor systems are very sensitive to modifications. Unfortunately, a numerical model that accounts for a wide range of structural modifications is not available.

Chapter 3

Model Overview

3.1 Introduction

As described in the Literature Review chapter, wood floor systems are sensitive to structural modification. Fortunately, we can use this to our advantage and investigate ways of improving wood floor performance through modification. Unfortunately, a model is not currently available that is capable of considering a wide range of modification. In response to the lack of an appropriate model, a displacement-based, Rayleigh-Ritz finite element model has been developed to investigate the vibratory response of stiffened plates (e.g. wood floors). Although not essential, the interested reader is referred to Appendix A for a short introduction regarding the general theory of displacement based finite elements, and how they can be used to represent dynamic motion. Model specifics, and detailed discussions, can be found in Appendices B and C. In all further discussions, due to the materially independent nature of the model, the word “stiffener” has been used instead of “joist” (in terms of wood floor systems, the two words are synonymous).

3.2 Modeling Environment

The model was hand coded in a 32-bit, Windows, mixed language environment. C++, FORTRAN, and Visual Basic were all utilized in application development.

3.3 Model Architecture

At a high level, the program can be considered to consist of three different layers: graphic user interface (GUI), preprocessor, and application engine. While the GUI and preprocessor are always a work in progress, the engine (where the finite element coding is applied) is consistent. Although the distinctions between layers may change, and new algorithms may be developed, the engine is essentially “cut in stone” from a procedural, finite element standpoint. Without going into code examples, the remainder of this chapter provides a high-level interpretation of the model, as designed in the application engine.

3.4 Application Engine

3.4.1 Elements

Wood floor systems are generally composed of two structural components, sheathing and stiffeners (i.e. joists). To account for the sheathing behavior, a quadratic, 9 node, 45 degree-of-freedom plate element is implemented. In terms of cartesian coordinates, all nodal degrees-of-freedom are active except for rotation about the vertical axis. In terms of stiffness, consideration has been given to vertical bending, transverse shear, and in-plane components. In terms of mass, consideration has been given to vertical and horizontal translational inertia, and rotary inertia.

To account for the stiffener behavior, a quadratic, 3 node, 12 degree-of-freedom beam element is implemented. In terms of cartesian coordinates all nodal degrees-of-freedom are active except for rotation about the vertical axis, and translation perpendicular to beam length. In terms of stiffness, consideration has been given to vertical bending, transverse shear, axial, and torsional components. In terms of mass, consideration has been given to vertical and axial translational inertia, and rotary inertia.

3.4.2 System Construction

From the two “base” elements just described, the entire structure is mapped using the direct stiffness method. However, as we know, sheathing and stiffeners do not act independently due to sheathing-stiffener connection behavior. If we assume that the sheathing-stiffener connections act rigidly (which is reasonable considering the widespread use of quality elastomeric adhesives), then a coordinate transformation can be applied such that the system is described by combined plate-beam elements, where only the plate degrees-of-freedom remain active.

3.4.3 System Size

As just mentioned, the direct stiffness method is used to map the entire structure. From this method, the system stiffness and mass matrices are obtained. Following the procedures found in the Appendix, a standard-form eigenvalue problem results. Unfortunately, due to the large number of active degrees-of-freedom, solution of the full system eigenvalue problem is not realistic. To remedy this concern, Ritz vectors have been applied to the full system matrices so that a reduced system eigenvalue

problem can be obtained. Results obtained from the reduced system analysis will be good approximations of the full system values.

It is important to realize that the large size of the full system is required to provide enough refinement so that modifications can be made to different parts of the floor system. For example, a model that initially generates 10 active degrees-of-freedom will not provide enough spatial refinement to consider modifications made at several different floor locations. However, a system that initially generates considerably more active degrees-of-freedom will provide more locations for modifications to occur. Once the modification information is in the full system, thanks to Ritz vectors, the system can be reduced to a size more comparable to 10 degrees-of-freedom than the full size, where the modification information is retained in the reduced system.

3.4.4 Frequency Analysis

With the reduced system eigenvalue problem at hand, IMSL routine DEVCSF is used to solve the free vibration problem. Results from the free vibration problem provide the reduced system eigenvalues and eigenvectors. From the eigenvalues, the natural frequencies can be calculated, and from the eigenvectors, the mode shapes can be calculated.

3.4.5 Time-History Analysis

Using the eigenvalues and eigenvectors obtained from the free vibration problem, the time-history is obtained using the modal analysis superposition method. Modal analysis allows the determination of the contributions of individual modes to the overall response, and allows modal viscous damping factors to be incorporated in the

time-history analysis without the need of calculating the system damping matrix.

Chapter 4

Model Verification

4.1 Introduction

In verifying the finite element model, that is, making sure that the model works as intended, both static and dynamic results will be compared to known exact plate solutions. Series solutions representing the exact solutions can be found in Appendix D. In the terms presented, considering the static solutions, “exact” can be considered “classical”. Only simply supported plates will be investigated. From a finite element standpoint, simply supported conditions can be achieved in either one of two ways. First, the transverse and perpendicular translation can be restricted along the boundary lines. This is commonly referred to as a “Soft” support. Second, in addition to the transverse and perpendicular translation being restricted along the boundary lines, the shear rotation can be restricted along the boundary lines. This is commonly referred to as a “Hard” support. For rectangular plates, the difference between the two essentially comes down to enforcing thin plate theory. Hard supports enforce thin plate theory, and soft supports do not. On the other hand, for thick plates, soft supports are necessary. Both support conditions will be investigated in the static ver-

ification section. In addition, due to potential numerical difficulties associated with evaluating the transverse shear stiffness (See Appendix B), the following results will consider both 2 and 3 point numerical integration.

4.2 Static Response

Five different plate scenarios will be considered that should adequately verify the static response. The first three scenarios consider simply supported plates whose material behavior can be characterized as either: Isotropic, Orthotropic, or Isotropic (Transverse Shear Flexible). While the fourth scenario will consider a simply supported, Isotropic plate reinforced with equidistant stiffeners, the fifth will consider a simply supported, Isotropic, dual span plate. Unless otherwise noted, Table 4.1 shows the plate material and geometric properties, and the corresponding values used throughout this chapter. For the Isotropic plate reinforced with equidistant stiffeners, the stiffeners will be taken as 100 mm x 300 mm (2 in x 12 in) rectangular sections spaced at 600 mm (24 in) intervals.

Tables 4.2 through 4.6 show the model results and how they compare to the exact solutions, considering a center-point 2225 N (500 lb) concentrated load. It is noted that the exact solution provided for the isotropic, stiffened plate example is actually a rough estimate of the exact solution (See Appendix D). Several different mesh layouts have been included so that a minimum required mesh can be determined. As a general rule, the smaller the mesh, the faster the solution. A (2x2) mesh layout means that there were two elements spanning along the x-axis, and two elements spanning along the y-axis; thus, there were four square elements used in the analysis.

Table 4.1 Plate Properties and Values Used Throughout This Chapter.
(See Appendix D For Property Definitions)

Property	Value
E, E_x	1.38D4 N/mm ² (2.0D6 lb/in ²)
E_y	6.89D3 N/mm ² (1.0D6 lb/in ²)
G	6.89D1 N/mm ² (1.0D4 lb/in ²)
ν	0.3
ν_x	0.2
ν_y	0.4
k	1.2
h	25 mm (1.0 in)
a	2.44 m (96 in)
b	2.44 m (96 in)

It is evident from Tables 4.2 through 4.6 that, for the most part, the model solutions agree well with the exact solutions. However, it is apparent that the 2 point integration. Hard support conditions provide the most accurate results with mesh sizes smaller than those required by the other conditions. As we now move on to consider the dynamic response, consideration will be given to 2 point integration. Hard support conditions.

It should be noted that 2 point integration is equivalent to a reduced integration state. One particular drawback of reduced integration is that there is no guarantee of monotonic convergence in energy (i.e. the displacements are not guaranteed to monotonically converge to the exact solutions from below as the mesh is refined). Considering symmetric mesh refinement for the (2x2), (4x4), and (8x8) mesh layouts, the results in Tables 4.2 through 4.6 bear this out. However, other than for the transverse shear flexible plate, the displacement results show essentially no change

between the (4x4) and (8x8) mesh layouts. Thus, taking convergence characteristics into account, even though convergence in energy is lost using 2 point integration, the results indicate good reliable agreement with the exact solutions. The relatively large difference found for the transverse shear flexible plate is due to the low G value used (6.89D1 N/mm² (1.0D4 lb/in²)). This G value was used deliberately to indicate a lower limit value where the results are borderline acceptable. If G is assigned a lower value, the stiffness is not adequately represented.

Table 4.2 Center-Point Displacement Results for Isotropic Plate.
(Exact = 7.42 mm)

Mesh	Soft Support		Hard Support	
	2 Point Integration	3 Point Integration	2 Point Integration	3 Point Integration
(2x2)	8.10	5.11	7.47	5.11
(4x4)	7.57	6.58	7.39	6.58
(2x8)	7.82	5.99	7.42	5.99
(4x8)	7.52	6.86	7.42	6.86
(8x8)	7.44	7.14	7.42	7.14

Table 4.3 Center-Point Displacement Results for Orthotropic Plate.
(Exact = 14.17 mm)

Mesh	Soft Support		Hard Support	
	2 Point Integration	3 Point Integration	2 Point Integration	3 Point Integration
(2x2)	14.79	9.53	14.33	9.53
(4x4)	14.25	12.57	14.16	12.57
(2x8)	14.47	11.19	14.23	11.19
(4x8)	14.22	13.10	14.17	13.10
(8x8)	14.19	13.67	14.18	13.67

Table 4.4 Center-Point Displacement Results for Isotropic.
Transverse Shear Flexible Plate.
(Exact = 8.38 mm)

Mesh	Soft Support		Hard Support	
	2 Point Integration	3 Point Integration	2 Point Integration	3 Point Integration
(2x2)	9.09	7.08	8.38	6.89
(4x4)	9.09	8.45	8.65	8.15
(2x8)	8.99	7.85	8.38	7.57
(4x8)	9.13	8.65	8.70	8.31
(8x8)	9.43	8.92	9.00	8.52

Table 4.5 Center-Point Displacement Results for Isotropic.
Stiffened Plate.
(Exact = 0.241 mm)

Mesh	Soft Support		Hard Support	
	2 Point Integration	3 Point Integration	2 Point Integration	3 Point Integration
(2x2)	0.183	0.074	0.182	0.074
(4x4)	0.218	0.178	0.218	0.178
(2x8)	0.221	0.174	0.221	0.174
(4x8)	0.221	0.206	0.221	0.206
(8x8)	0.221	0.214	0.221	0.214

Table 4.6 Center-Point Displacement Results for Isotropic.
Dual Span Plate.
(Exact = -0.508 mm)

Mesh	Soft Support		Hard Support	
	2 Point Integration	3 Point Integration	2 Point Integration	3 Point Integration
(2x2)	-0.526	-0.790	-0.610	-0.790
(4x4)	-0.498	-0.668	-0.503	-0.668
(2x8)	-0.556	-1.003	-0.620	-1.003
(4x8)	-0.498	-0.711	-0.503	-0.711
(8x8)	-0.508	-0.544	-0.508	-0.544

4.3 Dynamic Response

A preliminary investigation of mesh sizes showed that a minimum (4x8) mesh was needed to obtain an accurate dynamic response. This result, and the results from the static verification, lead to considering a (4x8), 2 point integration, Hard support condition plate for the dynamic verification. For simplicity and brevity, consideration will be given to an Isotropic plate; therefore, in the following discussion, an Isotropic, (4x8), 2 point integration, Hard support condition plate will be analyzed.

Table 4.7 shows a comparison between the model predictions and exact natural frequencies. Predictions match well with the exact natural frequencies. The first ten modes have been included since frequencies corresponding to modes higher than the tenth are not particularly well predicted by the (4x8) mesh. Table 4.7 also shows that the square plate behavior is not modelled “exactly” by the rectangular elements

(a (4x8) mesh leads to an element with a 2-1 aspect ratio). This can be seen by the failure of the (4x8) mesh to reproduce the repeated frequencies associated with the square plate.

Table 4.7 Comparison of Predicted and Exact Natural Frequencies (Hz)
for an Isotropic, Square Plate.

Mode #	Predicted (4x8)	Exact	% Difference
1	37.7	37.7	0
2	94.2	94.2	0
3	95.0	94.2	<1
4	151.5	150.7	<1
5	189.0	188.4	<1
6	197.1	188.4	4
7	246.2	244.9	<1
8	253.3	244.9	3
9	323.6	320.2	1
10	347.3	320.2	8

In verifying the time-histories, we will consider displacement, velocity, and acceleration in response to a 2225 N (500 lb) time-zero step function. Both continuous time and discrete time representations will be discussed. As a reminder, the exact time-history representations can be found in Appendix D.

In the following analyses, a viscous damping factor of 0.03 has been used where the first 10 modes have been included in the time-history responses. Furthermore, in order obtain a sufficient time-history representation, a sample rate of 1000 points/second has been used. Figure 4.1 shows a comparison between the predicted and exact displacement time-histories in response to the time-zero step function. A distinction

has not been made between the predicted and exact response in Figure 4.1 since they are almost identical. Figure 4.2 provides a closer (zoom) look at the displacement time-histories, where it is evident that the predicted time-history matches closely with the exact time-history. Similar conclusions can be drawn for the velocity time-histories (Figures 4.3 and 4.4), and acceleration time-histories (Figures 4.5 and 4.6).

The predicted time-histories in Figures 4.1 - 4.6 were constructed using a continuous time representation as described in Appendix C. While continuous time representations are applicable for simple geometric input forces (such as step functions), they are not applicable for arbitrary input forces. When arbitrary input forces are needed, a discrete time representation must be utilized. Utilizing the convolution sum (Appendix C), Figures 4.7 - 4.9 show how the predicted time-histories compare to the exact time-histories at a sample rate of 2000 points/second with regard to the same time-zero step function as used previously. The sample rate of 2000 points/second was determined during a preliminary investigation that found the value to be a minimum required for accurate response when considering a time-zero, non-zero load. As seen from Figures 4.7 - 4.9, the discrete time implementation predicts the exact responses well.

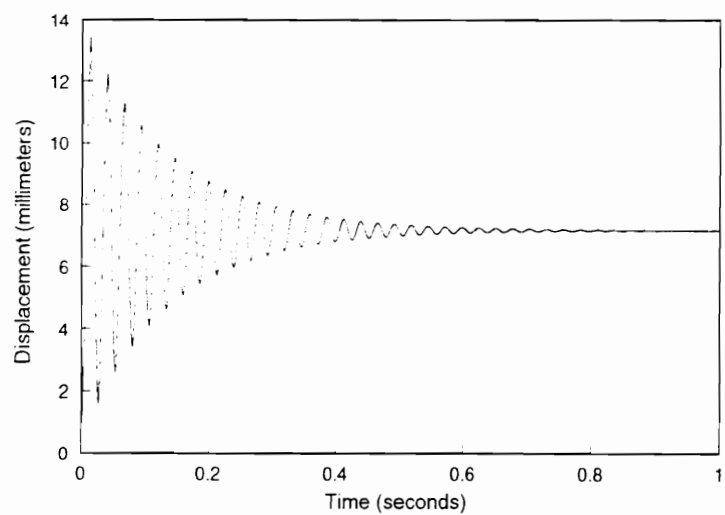


Figure 4.1 Comparison of Predicted and Exact Displacement Time-Histories
for an Isotropic. Square Plate.

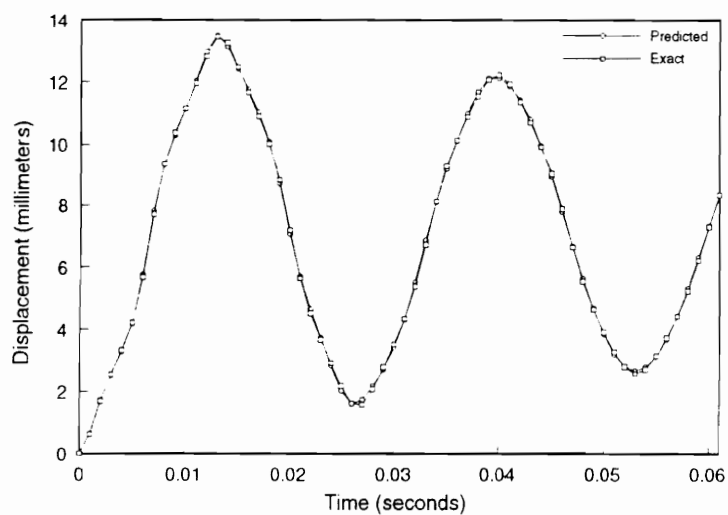


Figure 4.2 Zoom Comparison of Predicted and Exact Displacement Time-Histories
for an Isotropic. Square Plate.

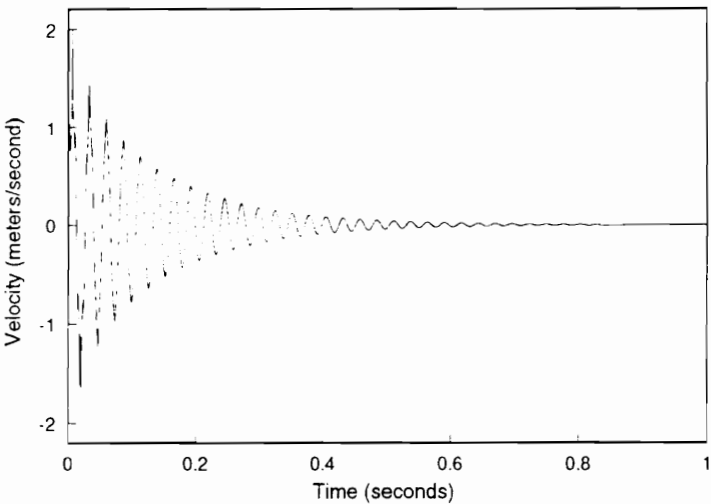


Figure 4.3 Comparison of Predicted and Exact Velocity Time-Histories
for an Isotropic, Square Plate.

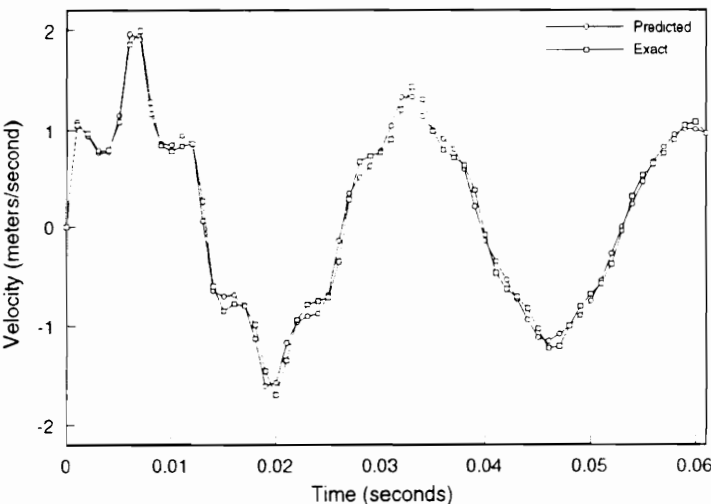


Figure 4.4 Zoom Comparison of Predicted and Exact Velocity Time-Histories
for an Isotropic, Square Plate.

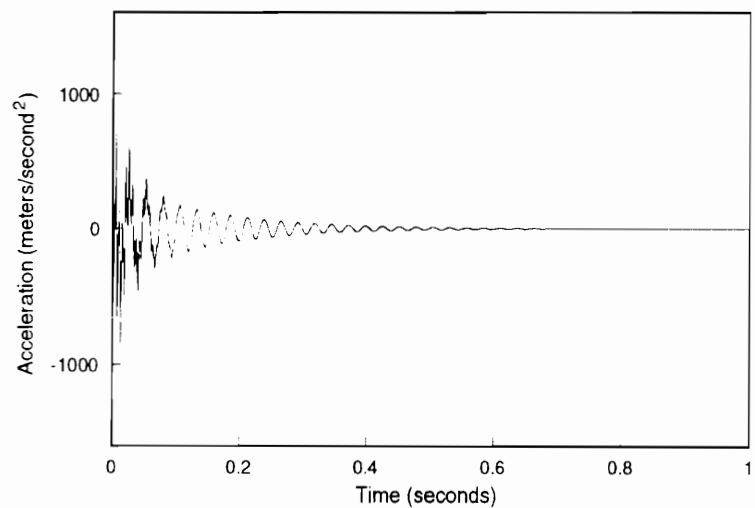


Figure 4.5 Comparison of Predicted and Exact Acceleration Time-Histories for an Isotropic, Square Plate.

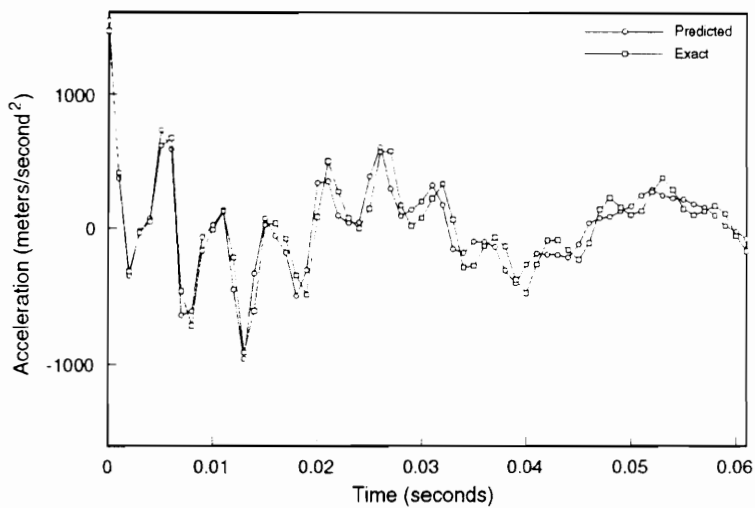


Figure 4.6 Zoom Comparison of Predicted and Exact Acceleration Time-Histories for an Isotropic, Square Plate.

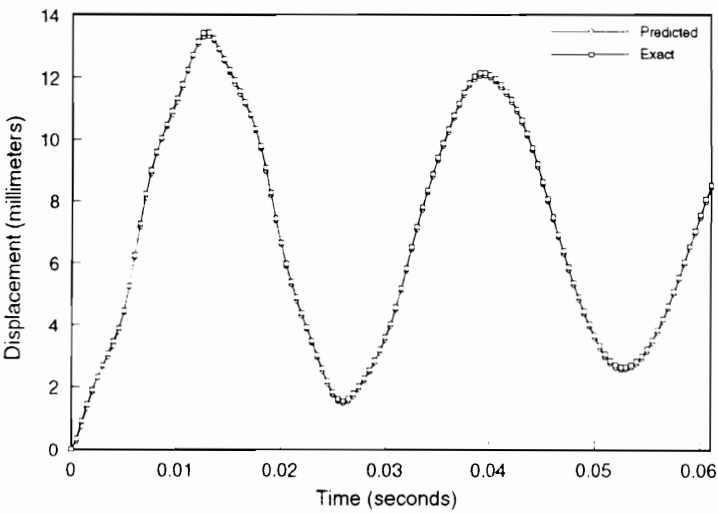


Figure 4.7 Zoom Comparison of Predicted and Exact Displacement Time-Histories for an Isotropic, Square Plate, Using the Convolution Sum.

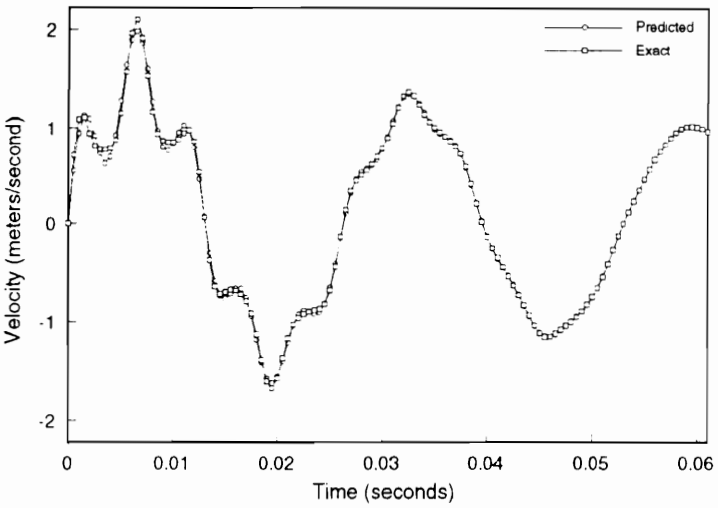


Figure 4.8 Zoom Comparison of Predicted and Exact Velocity Time-Histories for an Isotropic, Square Plate, Using the Convolution Sum.

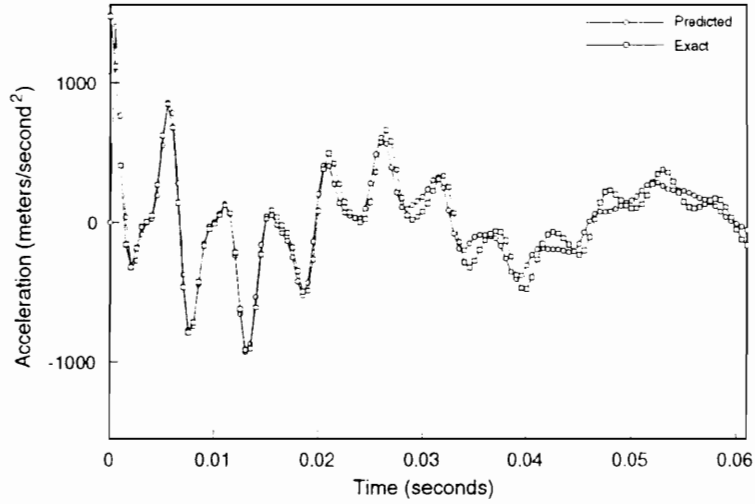


Figure 4.9 Zoom Comparison of Predicted and Exact Acceleration Time-Histories for an Isotropic, Square Plate. Using the Convolution Sum.

4.4 Summary

The results found in this chapter have emphasized model verification, that is, making sure that the model works as intended. By comparing both the static and dynamic predictions to the exact series solutions, it has been seen that the model does indeed produce the desired results. Going one step further, the results have indicated minimum required model parameters such as mesh size and sample rate. From this chapter, we can be confident that the model will provide a reliable prediction of plate response.

Chapter 5

Model Validation

This chapter focuses on model validation, that is, making sure that the model accurately represents a chosen physical system. For this purpose, model (predicted) results will be compared to experimental results obtained from selected wood floors. The experimental results used in this chapter were part of a larger experimental study conducted by Li (1993), Stark (1993), and Steiss (1994).

5.1 Experimental Floor Background

In experiments conducted by Li (1993), Stark (1993), and Steiss (1994), thirteen 4.88 m x 4.88 m (16 ft x 16 ft) wood floors were constructed and experimentally evaluated for vibrational response. For each individual floor, imposed loads of 0 N/m² (0 lb/ft²), 957 N/m² (20 lb/ft²), or 1914 N/m² (40 lb/ft²) were considered where the stiffeners were either solid-sawn joists, parallel-chord-trusses, or I-Joists. Plywood was used as a sheathing material where the sheathing-to-stiffener connections were a combination of common nails and elastomeric adhesive.

Consideration will be given to the center-point displacement time-histories and power densities under an imposed load of 957 N/m^2 and under the action of a center-point drop-weight input force. Displacement time-histories have been chosen since acceleration instrumentation problems were apparent (i.e. saturation). In addition, since the steel frame used to support the floors had a significant effect of the floor vibrational response at 0 N/m^2 , an imposed load of 957 N/m^2 has been chosen where the steel frame interaction effects are believed to be minimal (Runte, 1993).

5.2 Experimental Modal Analysis

In order to determine the natural frequencies and equivalent viscous damping factors of the experimental floors, frequency response functions (FRF's) were constructed for each floor from the displacement time-histories and input force time-history. If we assume that the input is x (force), and the output is y (displacement), an FRF can be expressed:

$$FRF = \frac{|Y|^2}{|X|^2} \quad (5.1)$$

where: Y are the fourier coefficients of y , and X are the fourier coefficients of x . The equivalent viscous damping factor at each FRF peak (natural frequency) can be determined by the half power method:

$$\zeta = \frac{f_2 - f_1}{f_2 + f_1} \quad (5.2)$$

where: f_1 and f_2 correspond to the frequencies that intersect the FRF at the values of peak/2.

5.3 Model Parameter Specifics

All material values, dimensions, etc... were obtained from the documentation notes of Li, Stark, and Steiss. Each sheathing panel was measured for directional bending stiffness, and each stiffener was measured for bending modulus of elasticity. Since shear modulus was not measured for any component, the sheathing shear modulus used in the model was taken as the American Plywood Association (APA) published design value of 621 N/mm^2 (90000 lb/in^2). Similar to Chui (1990), the shear modulus for the solid sawn joists was taken as $1/16^{th}$ the joist modulus of elasticity. When considering the parallel-chord-trusses, the shear modulus was taken as 276 N/mm^2 (40000 lb/in^2). This value was obtained by equating the displacements of a shear flexible, and non-shear flexible center-point loaded beam with respect to a 75 percent actual area moment of inertia. The 0.75 factor is commonly used in industry to account for shear in parallel-chord-trusses. For the I-Joists, it has been assumed that the oriented strand board (OSB) web material is comparable to plywood, thus a value of 621 N/mm^2 (90000 lb/in^2) has been used.

In order for orthotropic plate theory to hold, the following relation must be satisfied:

$$E_x \nu_y = E_y \nu_x \quad (5.3)$$

where: E_x and E_y are the directional sheathing moduli of elasticity, and ν_x and ν_y are the directional sheathing Poisson's ratio. Although the E_x and E_y were measured, ν_x and ν_y were not. Since the Poisson's ratios were not measured, values were assigned such that the values centered around 0.3 (an acceptable value for wood).

As previously mentioned, the sheathing-to-stiffener floor connections were a combination of common nails and elastomeric adhesive. The elastomeric adhesive used in the majority of the floor tests was Franklin Tilebond Construction Adhesive, which is comparable to the Scotch 3M 5230 elastomeric adhesive. Although neither of these adhesives will produce a “truly” rigid connection, they are stiff enough to assume so (especially when considering the small slip displacements associated with typical floor vibrations). Therefore, rigid sheathing-to-stiffener connections have been assumed in the model.

When considering transverse shear, a form (shear correction) factor must be determined that is based on physical geometry (see Appendix B). Most elementary strength of materials books show that for a rectangular section, the form factor can be taken as $6/5$. This value was used for both the solid-sawn joists and parallel-chord-trusses. For the I-Joists, the form factor was taken as the area of the entire section divided by the area of the web (which is valid if we assume that the web resists all the shear).

With respect to the sheathing mass density, an APA equivalent value of 5498 N/m^3 (35 lb/ft^3) was used for the 18 mm ($23/32 \text{ in}$) plywood sheathing. The average stiffener mass densities were determined from the documentation notes of Li, Stark, and Steiss. Average mass densities of the solid-sawn joists were found to be 6283 N/m^3 (40 lb/ft^3), and average mass densities of the I-Joists were found to be 7069 N/m^3 (45 lb/ft^3). For the parallel-chord-trusses, a value of 9425 N/m^3 (60 lb/ft^3) was used since an equivalent “chord-only” representation was used in the model.

The input force was taken from a mechanical dropweight mechanism used to excite the floors during experimental testing. The mechanism had a self-weight of 650

N (146 lb), and a graphical representation of the force time-history can be found in Figure 5.1. It should be noted that the force time-history shown is only an approximation with regard to what the floors actually received during a test since the force time-history was measured directly by a load cell placed on a rigid floor, where the mechanism was held tightly to the load cell by ropes.

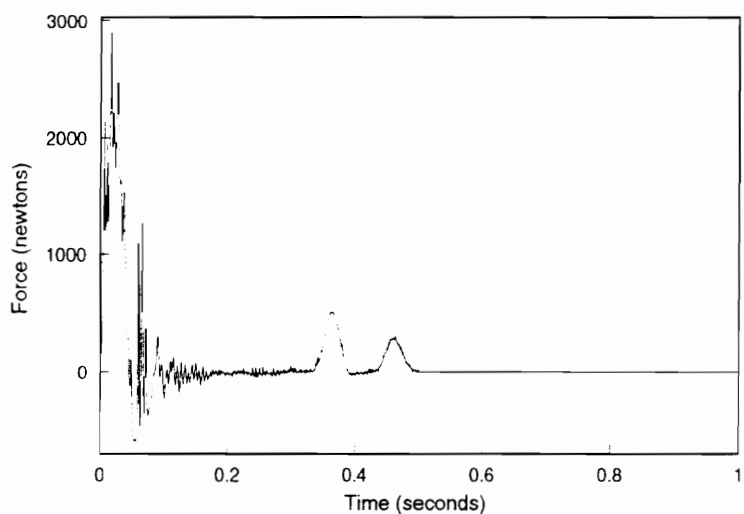


Figure 5.1 Mechanical Dropweight Force Time-History Recorded on Rigid Floor.

Due to the center-point experimental acquisition instrumentation being located on the bottom of the center stiffener, load sharing was taken into account to provide the input force experienced by the center stiffener. Based on a static procedure, Steiss (1994) reported load sharing factors for the solid-sawn and I-Joist floors. Factors for the parallel-chord-truss floors were determined from the experimental documentation of Li, Stark, and Steiss. Table 5.1 shows the load sharing factors (and

stiffener specifics), which represent the percentage of load carried by the center stiffener when a static load is applied to the center of the floor. If we assume that dropweight forces are transmitted in quantities similar to static loads, then the load sharing factors can be used to scale the input force to account for load sharing. Using this technique, it is assumed that the majority of the center-point response is a result of the scaled input force. The later assumption seems further justified by the difficulty involved in envisioning how to represent the loads transmitted to adjacent joists.

Table 5.1 Stiffener Specifics and Experimental Load Sharing Factors.
(See Appendix E for Actual Stiffener Dimensions)

Floor	Stiffener Type	Stiffener Dimensions	Load Sharing Factor (Percent)
a	solid-sawn	50 x 300 mm	42
b	solid-sawn	50 x 300 mm	47
c	parallel-chord-truss	100 x 300 mm	47
d	parallel-chord-truss	100 x 300 mm	51
e	parallel-chord-truss	100 x 300 mm	34
f	I-Joist	50 x 250 mm	51
g	I-Joist	50 x 250 mm	38
h	I-Joist	50 x 300 mm	44
i	I-Joist	50 x 300 mm	39
j	I-Joist	100 x 300 mm	50
k	I-Joist	100 x 300 mm	45

5.4 Validation Results

Of the data associated with the thirteen floors tested, two sets were found unusable. The first set was inadequate due to short data length, and the second set was found unusable due to a lack of documented sheathing property values. Thus, eleven floors will be used for direct comparison. Figure 5.2 shows a typical floor configuration, where in all cases, the stiffeners are placed at 600 mm (24 in) intervals. In modeling terms, a (4x8) mesh has been used to represent all floor systems in this chapter, where a plate element aspect ratio of 2:1 has been maintained. The reader is referred to Appendix E for a quick reference regarding these floors.

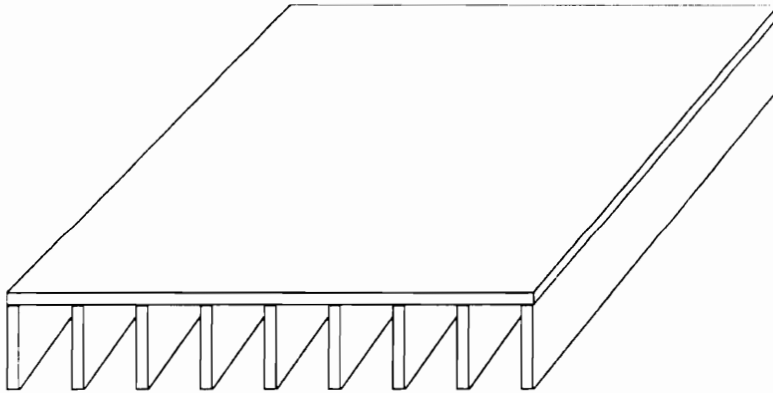


Figure 5.2 Typical Floor Configuration.

Table 5.2 shows the stiffener specifics and viscous damping factors obtained from the experimental displacement FRF's. Surprisingly, the fundamental viscous damping factors are higher than those typically associated with wood floors (< 0.05). Although it is unclear why the values were so high, it is most likely the result of applied load and connector properties.

Table 5.2 Stiffener Specifics and Experimental Viscous Damping Factors.

(See Appendix E for Actual Stiffener Dimensions)

Floor	Stiffener Type	Stiffener Dimensions	Damping (Mode 1)	Damping (Mode 2)	Damping (Mode 3)
a	solid-sawn	50 x 300 mm	0.086	0.036	0.025
b	solid-sawn	50 x 300 mm	0.044	0.03	0.024
c	parallel-chord-truss	100 x 300 mm	0.061	0.033	0.023
d	parallel-chord-truss	100 x 300 mm	0.067	0.053	0.023
e	parallel-chord-truss	100 x 300 mm	0.058	0.027	0.029
f	I-Joist	50 x 250 mm	0.062	0.034	0.017
g	I-Joist	50 x 250 mm	0.043	0.028	0.03
h	I-Joist	50 x 300 mm	0.085	0.034	0.022
i	I-Joist	50 x 300 mm	0.073	0.045	0.021
j	I-Joist	100 x 300 mm	0.115	0.021	0.018
k	I-Joist	100 x 300 mm	0.093	0.03	0.02

Table 5.3 shows how the predicted natural frequencies compare to the experimental natural frequencies obtained from the displacement FRF's. It should be kept in mind that predicted natural frequencies are not required to participate in the response. That is, the modal response at a particular point in the floor can be zero. On the other hand, only those frequencies contributing to the response can be detected experimentally. Therefore, a frequency by frequency comparison between predicted

and experimental values will generally show discrepancies of this type. In any event, the predicted fundamental frequencies are all within 18 percent of the experimental frequencies.

Table 5.3. Comparison of Predicted and Experimental () Natural Frequencies (Hz).

Floor	Mode 1	Mode 2	Mode 3	Mode 4	Mode 5	Mode 6
a	8.3 (7.8)	9.7 (12.0)	10.2 (16.1)	12.2	13.6	17.2
b	8.3 (7.8)	9.6 (10.5)	10.0 (14.4)	11.7	12.8	15.5
c	7.4 (8.5)	8.3 (12.0)	8.8 (16.4)	10.2	11.6	14.6
d	7.5 (8.5)	8.3 (11.7)	8.8 (16.1)	10.2	11.3	14.0
e	7.0 (8.5)	8.5 (12.0)	8.9 (16.4)	10.1	11.5	14.4
f	6.3 (6.8)	7.0 (9.3)	7.6 (13.9)	9.2	10.6	13.7
g	6.2 (6.8)	6.8 (9.0)	7.3 (13.4)	8.9	10.3	13.6
h	7.8 (7.8)	8.8 (10.5)	9.2 (15.1)	10.9	12.1	15.1
i	7.6 (7.8)	8.7 (10.3)	9.1 (15.4)	10.8	12.1	15.3
j	8.6 (8.5)	9.5 (9.8)	10.0 (12.5)	11.8 (16.4)	13.2	16.3
k	8.2 (9.0)	9.4 (10.0)	10.0 (12.2)	11.7 (16.8)	13.0	16.2

Figures 5.3 through 5.24 show how the displacement time-histories and power densities compare between the predicted and experimental representations (at a sample rate of 1000 points/second). Out of practical necessity, in obtaining the predicted time-history results, two assumptions were made. First, it was assumed that all frequencies in the experimental frequency range contributed to the response (regardless

of evidence suggesting otherwise). Second, since viscous damping factors were obtained from experimental FRF's, it was difficult to apply these values to the model since modes that contribute little or nothing to the response are included in the predictions. For example, an experimental mode 2 may actually correspond to a predicted mode 3 since the predicted mode 2 did not contribute to the response. Due to this concern, modal damping factors were specified in groups that surrounded the experimental modes.

Given that the raw input force time-history is an approximation, that the load sharing factors are dynamic point-equivalent approximations, that several material properties have been specified via "book" values, and that equivalent viscous damping factors have been approximately specified, the displacement time-histories and power densities indicate that the finite element model provides reasonable predictions of experimental wood floor behavior. The qualitative visual assessment was based on trend resemblance, peak location, and peak magnitude. A rigorous validation procedure was not implemented due to the data limitations just described.

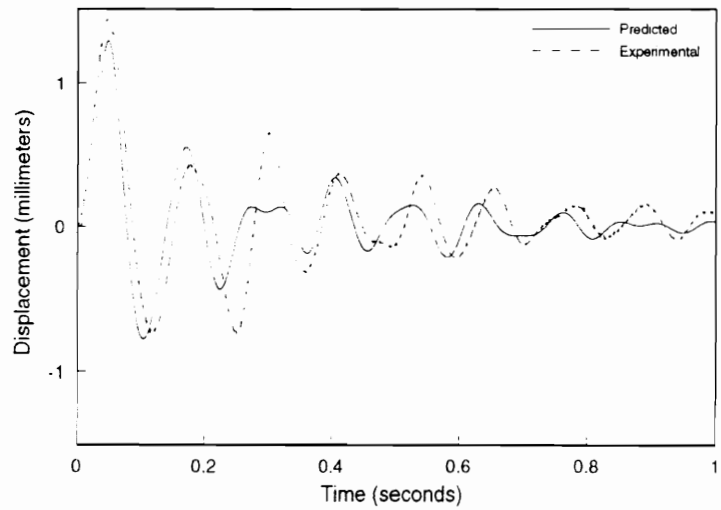


Figure 5.3 Comparison of Predicted and Experimental Displacements for Floor a (Solid-Sawn Stiffeners).

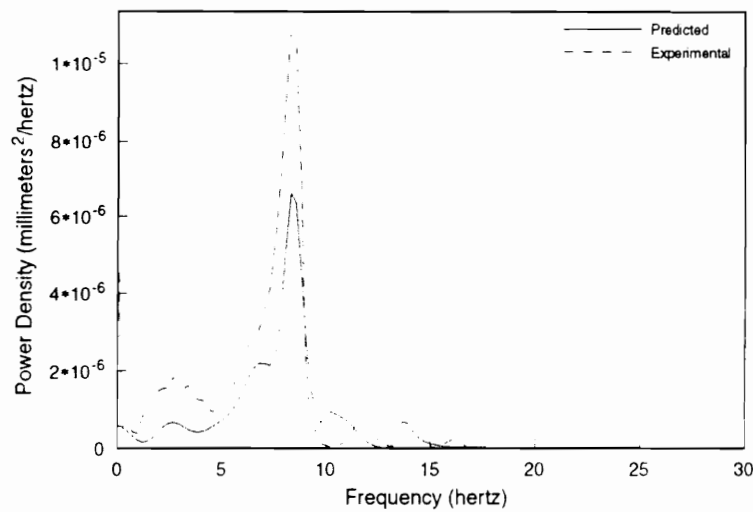


Figure 5.4 Comparison of Predicted and Experimental Power Densities for Floor a (Solid-Sawn Stiffeners).

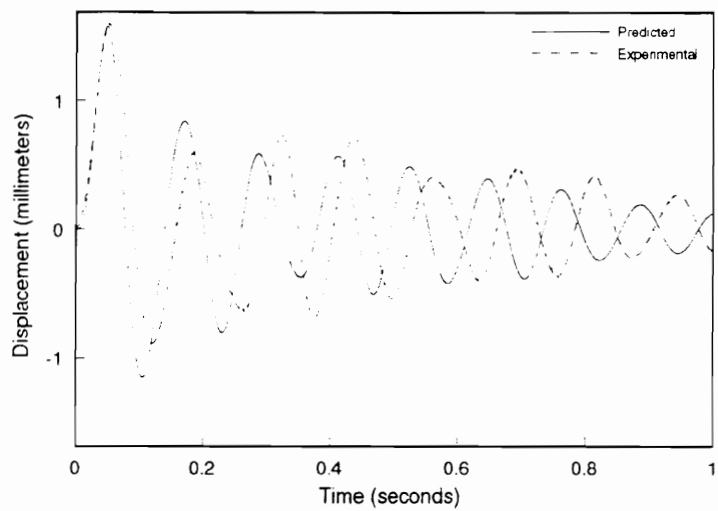


Figure 5.5 Comparison of Predicted and Experimental Displacements for Floor b (Solid-Sawn Stiffeners).

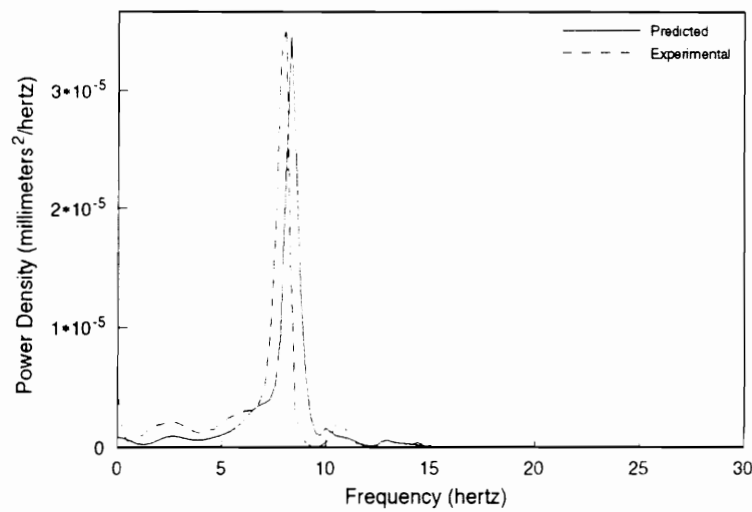


Figure 5.6 Comparison of Predicted and Experimental Power Densities for Floor b (Solid-Sawn Stiffeners).

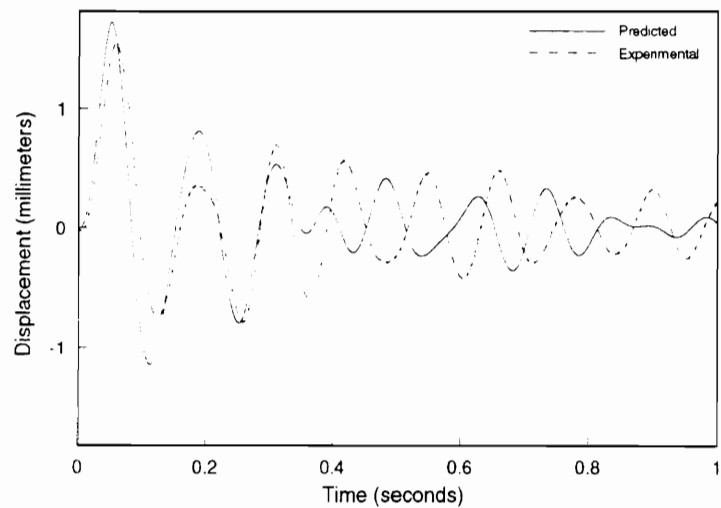


Figure 5.7 Comparison of Predicted and Experimental Displacements for Floor c (Parallel-Chord-Truss Stiffeners).

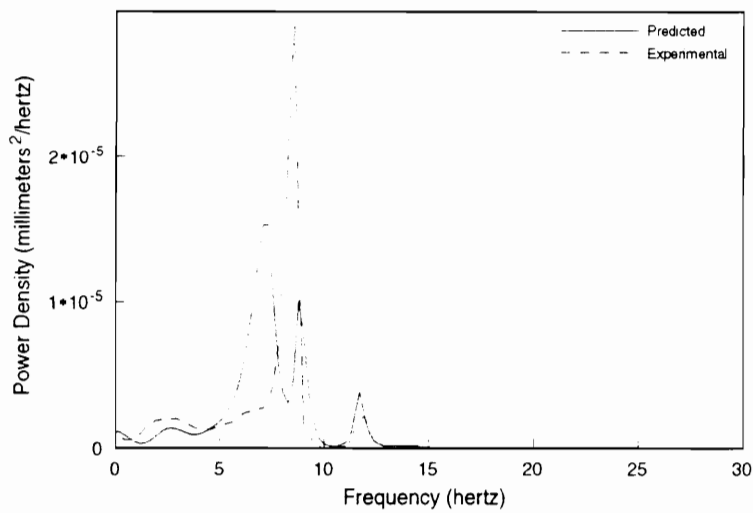


Figure 5.8 Comparison of Predicted and Experimental Power Densities for Floor c (Parallel-Chord-Truss Stiffeners).

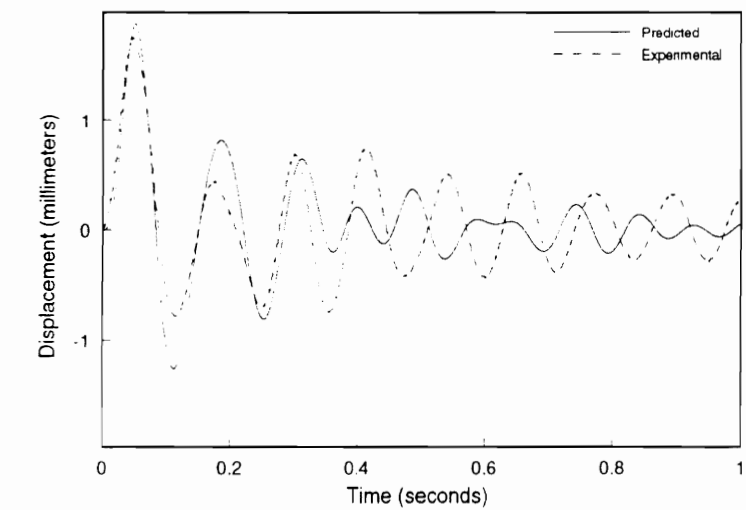


Figure 5.9 Comparison of Predicted and Experimental Displacements for Floor d (Parallel-Chord-Truss Stiffeners).

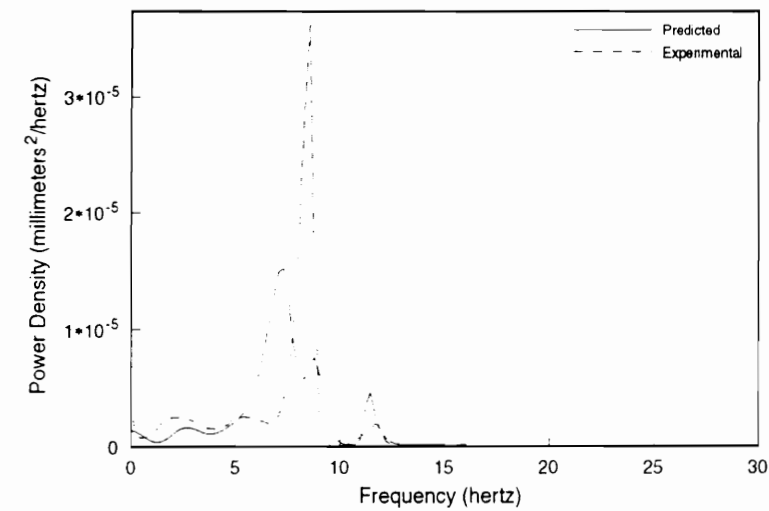


Figure 5.10 Comparison of Predicted and Experimental Power Densities for Floor d (Parallel-Chord-Truss Stiffeners).

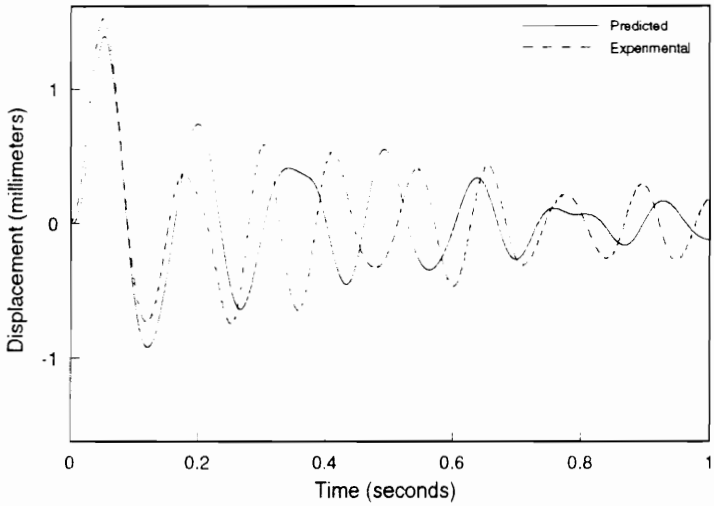


Figure 5.11 Comparison of Predicted and Experimental Displacements for Floor e (Parallel-Chord-Truss Stiffeners).

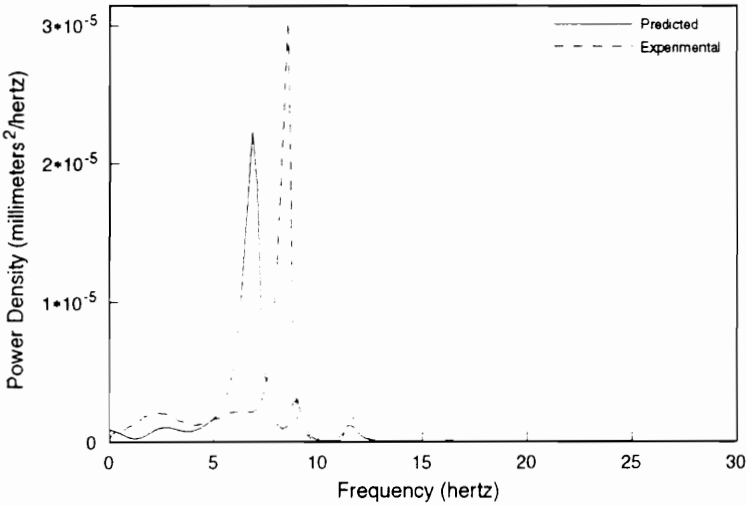


Figure 5.12 Comparison of Predicted and Experimental Power Densities for Floor e (Parallel-Chord-Truss Stiffeners).

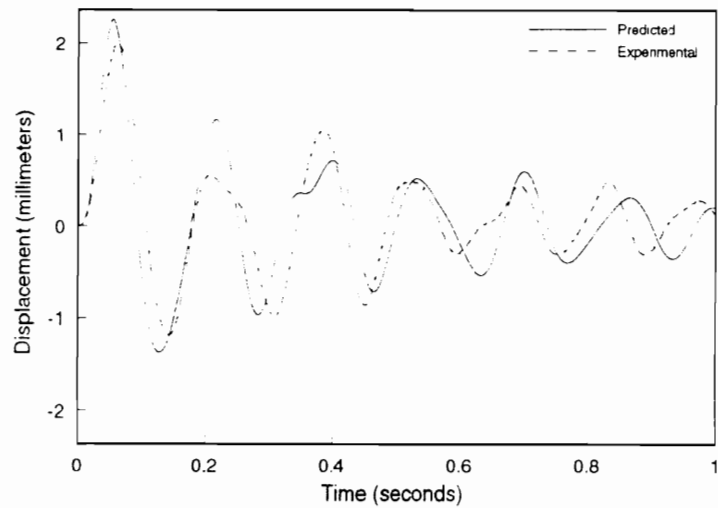


Figure 5.13 Comparison of Predicted and Experimental Displacements for Floor f (I-Joist Stiffeners).

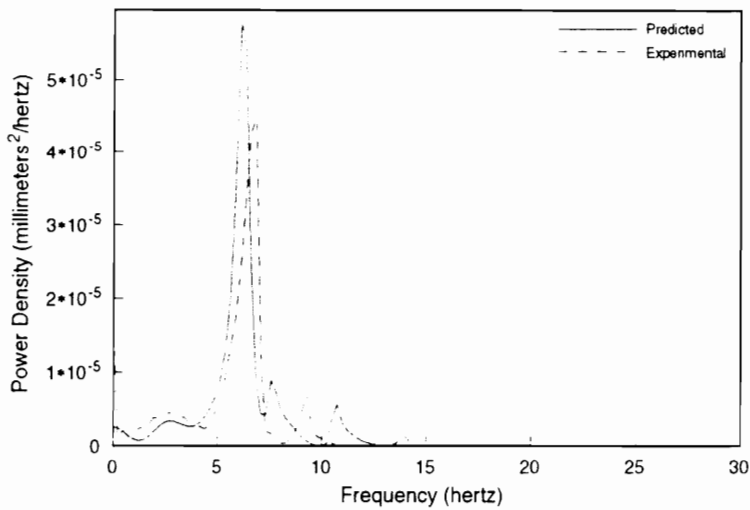


Figure 5.14 Comparison of Predicted and Experimental Power Densities for Floor f (I-Joist Stiffeners).

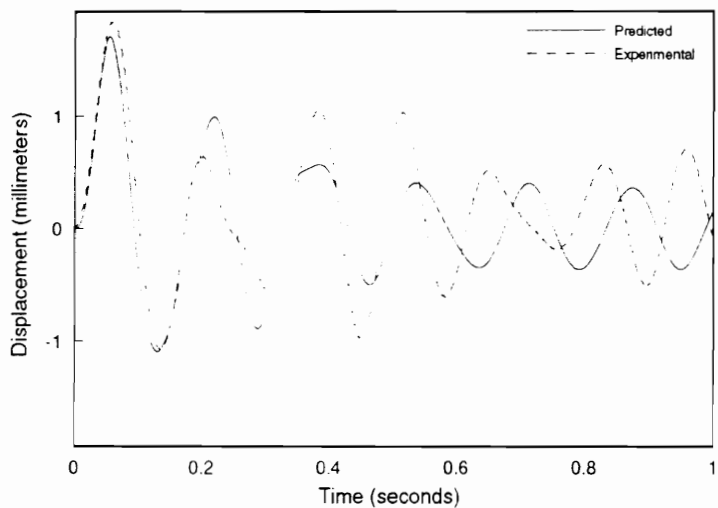


Figure 5.15 Comparison of Predicted and Experimental Displacements for Floor g (I-Joist Stiffeners).

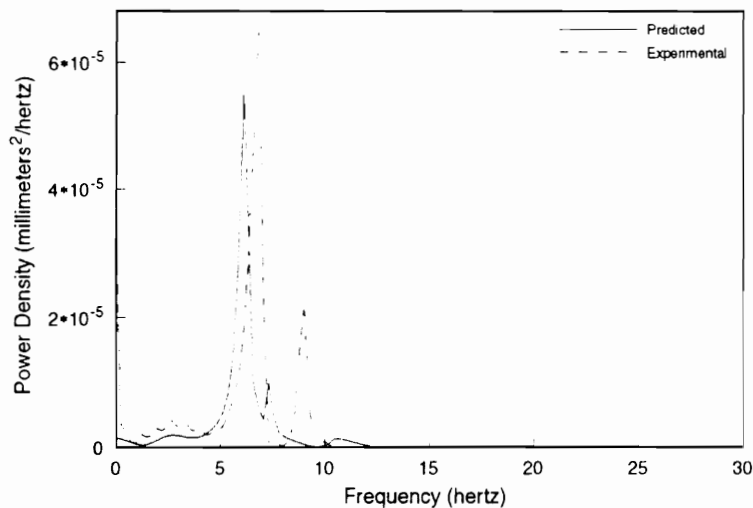


Figure 5.16 Comparison of Predicted and Experimental Power Densities for Floor g (I-Joist Stiffeners).

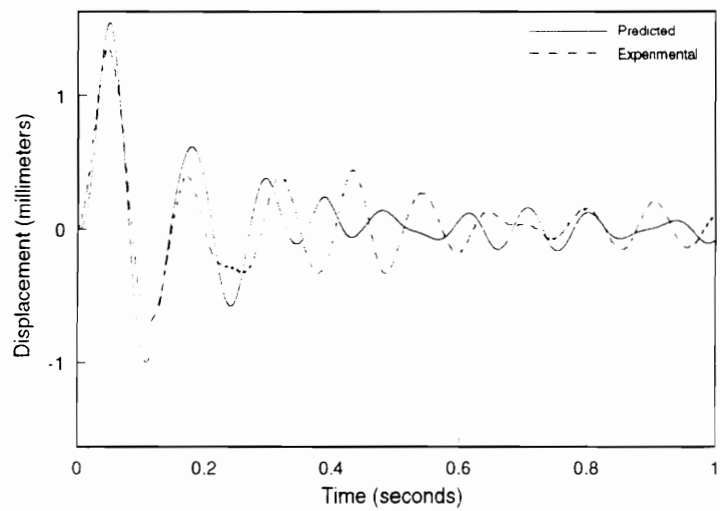


Figure 5.17 Comparison of Predicted and Experimental Displacements for Floor h (I-Joist Stiffeners).

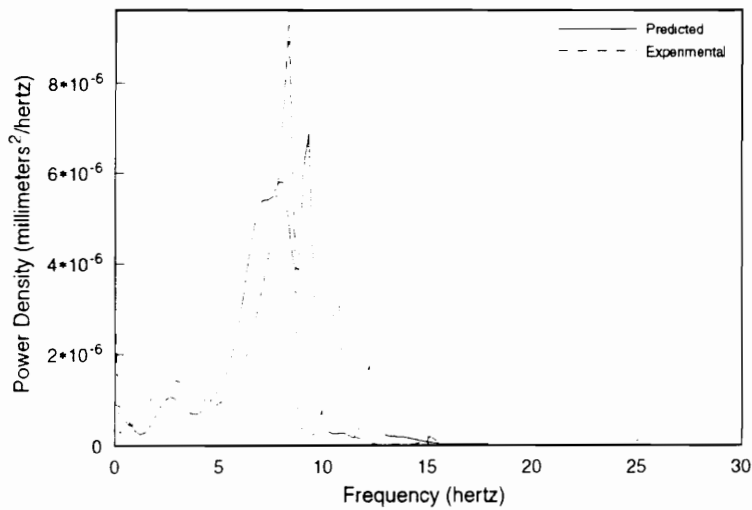


Figure 5.18 Comparison of Predicted and Experimental Power Densities for Floor h (I-Joist Stiffeners).

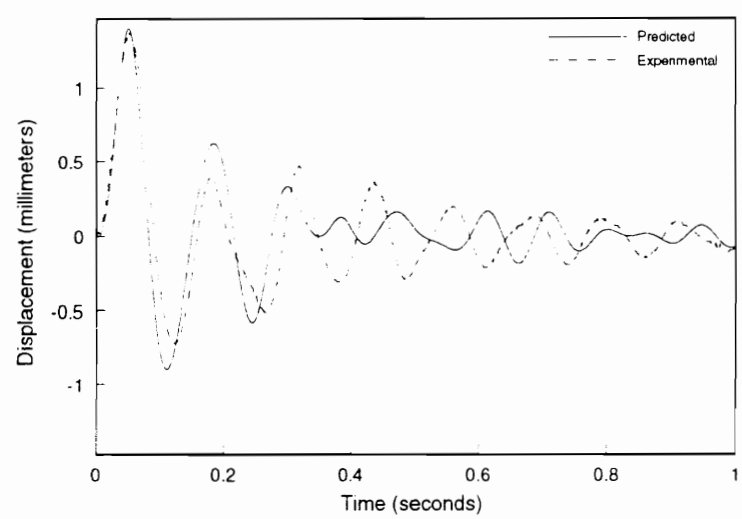


Figure 5.19 Comparison of Predicted and Experimental Displacements for Floor i (I-Joist Stiffeners).

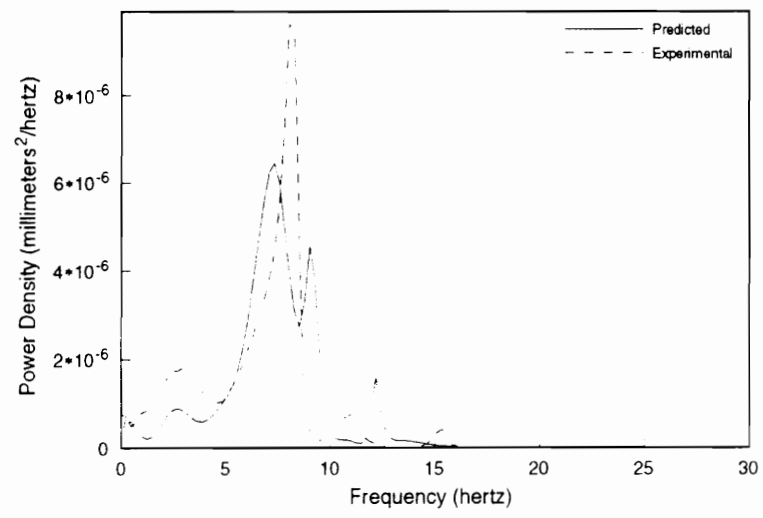


Figure 5.20 Comparison of Predicted and Experimental Power Densities for Floor i (I-Joist Stiffeners).

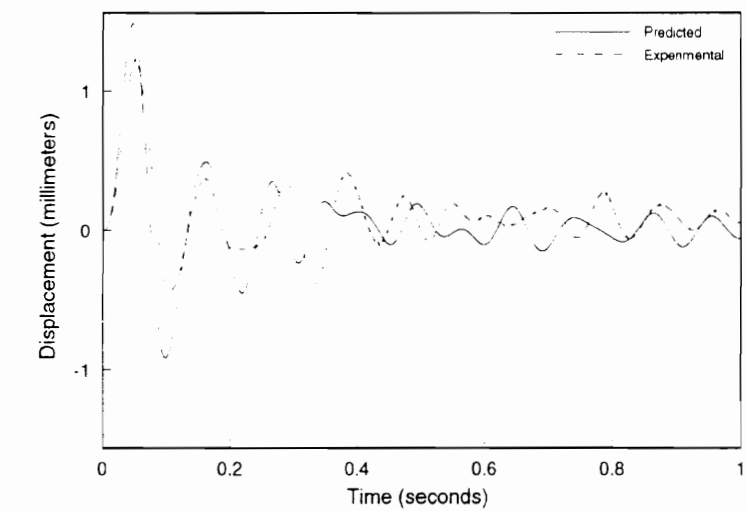


Figure 5.21 Comparison of Predicted and Experimental Displacements for Floor j (I-Joist Stiffeners).

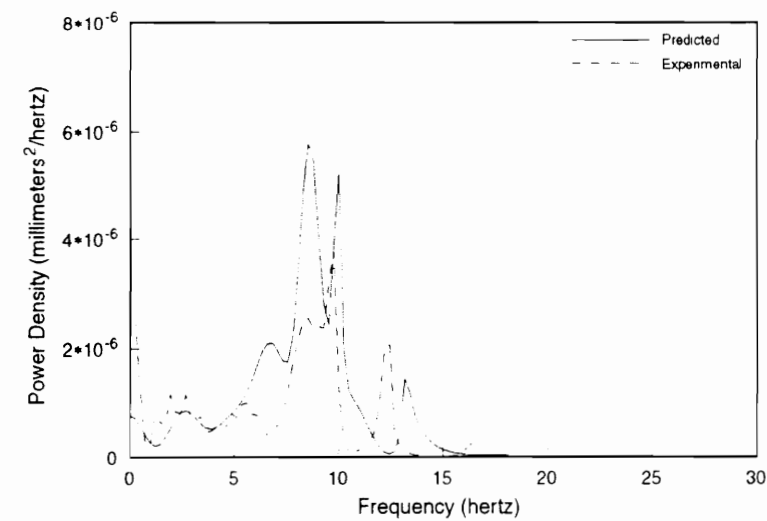


Figure 5.22 Comparison of Predicted and Experimental Power Densities for Floor j (I-Joist Stiffeners).

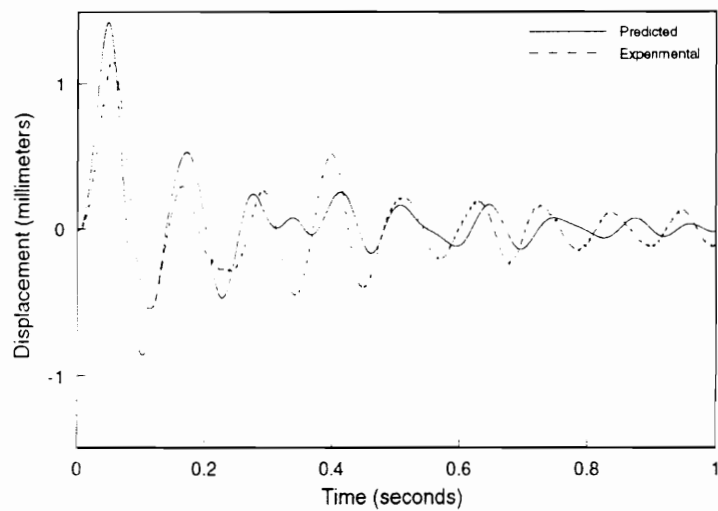


Figure 5.23 Comparison of Predicted and Experimental Displacements for Floor k (I-Joist Stiffeners).

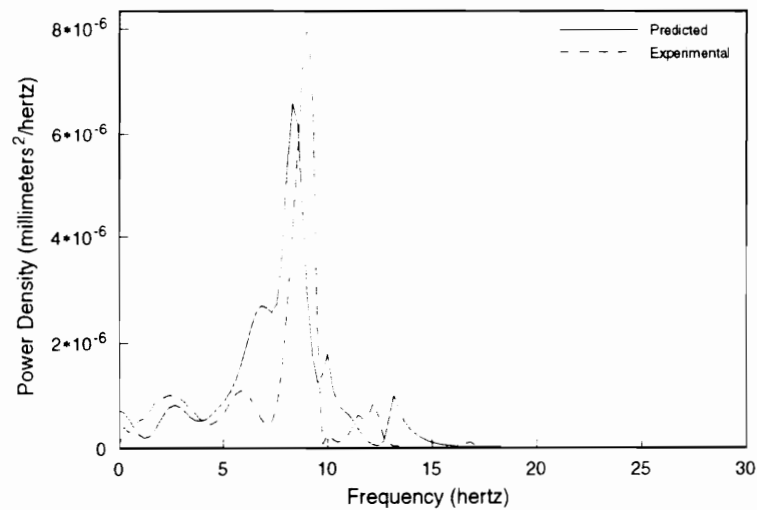


Figure 5.24 Comparison of Predicted and Experimental Power Densities for Floor k (I-Joist Stiffeners).

5.5 Summary

The results from this chapter have emphasized model validation, that is, making sure the model accurately represents a chosen physical system. Given the data limitations, it was shown that the predicted natural frequencies, displacement time-histories, and power densities were reasonable approximations of experimental wood floor behavior.

Chapter 6

Performance Improvement Investigation

Having the Rayleigh-Ritz finite element model verified and validated, consideration will now be given to investigating wood floor vibration performance improvement techniques. These techniques are passive in nature and are targeted towards implementation during construction. Active control and post construction implementations (“retro-fits”) will not be considered.

Both single span and dual span floors will be discussed. Table 6.1 shows the floor and stiffener dimensions used throughout this chapter for both span conditions. The only differences between the material properties of these floors and those in the model validation chapter, is that the stiffener moduli of elasticity will now be taken as published design values: solid-sawn, $1.1\text{D}4 \text{ N/mm}^2$ ($1.6\text{D}6 \text{ lb/in}^2$); parallel-chord-truss, $1.1\text{D}4 \text{ N/mm}^2$ ($1.6\text{D}6 \text{ lb/in}^2$); and I-Joist, 1.38 N/mm^2 ($2.0\text{D}6 \text{ lb/in}^2$). Additionally, the sheathing moduli of elasticity will now be taken as the model validation value averages: $E_x = 3.7\text{D}3 \text{ N/mm}^2$ ($5.4\text{D}5 \text{ lb/in}^2$), and $E_y = 4.1\text{D}3 \text{ N/mm}^2$ ($5.9\text{D}5 \text{ lb/in}^2$). As before, the stiffener-to-sheathing connections will be considered rigid, the stiffen-

ers will be spaced at 600 mm (24in) intervals, and the first six modes will be used in the response. To represent a realistic occupancy (live) load, a uniform imposed load of 240 N/m² (5 lb/ft²) has been included in the analyses. The reader is referred to Appendix E for a quick reference regarding these floors.

To compare floor performance, the velocity resulting from a time-zero unit impulse has been used. This is an accepted indicator of floor performance (Ohlsson, 1991), and has the added benefit that the time-zero response is independent of viscous damping factors. For the single span floors, where we are interested in the center-point response to a center-point time-zero unit impulse, the peak velocity will be at time-zero. For the dual span floors, consideration will be given to the center-point right-span response to a center-point left-span time-zero unit impulse. For these floors, the peak velocity will not necessarily be at time-zero; however, the time-zero response can be viewed as an indicator of velocity transmission. In summary, by considering the time-zero velocity response to a time-zero unit impulse, an accepted performance indicator can be obtained that is independent of viscous damping factors.

Table 6.1 Floor and Stiffener Dimensions Used Throughout This Chapter.
(See Appendix E for Actual Stiffener Dimensions)

Floor	Stiffener Type	Stiffener Dimensions	Floor Dimensions
A	solid-sawn	50 x 300 mm	4.88 x 4.88 m
B	parallel-chord-truss	100 x 300 mm	4.88 x 4.88 m
C	parallel-chord-truss	100 x 400 mm	4.88 x 7.32 m
D	parallel-chord-truss	100 x 500 mm	4.88 x 9.15 m
E	I-Joist	100 x 300 mm	4.88 x 4.88 m
F	I-Joist	100 x 400 mm	4.88 x 7.32 m
G	I-Joist	100 x 500 mm	4.88 x 9.15 m

6.1 Single Span Floors

The performance improvement techniques that will be considered for single span floors are: imposed mass, double stiffeners, continuous blocking, and additional sheathing. The key to the success of any of these techniques is how well they suppress the responses of the contributing modes. From preliminary analyses, it was evident that the mode shapes for the floors considered were most “flexible” in the perpendicular to stiffener direction, approximately near the mid-span. Thus, for the first three techniques, the greatest improvements in performance will be obtained by considering the mid-span locations.

6.1.1 Imposed Mass

One potential way of improving the performance of wood floors is to add mass to the system. As just mentioned, if we concentrate our efforts on reducing the mid-point responses, the greatest benefits should be seen. For this investigation, masses have been placed at the mid-span of all interior stiffeners. This is advantageous since the “line-load” will affect all of the modes considered, where load sharing need not be explicitly accounted for. Figure 6.1 shows a representation of where the masses would be imposed in practice (the area within the dotted lines indicating the location). One way in which the masses could be imposed is through the use of sheet-metal bins (Figure 6.2). Considering the practical range for these imposed weights (222 N - 445 N - 100 lb)), typical site soil (1.6D4 N/m^3 (100 lb/ft^3)) could be used as a fill material.

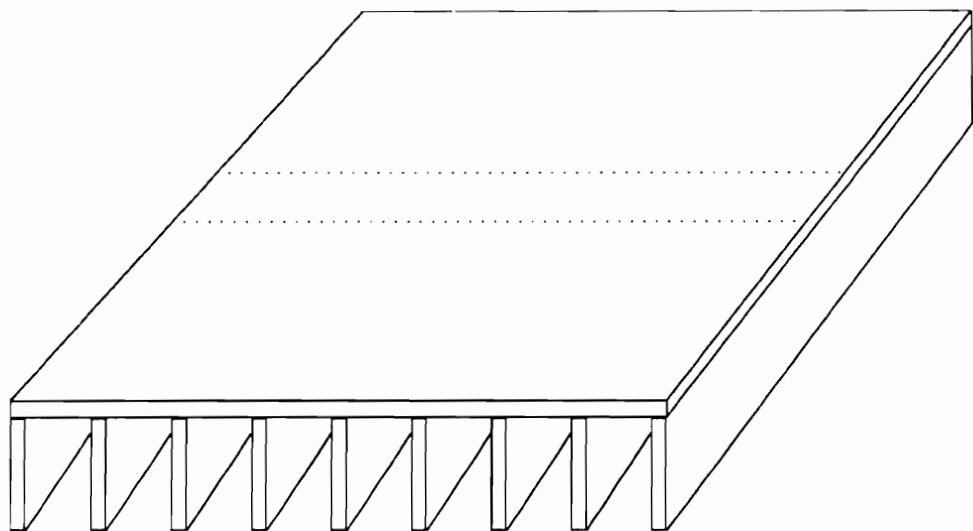


Figure 6.1 Location of Imposed Mass (Area Within the Dotted Lines).

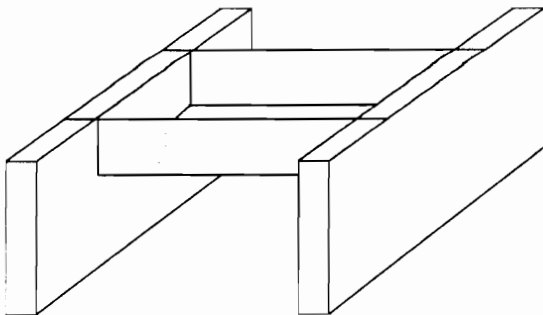


Figure 6.2 Hypothetical Bin Used to Impose Mass.

Table 6.2 shows how the natural frequencies and peak velocities compare based on imposed line-loads of 0 N, 222 N, and 445 N per bin. As expected, the natural frequencies and peak velocities are reduced as the imposed line-load increases. Furthermore, differences in peak velocity due to stiffener type are essentially non-existent. This is reasonable considering that an imposed uniform load of 240 N/m^2 has been included in the analyses to account for a service load.

Considering the 222 N line-load, the results indicate that an approximate 20 percent reduction in peak velocity occurs for the floors spanning 4.88 m. Similarly, 15 percent and 10 percent reductions occur for the floors spanning 7.32 m and 9.15 m respectively. For the 445 N line-load, the reductions are approximately double those of the 222 N line-load. These results indicate that imposed mass, applied along the center-line of the floor perpendicular to stiffener length, can improve wood floor performance. However, it should be noted, that the reduction in natural frequencies may reduce these benefits due to human annoyance of low frequency vibration.

6.1.2 Double Stiffeners

In addition to adding mass to the system, adding stiffness to the system should also improve the performance of wood floor systems. To increase the floor stiffness parallel to stiffener length, double stiffeners may be used. As with applied mass, we would expect the most benefit from double stiffeners located along the center-line (in this case, in a direction along the stiffener length rather than perpendicular to the stiffener length). Figures 6.3 to 6.5 show the cases that have been considered.

Table 6.2 Comparison of Natural Frequencies (Hz). and Peak Velocity
(millimeters/second) Based on Imposed Line-Load (N/bin).

Floor	Imposed Line-Load	Mode 1	Mode 2	Mode 3	Mode 4	Mode 5	Mode 6	Peak Velocity
A	0	15.4	16.5	18.0	20.1	23.1	27.2	53
	222	13.2	14.1	15.4	17.2	19.7	23.3	40
	445	11.7	12.5	13.7	15.3	17.4	20.4	32
B	0	14.7	15.5	16.8	18.7	21.5	25.7	53
	222	12.5	13.2	14.3	16.0	18.4	21.9	41
	445	11.1	11.7	12.6	14.1	16.2	19.2	33
C	0	9.7	10.5	11.8	13.9	17.3	22.1	37
	222	8.7	9.4	10.6	12.4	15.4	19.5	31
	445	7.9	8.6	9.6	11.3	13.9	17.5	26
D	0	8.0	8.7	10.0	12.3	15.8	20.9	30
	222	7.2	7.9	9.1	11.2	14.3	18.8	26
	445	6.7	7.3	8.4	10.3	13.2	17.1	23
E	0	15.9	16.9	18.4	20.6	23.5	27.6	53
	222	13.6	14.4	15.7	17.6	20.1	23.6	41
	445	12.0	12.7	13.9	15.5	17.7	20.7	33
F	0	11.0	11.9	13.3	15.4	18.6	23.2	36
	222	9.9	10.7	11.9	13.8	16.6	20.6	30
	445	9.0	9.7	10.8	12.5	15.1	18.6	26
G	0	9.4	10.4	11.7	13.8	17.1	21.8	29
	222	8.6	9.5	10.7	12.6	15.6	19.8	25
	445	8.0	8.8	9.9	11.6	14.3	18.1	22

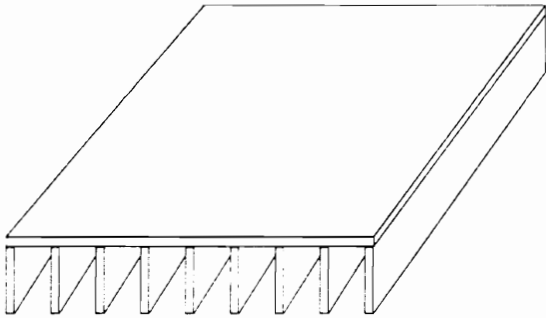


Figure 6.3 Floor With No Double Stiffeners (None).

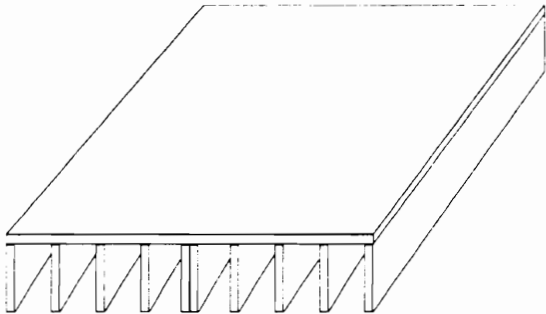


Figure 6.4 Floor With One Double Stiffener (Center).

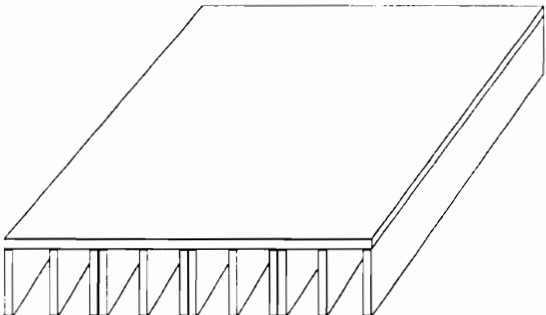


Figure 6.5 Floor With Three Double Stiffeners (Adjacent).

Table 6.3 shows how the natural frequencies and peak velocities compare based on the double stiffener locations shown in Figures 6.3 to 6.5. As expected, the natural frequencies increase, and the peak velocities decrease with the addition of double stiffeners. Similar to the results obtained for the imposed mass, differences in peak velocities due to stiffener type are minimal. Furthermore, it is evident that the Adjacent condition adds little if any performance improvement over the Center condition. This is further evidence suggesting that off-center placement does not provide the performance improvement benefits of on-center placement. For the Center condition,

an approximate 20 percent reduction in peak velocity occurs for the floors spanning 4.88 m. For the floors spanning 7.32 m and 9.15 m, an approximate 15 percent reduction in peak velocity is observed. In all cases, since the natural frequencies increase, no performance degradation is expected due to human annoyance of low frequency vibration.

6.1.3 Continuous Blocking

As discussed in the literature review, conventional blocking systems are not effective in improving the performance of wood floor systems. It would seem reasonable that the failure of these systems is due to their non-continuous nature. It would also seem reasonable that if the blocking systems were continuous, an improvement in floor performance would result. If we assume that a continuous blocking system could be achieved, then it would be of interest to determine the potential improvements in floor performance.

Considering solid-sawn and I-Joist stiffened floors, a continuous blocking system may be possible through the use of a hanger/adhesive/solid blocking system. Figure 6.6 shows how the system might be implemented. In practice, the hangers could be attached to the stiffeners first. Then, an elastomeric adhesive, or potentially rigid adhesive, could be applied to the hanger location where the solid blocking is slid down into place. After nailing the hanger to the solid blocking, and after the adhesive has had time to cure, it is believed that a rigid, or near rigid connection may be possible. By placing these “mechanisms” in a coincident row, a continuous blocking system (i.e. stiffener) would result.

Table 6.3 Comparison of Natural Frequencies (Hz). and Peak Velocity
(millimeters/second) Based on Double Stiffener Locations.

Floor	Double Stiffeners	Mode 1	Mode 2	Mode 3	Mode 4	Mode 5	Mode 6	Peak Velocity
A	None	15.4	16.5	18.0	20.1	23.1	27.2	53
	Center	16.0	16.5	18.8	20.2	23.7	27.4	42
	Adjacent	16.9	17.8	19.2	20.3	24.4	28.1	43
B	None	14.7	15.5	16.8	18.7	21.5	25.7	53
	Center	15.3	15.5	17.7	18.7	22.3	25.8	41
	Adjacent	16.5	17.1	18.0	18.7	23.1	26.7	43
C	None	9.7	10.5	11.8	13.9	17.3	22.1	37
	Center	10.2	10.5	12.5	13.9	17.7	22.1	31
	Adjacent	11.1	11.8	12.9	14.0	18.1	22.4	31
D	None	8.0	8.7	10.0	12.3	15.8	20.9	30
	Center	8.4	8.7	10.6	12.3	16.1	20.9	26
	Adjacent	9.1	9.8	10.9	12.3	16.3	21.0	26
E	None	15.9	16.9	18.4	20.6	23.5	27.6	53
	Center	16.6	16.9	19.4	20.6	24.3	27.7	41
	Adjacent	18.0	18.7	19.8	20.7	25.1	28.6	42
F	None	11.0	11.9	13.3	15.4	18.6	23.2	36
	Center	11.6	11.9	14.0	15.4	19.1	23.3	29
	Adjacent	12.5	13.3	14.4	15.5	19.6	23.7	30
G	None	9.4	10.4	11.7	13.8	17.1	21.8	29
	Center	9.9	10.4	12.3	13.8	17.4	21.9	24
	Adjacent	10.6	11.5	12.7	13.8	17.8	22.0	24

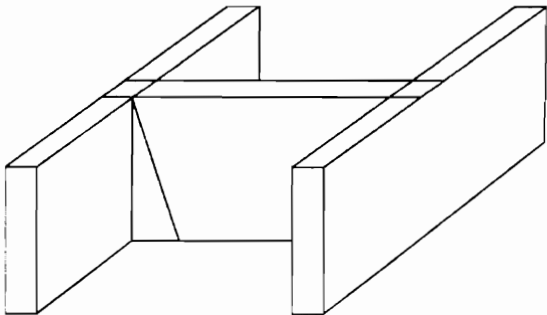


Figure 6.6 Hypothetical Continuous Blocking System.

Table 6.4 shows how the natural frequencies and peak velocities compare based on the number of rows of continuous blocking. For each floor, one row of continuous blocking corresponds to mid-span placement, perpendicular to stiffener span. For the floors spanning 4.88 m, two rows of continuous blocking correspond to quarter-span placement, perpendicular to stiffener span. For the floors spanning more than 4.88 m, two rows of continuous blocking correspond to an approximate third-span placement, perpendicular to stiffener span. In all cases, it has been assumed that the solid blocking properties are equivalent to those of the stiffeners.

Table 6.4 Comparison of Natural Frequencies (Hz), and Peak Velocity
(millimeters/second) Based on Rows of Continuous Blocking.

Floor	Continuous Blocking	Mode 1	Mode 2	Mode 3	Mode 4	Mode 5	Mode 6	Peak Velocity
A	0	15.4	16.5	18.0	20.1	23.1	27.2	53
	1	18.0	31.0	44.4	45.0	45.2	46.1	23
	2	18.0	31.0	44.6	45.7	47.3	49.5	43
E	0	15.9	16.9	18.4	20.6	23.5	27.6	53
	1	18.4	27.6	35.7	40.7	40.9	42.2	22
	2	18.4	27.7	35.9	40.9	42.0	42.6	43
F	0	11.0	11.9	13.3	15.4	18.6	23.2	36
	1	14.3	22.8	28.8	30.6	31.6	32.6	13
	2	15.7	27.7	32.5	37.3	38.1	40.5	27
G	0	9.4	10.4	11.7	13.8	17.1	21.8	29
	1	13.3	21.3	26.3	26.8	27.7	29.1	10
	2	15.4	28.1	30.2	30.6	36.2	39.8	27

The results in Table 6.4 indicate as expected that the natural frequencies increase, and the peak velocities decrease when continuous blocking is used. As with the techniques discussed earlier, differences in peak velocity based on stiffener type

are negligible. Although peak velocities are reduced using two off-center rows of continuous blocking, the largest reductions are apparent when using one on-center row of continuous blocking. Specifically, for the floors spanning 4.88 m, an approximate 55 percent reduction in peak velocity is obtained using one on-center row of continuous blocking. For the floors spanning longer than 4.88 m, an approximate 65 percent reduction in peak velocity is observed. In all cases, since the natural frequencies increase, no performance degradation is expected due to human annoyance of low frequency vibration.

6.1.4 Additional Sheathing

While the previous three performance improvement techniques were concerned with placement along discrete lines, additional sheathing is concerned with placement over the entire floor. Given that the typical design calls for an 18 mm (23/32 in) thickness, it is believed that 25 mm (1 in) and 38 mm (1.5 in) thicknesses represent reasonable design alternatives. By evaluating the results due to these three sheathing thicknesses, it will be possible to determine whether additional sheathing can improve wood floor performance.

Table 6.5 shows how the natural frequencies and peak velocities compare based on sheathing thickness. As expected, the peak velocities decrease as the sheathing thickness increases, where differences in peak velocity based on stiffener type are negligible. Interestingly, as the sheathing thickness increases, the fundamental frequencies for the parallel-chord-truss and I-Joist floors decrease while all other natural frequencies increase. These reductions in fundamental frequency are probably the result of a small relative stiffness increase in the stiffener direction that is unable to

compensate for the increase in mass associated with the sheathing.

Table 6.5 Comparison of Natural Frequencies (Hz), and Peak Velocity
(millimeters/second) Based on Sheathing Thickness (mm).

Floor	Sheathing Thickness	Mode 1	Mode 2	Mode 3	Mode 4	Mode 5	Mode 6	Peak Velocity
A	18	15.4	16.5	18.0	20.1	23.1	27.2	53
	25	15.8	17.0	19.2	22.7	28.0	35.6	49
	38	16.1	17.9	21.9	28.8	39.2	52.3	43
B	18	14.7	15.5	16.8	18.7	21.5	25.7	53
	25	14.6	15.7	17.8	21.3	26.7	34.5	50
	38	14.4	16.2	20.3	27.6	38.3	39.2	43
C	18	9.7	10.5	11.8	13.9	17.3	22.1	37
	25	9.6	10.7	13.0	17.0	23.1	26.8	34
	38	9.4	11.4	16.1	24.2	26.0	28.6	19
D	18	8.0	8.7	10.0	12.3	15.8	20.9	30
	25	7.8	8.9	11.3	15.6	21.7	22.0	27
	38	7.7	9.8	14.8	21.0	23.2	23.4	15
E	18	15.9	16.9	18.4	20.6	23.5	27.6	53
	25	15.8	17.1	19.5	23.2	28.6	36.2	49
	38	15.5	17.7	22.1	29.3	39.2	39.8	43
F	18	11.0	11.9	13.3	15.4	18.6	23.2	36
	25	10.9	12.1	14.4	18.3	24.1	29.9	33
	38	10.8	12.8	17.3	25.1	29.0	31.6	19
G	18	9.4	10.4	11.7	13.8	17.1	21.8	29
	25	9.3	10.6	12.8	16.8	22.8	26.2	26
	38	9.2	11.2	15.9	23.9	25.3	27.5	15

For the floors spanning 4.88 m, an approximate 6 percent and 20 percent reduction in peak velocity is obtained using 25 mm and 38 mm sheathing respectively. For the floors spanning longer than 4.88 m, an approximate 8 percent and 50 percent reduction in peak velocity is obtained when using 25 mm and 38 mm sheathing respectively. Considering the reduction in fundamental frequencies for the parallel-chord-truss and

I-Joist floors, it is possible that performance degradation may result due to human annoyance of low frequency vibration.

6.1.5 Summary

Four performance improvements techniques have been investigated for single span floors. The results indicate that all are effective in reducing the peak center-point velocity in response to a center-point time-zero unit impulse. The largest improvement in floor performance was achieved using a single row of continuous blocking placed mid-span, perpendicular to stiffener span. This was to be expected since wood floors are most “flexible” in the perpendicular to stiffener direction. To a lesser extent, the use of a center double stiffener also improved the floor performance. In each of these cases, where additional stiffness was added to the system, off-center placement was shown to produce less desirable performance benefits than on-center placement. This finding was also to be expected since for a center-point excitation, regions of high modal activity will generally extend from the center-point both parallel and perpendicular to stiffener span.

For the cases where significant mass was added to the system (imposed mass and additional sheathing), a reduction in fundamental frequencies was evident. Since performance degradation may result due to human annoyance of low frequency vibration, these two techniques should be used with caution.

6.2 Dual Span Floors

In typical wood construction, dual span floors are common. In general, the interior support may arise from a beam, wall, or wall/partition. For these types of floors,

two performance improvement techniques have been considered: beam supports and rotationally resistant supports. In all cases, it is sought to reduce the right-span center-point response resulting from a left-span center-point unit impulse. Furthermore, in all cases, the interior support has been located at the floor mid-span.

6.2.1 Beam Supports

In many instances, beams provide the interior support for a dual span floor. These supports may either be single span or part of a multi-span beam. For this investigation, only single span beam supports have been evaluated. Figure 6.7 shows how a typical interior beam support might be implemented. In common practice, the supporting beams generally consist of four, 50 mm x 250 mm (2 in x 10 in) or 50 mm x 300 mm (2 in x 12 in) nail laminated solid-sawn members; or equivalently, 150 mm x 250 mm (6 in x 10 in) or 150 mm x 300 mm (6 in x 12 in) sections. In evaluating the floor response with regard to these two common supporting beam sections, it will be possible to determine whether an increase in supporting beam section can be used to improve the performance of dual span floors.

With regard to the floors spanning 9.15 m, Table 6.6 indicates how the natural frequencies, time-zero velocity, and peak velocity compare based on the supporting beam section. Since the time-zero velocities do not correspond to the peak velocities for dual span floors with interior beam supports, both velocity indicators have been included. Differences between the velocity indicators are due to the beam-floor interaction that enhances higher mode activity.

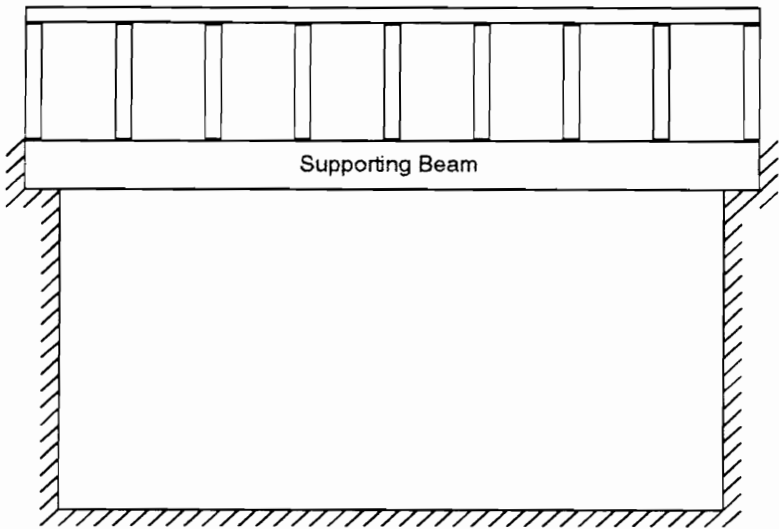


Figure 6.7 View of Interior Supporting Beam.

Table 6.6 Comparison of Natural Frequencies (Hz), Right-Span Time-Zero Velocity (millimeters/second) and Peak Velocity (millimeters/second) Based on Supporting Beam Section (millimeters).

Floor	Beam Section	Mode 1	Mode 2	Mode 3	Mode 4	Mode 5	Mode 6	Time-Zero Velocity	Peak Velocity
D	150x250	9.8	19.6	22.2	23.3	24.9	25.1	-5.1	-11.1
	150x300	11.0	21.5	22.2	23.3	24.9	25.8	-4.7	-12.2
G	150x250	11.0	21.5	26.8	27.7	28.6	29.0	-5.2	-9.9
	150x300	12.1	24.1	26.8	27.7	29.0	29.7	-4.9	-10.9

Figures 6.8 and 6.9 show the right-span center-point velocity time-histories resulting from left-span center-point unit impulses when a viscous damping factor of 0.06 has been specified to all modes. From these Figures, it is clear that peak velocities increase as a result of the larger interior beam section. Thus, contrary to expectation, increasing the supporting beam section does not necessarily improve the performance of dual span floors. Based on these results, it is recommended that interior beam supports continue to be designed on static a basis, since increasing the section has not been shown to improve vibrational performance.

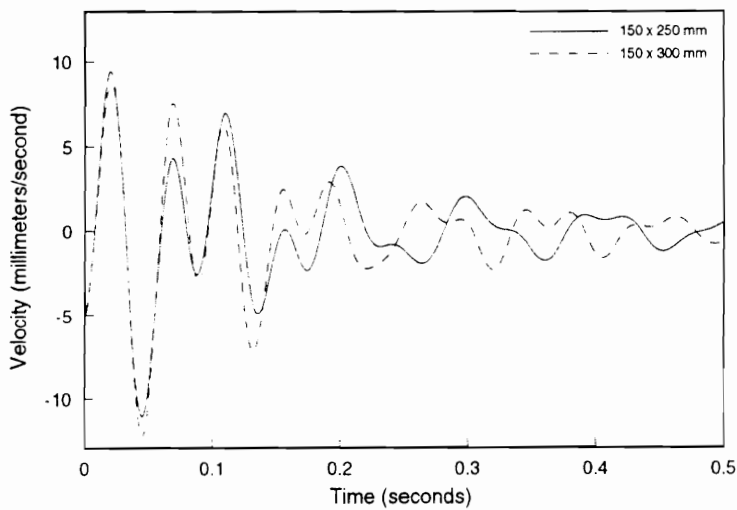


Figure 6.8 Floor D Comparison of Velocity Time-Histories Based on Supporting Beam Section Size.

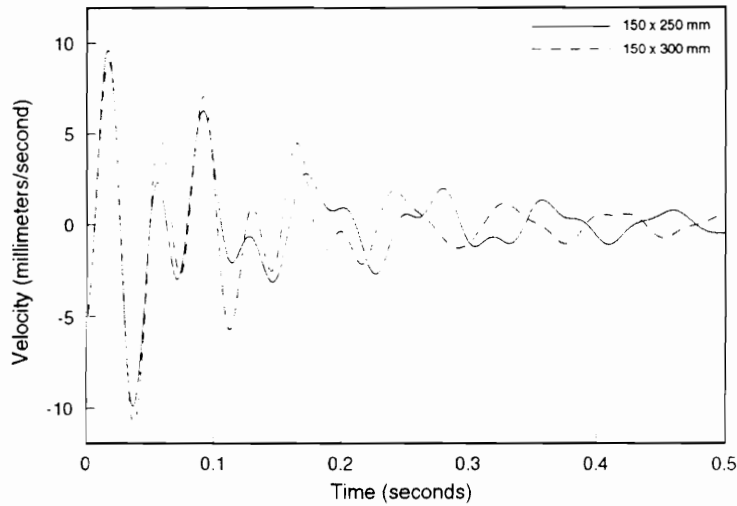


Figure 6.9 Floor G Comparison of Velocity Time-Histories Based on Supporting Beam Section Size.

6.2.2 Rotationally Resistant Supports

In many cases, the interior supports used in wood construction are of the wall, wall/partition variety. In the case of an interior supporting wall, Figure 6.10 provides a graphical representation. Assuming that the wall has infinite vertical stiffness, the wall can be represented in boundary condition terms as an interior simple support (where the vertical translation is restricted). Figure 6.11 shows a graphical representation of an interior supporting wall/partition (where the arrow in Figure 6.11 refers to the load bearing nature of the wall/partition). Given that an adequate connection has been made between the top plate of the supporting wall and the sole plate of the wall/partition, a rotational resistance may develop when either span is loaded.

In boundary condition terms, this situation can be represented by restricting vertical translation and adding a rotational spring (as viewed in Figure 6.12). In practice, the connection may be possible through the use of tie rods (Figure 6.13), or some other mechanism.

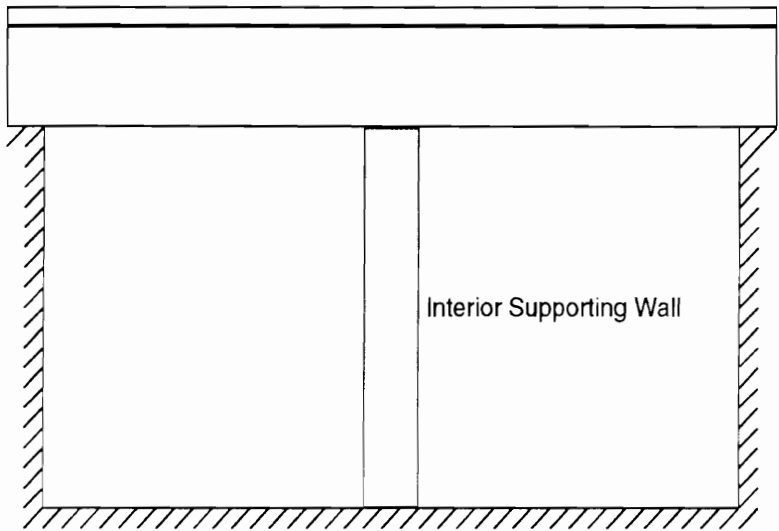


Figure 6.10 Floor with Interior Supporting Wall.

To compare the floor performance based on wall/partition rotational resistance, three spring stiffnesses have been chosen to span a practical value range: 0 Nm/rad (0 lb-in/rad), 1.0×10^3 Nm/rad (1.75×10^5 lb-in/rad), and 1.0×10^4 Nm/rad (1.75×10^6 lb-in/rad). These values have been specified with knowledge of Chui and Smith's (1990) findings that end clamped wooden beams generally have rotational spring stiffnesses between 10^3 Nm/rad and 10^6 Nm/rad. Table 6.7 compares how the natural frequencies, and peak velocity compare based on the three stiffness values. As expected, the natural frequencies increase with the addition of wall/partition spring stiffness.

However, the results also indicate that the rotational resistance of the wall/partition does not enhance the performance of the dual span floors investigated. The slight increase in peak velocity as rotational resistance is added is due to the slight increase in natural frequencies. From these results, it is apparent that within the practical limits of wall/partition rotational resistance, improvements in floor performance will not be achieved.

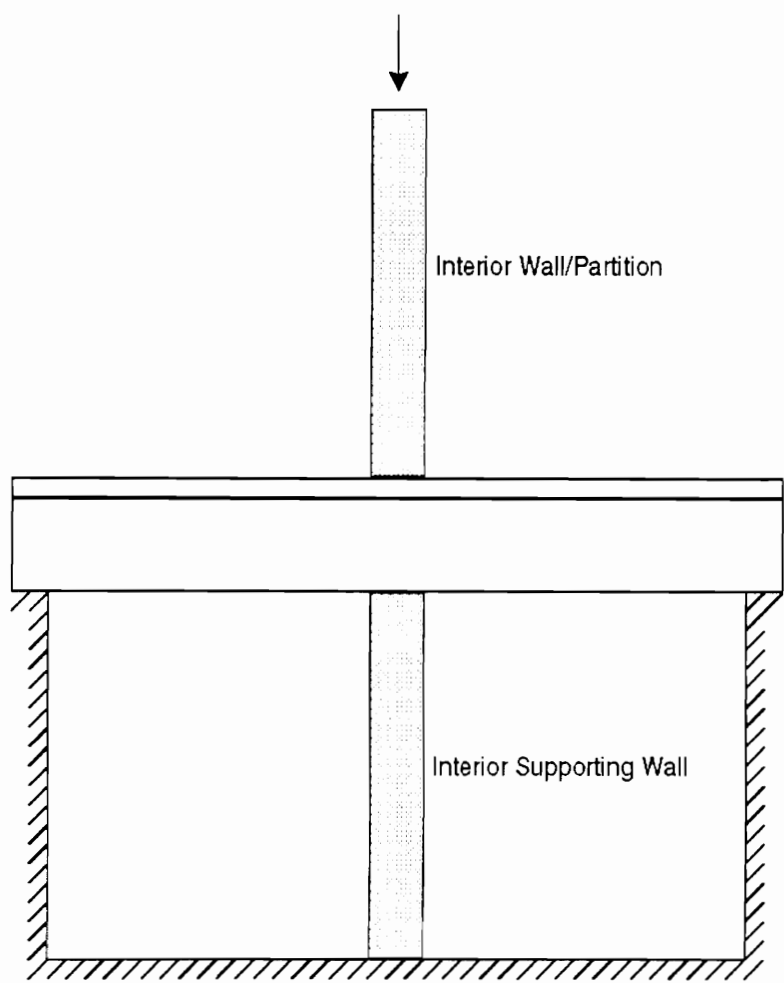


Figure 6.11 Floor with Interior Wall/Partition Support.

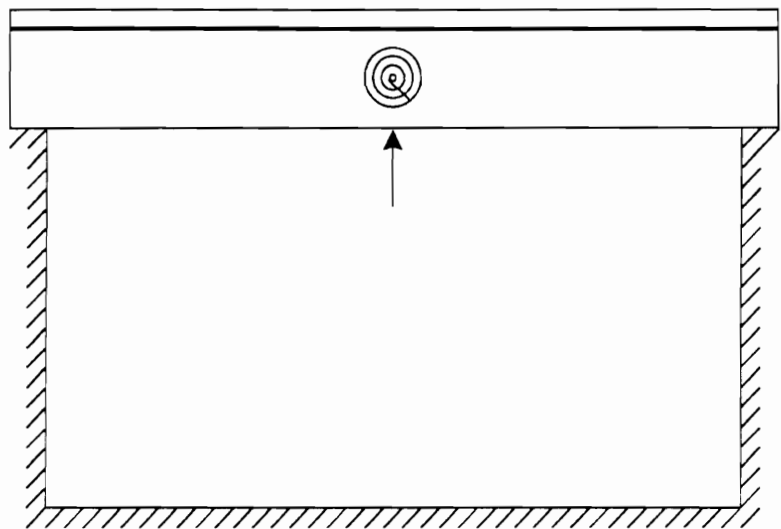


Figure 6.12 Boundary Condition Equivalent of Figure 6.11.

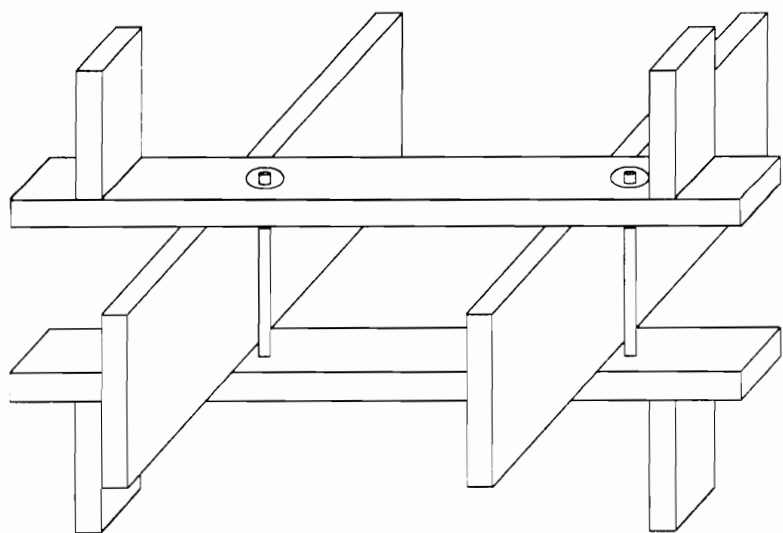


Figure 6.13 Hypothetical Tie-Rod System Used to Create an Adequate Interior Support Connection (Minus Sheathing for Clarity).

Table 6.7 Comparison of Natural Frequencies (Hz), and Right-Span Peak Velocity (millimeters/second) Based on Center-Support Rotational Stiffness (Nm/rad).

Floor	Rotational Stiffness	Mode 1	Mode 2	Mode 3	Mode 4	Mode 5	Mode 6	Peak Velocity
D	0	22.2	23.3	24.1	24.9	25.3	26.8	-8.8
	1.0D3	22.2	23.3	24.1	24.9	25.3	26.8	-8.9
	1.0D4	22.4	23.4	24.1	25.0	25.3	26.9	-9.0
G	0	26.8	27.7	29.0	29.5	30.4	30.8	-8.4
	1.0D3	26.9	27.8	29.1	29.5	30.4	30.9	-8.4
	1.0D4	27.0	27.9	29.2	29.5	30.4	30.9	-8.5

6.2.3 Summary

Two performance improvement techniques have been investigated for dual span floors. Within the practical limits of design, increases in beam support section and wall/ partition rotational resistance do not improve floor performance. However, by replacing an interior beam support with a wall support, improvements in performance may result. Table 6.8 compares how the natural frequencies, and peak velocity compare based on a 150 mm x 250 mm (6 in x 10 in) supporting beam section and an interior wall support. It is evident from Table 6.8 that reductions in peak velocity are possible when an interior wall is substituted for an interior beam support. In all of the cases presented for dual span floors, since the natural frequencies increase when the techniques are applied, no performance degradation is expected due to human annoyance of low frequency vibration.

Table 6.8 Comparison of Natural Frequencies (Hz) and Right-Span Peak Velocity (millimeters/second) Based on Interior Support Type.

Beam: 150 mm x 250 mm (6 in x 10 in)

Floor	Interior Support	Mode 1	Mode 2	Mode 3	Mode 4	Mode 5	Mode 6	Peak Velocity
D	Beam	9.8	19.6	22.2	23.3	24.9	25.1	-11.1
	Wall	22.2	23.3	24.1	24.9	25.3	26.8	-8.8
G	Beam	11.0	21.5	26.8	27.7	28.6	29.0	-9.9
	Wall	26.8	27.7	29.0	29.5	30.4	30.8	-8.4

6.3 Summary

Six performance improvement techniques have been investigated for wood floor systems, where performance has been measured by considering peak velocity resulting from a time-zero unit impulse. For the single span floors discussed, it was shown that imposed mass, double stiffeners, continuous blocking, and additional sheathing can be used to improve floor performance. However, imposed mass and additional sheathing should be used with caution since reductions in natural frequencies may result where performance degradation is possible due to human annoyance of low frequency vibration.

With regard to the dual span floors discussed, it was shown that within the practical limits of design, increases in beam support section and wall/partition rotational resistance do not improve floor performance. However, substituting a wall support for a beam support will improve floor performance. Since natural frequencies increase due to the implementation of either technique, no performance degradation is expected due to human annoyance of low frequency vibration.

Chapter 7

Tying Research to Practice

7.1 Introduction

To bridge the gap between research results and practice, a design example will be discussed that draws on the knowledge gained from the performance improvement investigation. Since design acceptability is ultimately predicated on an underlying design criterion, a design criterion must be chosen. Although there are several design criteria to choose from, Ohlsson's (1991) criterion has been chosen based on merit.

7.2 Design Example

In this example, a designer in the U.S.A. is responsible for ensuring the vibrational serviceability of a 4.88 m x 4.88 m (16 ft x 16 ft) floor system. Considering a 1400 N/m² (40 lb/ft²) live load, it is found that 50 mm x 300 mm (2 in x 12 in) solid-sawn stiffeners can be used to ensure the code requirement of limiting the live-load deflection to SPAN/360. Unfortunately, since this requirement does not address dynamic response, an additional design check is desired that specifically accounts for vibrational serviceability. In complying with Ohlsson's (1991) design criterion, the

following must be satisfied:

1. The fundamental frequency must be greater than 8 Hz.
2. The static deflection resulting from a static 1 kN (225 lb) center-point concentrated force must be less than 1.5 mm (0.059 in).
3. The maximum impulse velocity resulting from a time-zero unit impulse must be less than $100^{(f\zeta-1)}m/s$, where f is the fundamental frequency, and ζ is a viscous damping factor.

Although Ohlsson (1991) recommends using a viscous damping factor of 0.01, a viscous damping factor of 0.02 appears justified considering the experimental results obtained by Li (1993), Stark (1993), Steiss (1994), Johnson (1994), and Shue (1995). In order to evaluate this criterion, the designer chooses to use the model developed in this dissertation, which allows all three requirements to be addressed in the same computer run.

Using the same base design as found in Floor A of the Performance Improvement Investigation chapter, the model results show:

- Fundamental Frequency: 15.4 Hz
- Static Deflection: 1.13 mm
- Maximum Impulse Velocity: 0.053 m/s

Using a fundamental frequency of 15.4 Hz, and a viscous damping factor of 0.02, the maximum allowable velocity ($100^{(f\zeta-1)}m/s$) is 0.041 m/s. Although the first two

design requirements are satisfied, since the calculated impulse velocity is greater than the allowable impulse velocity, the design fails.

Fortunately, the designer knows that improvements in floor performance can be achieved using the methods discussed in this dissertation. More importantly, he or she knows where to properly make the modifications to maximize the performance improvement. For completeness, the designer chooses to evaluate imposed load, double stiffeners, continuous blocking, and additional sheathing. It should be noted that the static deflection will only benefit from these techniques, and thus it only needs to be evaluated for the base design.

Considering imposed load located along the floor center-line perpendicular to stiffener length, the results indicate that for this particular design, imposed load can not be used to satisfy the chosen design criterion.

1. 222 N (50 lb) line-load

- Fundamental Frequency: 13.2 Hz
- Maximum Impulse Velocity: 0.040 m/s
- Maximum Allowable Impulse Velocity: 0.034 m/s

2. 445 N (100 lb) line-load

- Fundamental Frequency: 11.7 Hz
- Maximum Impulse Velocity: 0.032 m/s
- Maximum Allowable Impulse Velocity: 0.029 m/s

Considering the use of a Center double stiffener, the results indicate that for this particular design, the use of a Center double stiffener can be used to satisfy the chosen design criterion.

1. Center double stiffener

- Fundamental Frequency: 16.0 Hz
- Maximum Impulse Velocity: 0.042 m/s
- Maximum Allowable Impulse Velocity: 0.044m/s

Considering the use of a single row of continuous blocking located along the floor center-line perpendicular to stiffener length, the results indicate that for this particular design, the use of the continuous blocking can be used to satisfy the chosen design criterion.

1. Single row of continuous Blocking

- Fundamental Frequency: 18.0 Hz
- Maximum Impulse Velocity: 0.023 m/s
- Maximum Allowable Impulse Velocity: 0.052m/s

Considering the use of additional sheathing, the results indicate that for this particular design, doubling the sheathing thickness can not be used to satisfy the chosen design criterion.

1. Doubling the sheathing thickness

- Fundamental Frequency: 16.1 Hz

- Maximum Impulse Velocity: 0.049 m/s
- Maximum Allowable Impulse Velocity: 0.044m/s

Based on these results, the designer has the choice of satisfying the chosen design criterion through the use of either a center double stiffener or continuous blocking system. It should be noted that any combination of the described methods can also be evaluated.

Chapter 8

Conclusions and Recommendations

8.1 Conclusions

This study investigated wood floor systems constructed with solid-sawn joists, I-Joists, and parallel-chord-trusses. No attempt was made to consider allowable notches or allowable holes in the joist products. Based on the information contained in this document, the following conclusions can be drawn for the floors investigated:

1. The assumption of rigid sheathing-to-stiffener connections is justified when predicting the vibrational response of wood floor systems if an elastomeric adhesive equivalent to Franklin Titebond is used.
2. For single span floors under an imposed uniform service load of 240 N/m^2 (5 lb/ft^2), when considering the peak center-point velocity resulting from a center-point time-zero unit impulse:
 - (a) Differences in peak velocity due to stiffener type (solid-sawn, parallel-chord-truss, and I-Joist) are negligible.

- (b) By imposing mass along the center-line perpendicular to stiffener length, improvements in floor performance (i.e. reductions in peak velocity) can be achieved (Table 8.1).
- (c) By implementing a double stiffener along the center-line parallel to stiffener length, improvements in floor performance (i.e. reductions in peak velocity) can be achieved (Table 8.2).
- (d) By placing a continuous blocking system along the center-line perpendicular to stiffener length, improvements in floor performance (i.e. reductions in peak velocity) can be achieved (Table 8.3).
- (e) By applying additional sheathing over the entire floor, improvements in floor performance (i.e. reductions in peak velocity) can be achieved (Table 8.4).
- (f) Imposed mass and additional sheathing should be used with caution since reductions in natural frequencies may result where performance degradation is possible due to human annoyance of low frequency vibration.
- (g) Considering the use of double stiffeners and continuous blocking, since natural frequencies increase, no performance degradation is expected due to human annoyance of low frequency vibration.
- (h) Considering the use of double stiffeners and continuous blocking, off-center placement is not as effective as on-center placement in improving floor performance.

3. For dual span floors under an imposed uniform service load of 240 N/m^2 (5 lb/ft^2), when considering the peak center-point right-span velocity resulting from a center-point left-span time-zero unit impulse:
 - (a) Performance improvements (i.e. reductions in peak velocity) should not be expected when larger beam sections are used to center-support the floor.
 - (b) Performance improvements (i.e. reductions in peak velocity) should not be expected when rotational resistance is added to a center-support wall/partition.
 - (c) Performance improvements (i.e. reductions in peak velocity) can be expected when a center-support wall is used in place of a center-support beam.
 - (d) Considering the use of either larger beam sections or wall/partition rotational resistance, since natural frequencies increase, no performance degradation is expected due to human annoyance of low frequency vibration.

8.2 Recommendations

Conclusions concerning performance improvement are intended to be used by designers as complimentary information. For example, current methods or criteria should be used to obtain a base design. If it is found that the performance of the floor design is inadequate, or if enhanced performance is desired, the appropriate techniques discussed can be implemented.

Table 8.1 Approximate Percent Reductions in Peak Velocity (millimeters/second)

Based on Center-Line Imposed Line-Load.

Floor Span	Imposed Line-Load	Approximate Reduction In Peak Velocity (%)
4.88 m	222 N	20
	445 N	40
7.32 m	222 N	15
	445 N	30
9.15 m	222 N	10
	445 N	20

Table 8.2 Approximate Percent Reductions in Peak Velocity (millimeters/second)

Based on Center-Line Double Stiffener Implementation.

Floor Span	Approximate Reduction In Peak Velocity (%)
4.88 m	20
7.32 m	15
9.15 m	15

Table 8.3 Approximate Percent Reductions in Peak Velocity (millimeters/second)

Based on Center-Line Continuous Blocking System Implementation.

Floor Span	Approximate Reduction In Peak Velocity (%)
4.88 m	55
7.32 m	65
9.15 m	65

Table 8.4 Approximate Percent Reductions in Peak Velocity (millimeters/second)
Based on Additional Sheathing (Base Thickness: 18 mm).

Floor Span	Sheathing Thickness	Approximate Reduction In Peak Velocity (%)
4.88 m	25 mm	6
	38 mm	20
7.32 m	25 mm	8
	38 mm	50
9.15 m	25 mm	8
	38 mm	50

Bibliography

- [1] Allen. D.E.. and J.H. Rainer. 1976. "Vibration Criteria for Long-Span Floors." *Canadian Journal of Civil Engineering*. 3(2):165-173.
- [2] Allen. D.E.. J.H. Rainer, and G. Pernica. 1985. "Vibration Criteria For Assembly Occupancies." *Canadian Journal of Civil Engineering*. 12:617-623.
- [3] Allen. D.E. 1990. "Floor Vibrations From Aerobics." *Canadian Journal of Civil Engineering*. 17:771-779.
- [4] Allen. D.L. 1974. "Vibrational Behavior of Long-Span Floor Slabs." *Canadian Journal of Civil Engineering*. 1:108-115.
- [5] Allen. D.L.. and J.C Swallow. 1975. "Annoying Floor Vibrations - Diagnosis and Therapy." *Journal of Sound and Vibration*. 3:12-17.
- [6] Atherton. G.H., A. Polensek, and S.E Corder. 1976. "Human Response to Walking and Impact Vibration of Wood Floors." *Forest Products Journal*. 26(10):40-47.
- [7] Becker. R. 1980. "Simplified Investigation Of Floors Under Foot Traffic." *Journal of Structural Engineering*. 106(11):2221-2234.

- [8] British Standards Institute. 1984. *Code of Practice for the Structural Use of Timber: Part 2. Standard 5268*. London, England.
- [9] Bulliet, W.M. 1987. "Markov Model For Wood Structural Systems." *ASCE Journal of Structural Engineering*. 113(9):2023-2031.
- [10] Bulliet, W.M. 1991. "Reliability-Based Design Of Wood Structural Systems." *International Timber Engineering Conference*, TRADA Technology Ltd., High Wycombe, U.K. II:2.417-2.423.
- [11] Chui, Y.H. 1986. "Vibrational Performance Of Timber Floors And The Related Human Discomfort Criteria." *Journal of the Institute of Wood Science*. 10(5):183-188.
- [12] Chui, Y.H. 1987. "Vibrational Performance Of Wooden Floors In Domestic Dwellings." *Dissertation accepted in partial fulfillment of PH.D.*, Brighton Polytech.
- [13] Chui, Y.H. 1988. "Evaluation Of Vibrational Performance Of Light-Weight Wooden Floors." *International Conference on Timber Engineering*. Forest Products Research Society, Madison, Wisconsin. I:707-715.
- [14] Chui, Y.H., and L.H. Hu. 1990. "Dynamic Response Of Floors Built With Wood I-Joists." *Proceedings For IURFO Timber Engineering Group*, Saint John, New Brunswick.

- [15] Chui, Y.H. 1990. "Influence Of Rotary Inertia, Shear Deformation And Support Condition On Natural Frequencies Of Wooden Beams." *Wood Science and Technology* 24: 233-245.
- [16] Chui, Y.H., and I. Smith. 1991. "Dynamic Response Of Light-Weight Floors With Wood I-Joists." *International Timber Engineering Conference*, TRADA Technology Ltd., High Wycomb, U.K. IV:4.378-4.385.
- [17] Cook, R.D., D.S. Malkus, and M.E. Plesha. 1989. *Concepts And Applications Of Finite Element Analysis*. 3rd ed., John Wiley and Sons.
- [18] Dawson, P.R., and J.R. Goodman. 1976. "Variability Simulations of Wood Joist Floor Systems." *Wood Science*. 8(4):242-251.
- [19] DeBonis, A.L. 1980. "Stochastic Simulation Of Wood Load-Sharing Systems." *ASCE Journal of Structural Engineering*. 106(2):393-410.
- [20] Dong, C.C., and R.H. Hoyle. 1976. "Elastomeric Adhesive Properties - Shear Strength, Shear Modulus, Creep, and Recovery." *Wood and Fiber*. 8(2):98-106.
- [21] Ellingwood, B., and A. Tallin. 1984. "Structural Serviceability: Floor Vibrations." *ASCE Journal of Structural Engineering*. 110(2):401-417.
- [22] Erki, M.A. 1991. "Modelling the load-slip behavior of timber joints with mechanical fasteners." *Canadian Journal of Civil Engineering*. 18:607-616.
- [23] Filliatrault, A., B. Folz, and R.O. Foschi. 1990. "Finite-Strip Free-Vibration Analysis Of Wood Floors." *ASCE Journal of Structural Engineering*. 116(8):2127-2143.

- [24] Folz, B., and R.O. Foschi. 1989. "Reliability-Based Design Of Wood Structural Systems." *ASCE Journal of Structural Engineering*. 115(7):1666-1680.
- [25] Foschi, R.O. 1974. "Load-Slip Characteristics of Nails." *Wood Science*. 7(1):69-76.
- [26] Foschi, R.O. and T. Bonac. 1977. "Load-Slip Characteristics for Connections With Common Nails." *Wood Science*. 9(3):118-123.
- [27] Foschi, R.O. 1982. "Structural Analysis Of Wood Floor Systems." *ASCE Journal of Structural Engineering*. 108(7):1557-1574.
- [28] Foschi, R.O. 1985. "Wood Floor Behavior: Experimental Study." *ASCE Journal of Structural Engineering*. 111(11):2497-2508.
- [29] Foschi, R.O., and A. Gupta. 1987. "Reliability of Floors Under Impact Vibration." *Canadian Journal of Civil Engineering*. 14:683-689.
- [30] Goodman, J.R., and E.P. Popov. 1968. "Layered Beam Systems With Interlayer Slip." *ASCE Journal of Structural Engineering*. 94(11):2535-2547.
- [31] Goodman, J.R. 1969. "Layered Wood Systems With Interlayer Slip." *Wood Science*. 1(3):148-158.
- [32] Goodman, J.R., M.D. Vanderbilt, M.E. Criswell, and J. Bodig. 1974. "Composite and Two-Way Action in Wood Joist Floor Systems." *Wood Science*. 7(1):25-33.
- [33] Grether, W.F. 1971. "Vibration and Human Performance." *Human Factors*. 13(3):203-216.

- [34] Gromola, S.D., D.J. Sharp, and R.C. Moody. 1991. "LRFD Concepts For Wood Systems." *ASCE 9th Structures Congress Proceedings*. pp 243-246.
- [35] Gupta, A.K., and P.S. Ma. 1977. "Error In Eccentric Beam Formulation." *International Journal For Numerical Methods In Engineering* 11:1473-1483.
- [36] Hoyle, R.J. 1976. "Designing Wood Structures Bonded With Elastomeric Adhesives." *Forest Products Journal*. 26(3):28-34.
- [37] Hoyle, R.H., and J.K. Hsu. 1978. "Shear Strength and Shear Modulus of an Elastomeric Adhesive Subject to Repeated Stress." *Wood Science*. 11(2):65-68.
- [38] Hoyle, R.H. 1988a. "Design of Wood Shear Joints Fastened With Nails and Structural Elastomeric Adhesives." *International Conference On Timber Engineering*. Forest Products Research Society, Madison, Wisconsin. Vol I. pp 38-45.
- [39] Hoyle, R.H. 1988b. "An Evaluation Of A Design Method For Wood Shear Joints Fastened With Nails And Structural Elastomeric Adhesives." Unpublished.
- [40] Hsu, J.K., and R.H. Hoyle. 1978. "Factors Affecting Measurement of Shear Modulus For an Elastomeric Construction Adhesive." *Wood Science*. 10(3):105-110.
- [41] Hu, L.J. 1990. "Vibration Analysis Of Wooden Floors By Modal Synthesis Part I: Frequency Analysis." *Proceedings For IUFRO Timber Engineering Group*. Saint John, New Brunswick.
- [42] Hu, L.J. 1992. "Prediction Of Vibration Responses Of Ribbed Plates By Modal Synthesis." *Dissertation accepted in partial fulfillment of PH.D.*, The University Of New Brunswick.

- [43] International Standards Organization (ISO). 1978. *Guide for the Evaluation of Human Exposure to Vibration. Standard 2631*. Geneva Switzerland.
- [44] Irwin. A.W. 1978. "Human Response To Dynamic Motion of Structures." *The Structural Engineer*. 9(56a):237-244.
- [45] Jizba. T.D. 1979. "Sheathing Joist Stiffness for Wood Joist Floors." *Thesis accepted in partial fulfillment of Master's of Science Degree*. Colorado State University.
- [46] Johnson. J.R. 1994. "Vibration Acceptability In Wood Floor Systems." *Thesis accepted in partial fulfillment of Master's of Science Degree*. Virginia Polytechnic Institute And State University.
- [47] Levin. E. 1975. "A Review Of Load-Sharing In Theory And Practice." *Interim Report, International Council For Building Research*, Paris.
- [48] Lenzen. K.H. 1966. "Vibration of Steel Joist-Concrete Slab Floors." *AISC Engineering Journal*. Third Quarter, pp. 133-136.
- [49] Li. X. 1993. "The Effect Of Stiffness And Mass On The Dynamic Response Of Wood Floors." *Thesis accepted in partial fulfillment of Master's of Science Degree*. Virginia Polytechnic Institute And State University.
- [50] McCutcheon. W.J. 1977. "Method For Predicting The Stiffness Of Wood-Joist Floor Systems With Partial Composite Action." *Forest Service Research Paper FPL 289*. Madison, Wisconsin.

- [51] McCutcheon, W.J., M.D. Vanderbilt, J.R. Goodman, and M.E. Criswell. 1981. "Wood Joist Floors: Effects of Joist Variability on Floor Stiffness." *Forest Service Research Paper FPL 405*, Madison, Wisconsin.
- [52] McGee, W.D., and R.H. Hoyle. 1974. "Design Method For Elastomeric Adhesive Bonded Wood Joist-Deck Systems." *Wood and Fiber*. 6(2):144-155.
- [53] McLain, T.E. 1976. "Curvilinear Load-Slip Relations In Laterally-Loaded Nailed Joints." *Dissertation accepted in partial fulfillment of Ph.D.*, Colorado State University.
- [54] Miller R.E. 1980. "Reduction Of The Error In Eccentric Beam Modelling." *International Journal For Numerical Methods In Engineering* 15:575-582.
- [55] Murray, T.M. 1981. "Acceptability Criterion for Occupant-Induced Floor Vibrations." *AISC Engineering Journal*. Second Quarter, pp. 62-70.
- [56] Murray, T.M. 1991. "Building Floor Vibrations." *AISC Engineering Journal*. Third Quarter, pp. 102-109.
- [57] National Association of Home Builders. 1961. "Bridging In Residential Floor Construction." *Report LR-6*.
- [58] National Building Code of Canada. 1990. *National Research Council Canada*. pp 388-390.
- [59] National Design Specification. 1991. *National Forest Products Association*. pp 19.

- [60] Ohlsson, S.V. 1982. "Floor Vibrations And Human Discomfort." *Dissertation accepted in partial fulfillment of PH.D.*, ISBN 91-7032-007-2, Chalmers University of Technology, Division of Steel & Timber Structures, Gothenburg, Sweden.
- [61] Ohlsson, S.V. 1984. "Springiness and Human-Induced Floor Vibrations: A Design Guide." *Swedish Council for Building Research*, Stockholm, Sweden.
- [62] Ohlsson, S.V. 1988a. "Ten Years Of Floor Vibration Research." *Paper Submitted To Symposium/Workshop On Serviceability Of Buildings*, University Of Ottawa, Canada.
- [63] Ohlsson, S.V. 1988b. "A Design Approach For Footstep-Induced Floor Vibration." *Proceedings For The International Conference On Timber Engineering*, Forest Products Research Society, Madison, Wisconsin, I:722-729.
- [64] Ohlsson, S.V. 1988c. "Stiffness Characteristics Of Wood-Joist Floors." *Proceedings For The International Conference On Timber Engineering*, Forest Products Research Society, Madison, Wisconsin, I:730-735.
- [65] Ohlsson, S.V. 1991. "Serviceability Criteria - Especially Floor Vibration Criteria." *Proceedings For The International Timber Engineering Conference*, TRADA Technology Ltd., High Wycomb, U.K. I:1.58-1.65.
- [66] Onysko, D.M. 1975. "Performance of Wood-Joist Floors: a Questionnaire Survey." *Eastern Forest Products Laboratory*, Ottawa, Report No. OPX12OE.

- [67] Onysko, D.M. 1985. "Serviceability Criteria For Residential Floors Based On A Field Study Of Consumer Response." *Forintek Canada Corporation*. Ottawa. Project No. 03-50-10-008.
- [68] Onysko, D.M. 1988. "Deflection Serviceability Criteria For Residential Floors." *Forintek Canada Corporation*. Ottawa. Project No. 43-10c-024.
- [69] Percival, D.H. 1979. "History of L/360." *Forest Products Journal*. 29(8):26-27.
- [70] Polensek, A. 1970. "Human Response to Vibration of Wood-Joist Floor Systems." *Wood Science*. 3(2):111-119.
- [71] Polensek, A., G.H. Atherton, S.E. Corder, and J.L. Jenkins. 1972. "Response of Nailed Wood-Joist Floors to Static Loads." *Forest Products Journal*. 22(9):52-61.
- [72] Polensek, A. 1975. "Damping Capacity of Nailed Wood-Joist Floors." *Wood Science*. 8(2):141-151.
- [73] Polensek, A. 1988. "Structural Damping And It's Effect On Human Response To Floor Vibrations." *Proceedings For The International Conference On Timber Engineering*. Forest Products Research Society, Madison. Wisconsin. I:746-755.
- [74] Reiher, H., and F.J. Meister. 1931. "The Effect of Vibration on People." *Forschung auf dem Gebiete des Ingenieurwesens*. 2(11):381-386. Translation: Rep. F-TS-616-RE. Air Material Command, Wright Field, Ohio (1946).

- [75] Rosowsky, D., and B. Ellingwood. 1991. "System Reliability and Load-Sharing Effects In Light-Frame Wood Construction." *ASCE Journal of Structural Engineering*. 117(4):1096-1114.
- [76] Sazinski, R.J., and M.D. Vanderbilt. 1979. "Behavior and Design of Wood Joist Floors." *Wood Science*. 11(4):209-220).
- [77] Schaefer, E.M., and M.D. Vanderbilt. 1983. "Comprehensive Analysis Methodology For Wood Floors." *ASCE Journal of Structural Engineering*. 109(7):1680-1694.
- [78] Shue, B.C . 1995. "Some Aspects Of Vibration Serviceability In Wood Floor Systems." *Thesis accepted in partial fulfillment of Master's of Science Degree*. Virginia Polytechnic Institute And State University.
- [79] Sliker, A. 1972. "Joist Deflections Simulated By a Computer Program." *Forest Products Journal*. 22(9):71-73.
- [80] Smith, I., and Y.H. Chui. 1988. "Design of Lightweight Wooden Floors To Avoid Human Discomfort." *Canadian Journal of Civil Engineering*. 15:254-262.
- [81] The Span Book. 1990. *Canadian Wood Council*.
- [82] Stark, J.W. 1993. "The Effect Of Lateral Bracing On The Dynamic Response Of Wood Floor Systems." *Thesis accepted in partial fulfillment of Master's of Science Degree*. Virginia Polytechnic Institute And State University.

- [83] Stiess, T.S. 1994. "The Effects Of Cutouts In Joists On The Vibrational Response Of Wood Floors." *Thesis accepted in partial fulfillment of Master's of Science Degree*. Virginia Polytechnic Institute And State University.
- [84] Thompson, E.G., M.D. Vanderbilt, and J.R. Goodman. 1977. "FEAFLO: A Program For The Analysis Of Layered Wood Systems." *Computers & Structures*. (7):237-248.
- [85] Timoshenko, S. and S. Woinowsky-Kreiger. 1959. *Theory Of Plates And Shells*. McGraw-Hill.
- [86] Tremblay, G.A., J.R. Goodman, and M.E. Criswell. 1976. "Analysis of Layer T-Beams With Interlayer Slip." *Wood Science*. 9(1):21-29.
- [87] Ugural, A.C. 1981. *Stresses In Plates And Shells*, McGraw-Hill.
- [88] Ungar, E.E. 1973. "The Status Of Engineering Knowledge Concerning The Damping Of Built-Up Structures." *Journal of Sound and Vibration*. 26(1):141-154.
- [89] Vanderbilt, M.D., J.R., Goodman, and M.E. Criswell. 1974. "Service And Overload Behavior Of Wood Joist Floor Systems." *ASCE Journal of Structural Engineering*. 100(1):11-29.
- [90] Vick, C.B. 1971. "Elastomeric Adhesives for Field-Gluing Plywood Floors." *Forest Products Journal*. 21(8):34-42.
- [91] Webster, A.C., and M.P. Levy. 1992. "A Case Of The Shakes". *Civil Engineering*. February 0885-7024-/92-0002-058.

- [92] Wheat, D.L., M.D. Vanderbilt, and J.R. Goodman. 1983. "Wood Floors With Nonlinear Nail Stiffness." *ASCE Journal of Structural Engineering*. 109(5):1290-1302.
- [93] Wheat, D.L., and R.C. Moody. 1984. "Predicting the Strength of Wood-Joist Floors." *Forest Service Research Paper FPL 445*. Madison, Wisconsin.
- [94] Wheat, D.L., D.S. Gromola, and R.C. Moody. 1986a. "Static Behavior Of Wood-Joist Floors At Various Limit States." *ASCE Journal of Structural Engineering*. 112(7):1677-1691.
- [95] Wheat, D.L., D.C. Shock, and L.M. Wolf. 1986b. "Nail Slip in Wood-Joist Floors." *Forest Products Journal*. 36(11/12):29-32.
- [96] Wheeler, J.E. 1982. "Prediction And Control Of Pedestrian-Induced Vibration In Footbridges." *ASCE Journal of Structural Engineering*. 108(9):2045-2065.
- [97] Wilkinson, T.L. 1972. "Analysis Of Nailed Joints With Dissimilar Members." *ASCE Journal of Structural Engineering*. 98(9):2005-2013.
- [98] Wiss, J.F., and R.A. Parmelee. 1974. "Human Perception Of Transient Vibrations." *ASCE Journal of Structural Engineering*. 100(4):773-787.
- [99] Yeh, C.T., B.J. Hartz, and C.B. Brown. 1971. "Damping Sources In Wood Structures." *Journal of Sound and Vibration*. 19(4):411-419.
- [100] Wilson, E.L., M-W Yuan, and J.M. Dickens. 1982. "Dynamic Analysis By Direct Superposition Of Ritz Vectors." *Earthquake Engineering And Structural Dynamics* 10:813-821.

- [101] Zornig, H.F., and C.B. Vick. 1974. "Methods of Nailing and Adhesive Consistency Affect the Strength of Nailed-Glued Construction Joints." *Forest Products Journal*. 24(12):17-22.

Appendix A

General Theory of Displacement Based Finite Elements

This appendix is intended to provide the reader with information concerning the derivation and construction of the system equations of motion through the use of displacement based finite elements. In the following discussion, bold letters will refer to non-scalar quantities.

A.1 Equation of Motion Generation

In analyzing continuous systems, it is necessary to generate a representative set of governing partial differential equations of motion. In obtaining the governing equations, two general approaches may be used: 1) direct, and 2) variational. Direct methods establish equilibrium, follow material laws, and ensure compatibility. Variational methods provide equivalent energy representations of the governing equations. The primary advantages of variational methods are convenience, and inherent inclusion of the natural boundary conditions. In general, the latter advantage increases the possibility of determining an accurate approximate solution since fewer boundary

conditions need be satisfied due to inclusion.

A.2 Variational Principles

In structural mechanics, the term “variational method” implies a work and energy method. By definition, work is the product of a force and displacement where both force and displacement directions are coincident. If we let F_r be a force moving through a displacement dr , the increment of work done is:

$$dW = F_r dr \quad (\text{A.1})$$

If energy is defined as the capacity to perform work, then the amount of work performed is proportional to the change in system energy (assuming that energy is neither created or destroyed). This implies that no net work is performed in moving on a closed path, that the work performed in the system is dependent on position alone, and that the system is conservative. In the case of conservative systems, dW is an exact differential of some functional (Π). This functional must be an expression that implicitly contains the governing equations of motion. For linear elastic structural components or systems, the functional can be taken as the total potential energy which corresponds to the work done in a conservative force field when moving from a fixed position to a reference position:

$$\Pi = U_i + U_e \quad (\text{A.2})$$

where: U_i = elastic strain energy, and U_e = potential energy of the external forces. This functional allows the following expression to be established:

$$dW = -d\Pi = -(dW_i + dW_e) \quad (\text{A.3})$$

where: dW_e = work performed by external forces, and dW_i = work performed by internal forces. Notice the substitution of work terms for energy terms. The equivalence of work and energy terms is due to the use of an exact differential.

If we now define virtual displacements as arbitrary, infinitesimal displacements that are compatible with system constraints and do not appreciably alter system geometry, virtual work can be expressed as:

$$\delta W = -(\delta W_i + \delta W_e) \quad (\text{A.4})$$

where: δW_i = internal virtual work, and δW_e = external virtual work. For a system in equilibrium, the virtual work is zero for all virtual displacements satisfying the system constraints where the constraint forces (i.e. friction) perform no work. This statement, the principle of virtual work, leads to the following:

$$\delta(W_i + W_e) = 0 \quad (\text{A.5})$$

which can alternatively be written for conservative systems as:

$$\delta(U_i + U_e) = 0 \quad (\text{A.6})$$

In the vast majority of cases, linear elastic structural systems are not conservative. The non-conservative nature arises from forces such as applied loads, damping, and friction. These non-conservative forces are labeled as such since they do not depend on position alone, and thus can not be derived from a functional (in this case, a potential). This means that work terms are needed to account for the non-conservative forces. Realizing that the non-conservative forces initiate external actions, and that internal potential energy is conservative for a linearly elastic material, the following

relationship can be established for non-conservative systems:

$$\delta(U_i - W_e) = 0 \quad (\text{A.7})$$

which can be written:

$$\delta(U_i + U_e^*) = 0 \quad (\text{A.8})$$

where: U_e^* is the external potential energy including non-conservative effects.

In either the conservative or non-conservative case, from calculus, we know that the first variation of a function, when set equal to zero, produces an extreme function value (stationary value). Evaluation of the second variation will show whether the stationary value is a maximum, minimum, or saddle point. In considering equations (A.6) and (A.8), we conclude that in order for equilibrium to be ensured, the total potential energy must be stationary (this is known as the principle of stationary potential energy). Furthermore, for linear elastic components or systems in equilibrium, changes in internal potential energy are always positive, which implies a minimum value of the stationary point.

In the following sections, the variational framework for theoretical development will center on seeking a minimum, stationary value of the non-conservative system potential energy:

$$\delta\Pi = \delta(U_i + U_e^*) \quad (\text{A.9})$$

A.3 Complexity

In analyzing components or structures, only elementary configurations lend themselves to closed-form solutions of the governing partial differential equation (s) of motion. For example, a uniform, arbitrarily loaded, simply supported beam can be

analyzed in closed-form. However, it may not be possible to obtain a closed-form solution for a non-uniform, arbitrarily loaded, simply supported beam. In lieu of exact solutions, we turn to approximate solutions.

Several approximate solution methods are available, including: subdomain, collocation, least squares, galerkin, and Rayleigh-Ritz. These solution methods are known as trial function methods. While the Rayleigh-Ritz method is considered a variational method, the remaining methods, in general form, fall under a class known as weighted residual methods. In trial function methods, we seek to approximate an unknown solution using a set of scaled basis functions that are problem dependent. The distinct advantage of the Rayleigh-Ritz method is that it operates on the functional (Π), as opposed to the weighted residual methods that operate on the direct formulation. This means that the Rayleigh-Ritz method trial functions need only satisfy the geometric boundary conditions, while the trial functions of the weighted residual methods need satisfy both geometric and natural (forced) boundary conditions. Since it may be difficult to find trial functions that satisfy both geometric and natural boundary conditions, the Rayleigh-Ritz method is preferred. Furthermore, in keeping with the spirit of variational principles, the Rayleigh-Ritz method will be used in all subsequent analysis.

In the classical Rayleigh-Ritz analysis, we seek a spatial displacement field $u(x)$. This displacement field can be approximated by a linear combination represented by:

$$u(x) = \sum_{i=1}^n a_i \phi_i \quad (\text{A.10})$$

where: a_i = unknown coefficients, and ϕ_i = trial functions. In this analysis, the trial functions need only be admissible, that is, trial functions that satisfy the geometric

boundary conditions and are differentiable half as many times as the order of the system. Once the functional (Π) has been cast in terms of the assumed displacement field, the principle of stationary potential energy can be utilized, so that:

$$\frac{\partial \Pi}{\partial a_i} = 0 \quad i = 1, 2, \dots, n \quad (\text{A.11})$$

Solving for the unknown coefficients, substitution into the linear combination will provide the approximated displacement field. This process has the effect of reducing an infinite-degree-of-freedom system into an n -degree-of-freedom system. In other words, a continuous problem represented by partial differential equations is replaced with a discrete problem represented by algebraic equations. Because only n terms are taken, the displacement field approximation has the effect of overestimating the functional (Π) so that a bound on the total potential energy is achieved. In the case of an elastic material, this has the implication of increasing stiffness and natural frequencies. As the number of terms increases, the stiffness and natural frequencies should monotonically approach the actual values from above.

The success of the Rayleigh-Ritz method depends on how well the trial functions represent the problem at hand. In many cases, for complex systems, trial functions that adequately represent the actual continuous situation are difficult if not impossible to determine. However, it would seem reasonable that the Rayleigh-Ritz method could be used in situations where the trial functions were valid over some known region of the continuous system. This is essentially what displacement-based finite elements try to accomplish: that is, to take a continuous system, divide it into known finite regions, and apply a Rayleigh-Ritz analysis on each finite region where the trial function limitation is not based on system complexity, but on how the trial function

is represented over the finite region. By then introducing inter-region compatibility relations, the complex system can be fully characterized by its much simpler, finite regions.

A.4 Finite Element Formulation

A.4.1 Overview

As just mentioned, displacement-based finite elements provide a vehicle for characterizing complex structural systems. The following discussion will center on finite elements that use the Rayleigh-Ritz method to minimize the total system potential energy. With external actions known, the ensuing analysis seeks to approximate the amplitude field (displacement, velocity, or acceleration).

Assume that we have divided a linear elastic, externally loaded, continuous system into several finite geometric regions where we seek to approximate the displacement field. Further assume that the finite regions are connected at locations called nodes. Applying the Rayleigh-Ritz method, we can approximate the finite region displacement field, \mathbf{u} , by writing:

$$\mathbf{u} = \mathbf{N}\mathbf{d} \quad (\text{A.12})$$

where: \mathbf{N} are trial functions, and \mathbf{d} are region nodal displacements. In finite element analysis, the trial functions are often referred to as shape functions. At this point, for clarity, we will consider the “finite regions” to be termed “finite elements”, where \mathbf{N} are shape functions, and \mathbf{d} are element nodal displacements. Continuing the formulation, the strain-displacement relation can be taken as:

$$\epsilon = \mathbf{L}\mathbf{u} \quad (\text{A.13})$$

where: \mathbf{L} is a problem dependent differential linear operator. Substituting equation (A.12) into equation (A.13) gives:

$$\epsilon = \mathbf{L}\mathbf{N}\mathbf{d} \quad (\text{A.14})$$

For convenience, let:

$$\mathbf{B} = \mathbf{L}\mathbf{N} \quad (\text{A.15})$$

The strain-displacement relation can now be expressed as:

$$\epsilon = \mathbf{B}\mathbf{d} \quad (\text{A.16})$$

Assuming no initial stress or strains, the stress-strain relation is:

$$\sigma = \mathbf{D}\epsilon \quad (\text{A.17})$$

where: \mathbf{D} is the elasticity matrix containing material properties. In a similar fashion, the shear strain-displacement relation can be taken as:

$$\gamma = \mathbf{B}_s\mathbf{d} \quad (\text{A.18})$$

where: \mathbf{B}_s will refer to the \mathbf{B} shear matrix. It is noted that \mathbf{L} will be different for ϵ and τ . The shear stress-strain relation can then described as:

$$\tau = \mathbf{D}_s\gamma \quad (\text{A.19})$$

where: \mathbf{D}_s is the shear elasticity matrix containing material properties. To take into account external actions, we may consider the effects of surface forces, body forces, concentrated nodal forces, inertial forces, and damping forces.

In summary, our basic finite element relations are:

$$\mathbf{u} = \mathbf{N}\mathbf{d} \quad (\text{A.20})$$

$$\epsilon = \mathbf{B}\mathbf{d} \quad (\text{A.21})$$

$$\gamma = \mathbf{B}_s\mathbf{d} \quad (\text{A.22})$$

$$\sigma = \mathbf{D}\epsilon \quad (\text{A.23})$$

$$\tau = \mathbf{D}_s\gamma \quad (\text{A.24})$$

By placing virtual displacements at the element nodes, we obtain:

$$\delta\mathbf{u} = \mathbf{N}\delta\mathbf{d} \quad (\text{A.25})$$

$$\delta\epsilon = \mathbf{B}\delta\mathbf{d} \quad (\text{A.26})$$

$$\delta\gamma = \mathbf{B}_s\delta\mathbf{d} \quad (\text{A.27})$$

A.4.2 Internal Potential Energy

Viewing the stress-strain diagram of Figure A.1, where it is assumed that we have a linear elastic material free of shear deformation, the internal potential energy (elastic strain energy) per unit volume (elastic strain energy density) generated as a result of the virtual displacements $\delta\epsilon$ is:

$$\delta\epsilon^T \sigma \quad (\text{A.28})$$

where it follows that:

$$\delta\mathbf{U}_i = \delta\epsilon^T \sigma \quad (\text{A.29})$$

Similarly, if we include the effects of shear deformation (Figure A.2), the following term must be included in determining the elastic strain energy density:

$$\delta\gamma^T \tau \quad (\text{A.30})$$

so that:

$$\delta\mathbf{U}_i = \delta\epsilon^T \sigma + \delta\gamma^T \tau \quad (\text{A.31})$$

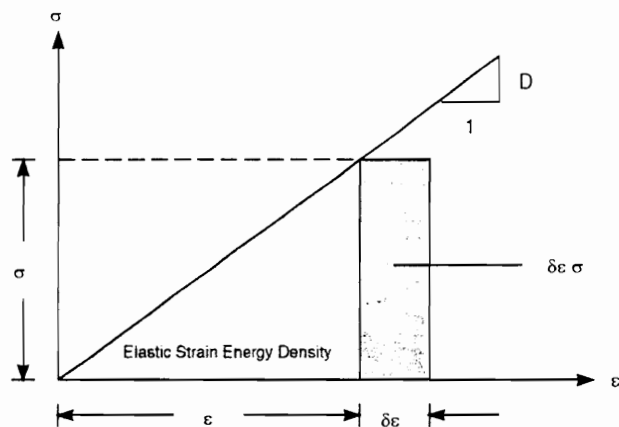


Figure A.1 Linear Elastic Stress-Strain Diagram.

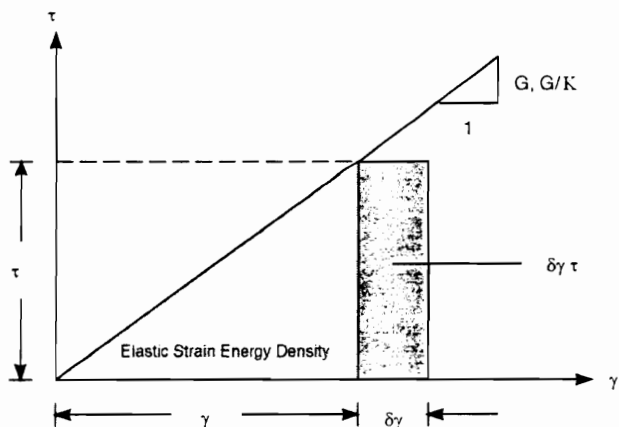


Figure A.2 Linear Elastic Shear Stress-Strain Diagram.

Integrating equation (A.31) over the volume of the element results in the first variation of internal potential energy (elastic strain energy):

$$\delta \mathbf{U}_i = \int \int \int_{vol} \delta \epsilon^T \boldsymbol{\sigma} dV + \int \int \int_{vol} \delta \gamma^T \boldsymbol{\tau} dV \quad (\text{A.32})$$

which, using the basic finite element relations, can be re-written as:

$$\delta \mathbf{U}_i = \left[\left(\int \int \int_{vol} \mathbf{B}^T \mathbf{D} \mathbf{B} dV + \int \int \int_{vol} \mathbf{B}_s^T \mathbf{D}_s \mathbf{B}_s dV \right) \mathbf{d} \right] \delta \mathbf{d}^T \quad (\text{A.33})$$

For convenience, let:

$$\delta \mathbf{U}_i = \mathbf{K} \mathbf{d} \delta \mathbf{d}^T \quad (\text{A.34})$$

where:

$$\mathbf{K} = \int \int \int_{vol} \mathbf{B}^T \mathbf{D} \mathbf{B} dV + \int \int \int_{vol} \mathbf{B}_s^T \mathbf{D}_s \mathbf{B}_s dV \quad (\text{A.35})$$

A.4.3 External Potential Energy

In determining the external potential energy, we will consider surface forces, body forces, concentrated nodal forces, inertial forces, and damping forces. Furthermore, the principle of virtual work will be used directly to obtain an equivalent external potential. The principle will allow us to generate the external work performed per unit volume or area by each of the given forces through the direct relation of: virtual work = (virtual displacement) (applied force).

Surface forces, also known as tractions, are those forces applied on a boundary in units of stress. From our basic principle of virtual work relation, the external work per unit area becomes:

$$\delta \mathbf{W}_{e(\text{surface})} = \delta \mathbf{u}^T \boldsymbol{\Phi} \quad (\text{A.36})$$

where: Φ are prescribed surface tractions. Integrating this relation over the surface area produces:

$$\int \int_{sur} \delta \mathbf{u}^T \Phi \, dS \quad (\text{A.37})$$

Body forces are those forces that are applied over the entire element volume. These forces may arise from gravity, rotating machinery, magnetic fields, etc. For our purposes, body forces are generated from the self-weight of the structure (gravity). The external work per unit volume associated with body forces is:

$$\delta \mathbf{W}_{e(\text{body})} = \delta \mathbf{u}^T \mathbf{b} \quad (\text{A.38})$$

where: \mathbf{b} are body forces. Integration over the volume leads to:

$$\int \int \int_{vol} \delta \mathbf{u}^T \mathbf{b} \, dV \quad (\text{A.39})$$

Concentrated nodal forces are self-explanatory and can be used to account for either concentrated or distributed applied element forces. Since these forces act at the nodes, the external virtual work can simply be expressed as:

$$\delta \mathbf{d}^T \mathbf{f} \quad (\text{A.40})$$

where: \mathbf{f} are nodal concentrated forces.

In performing a static analysis, the external virtual work can be taken as:

$$\delta \mathbf{W}_{e(\text{static})} = \delta \mathbf{W}_{e(\text{surface})} + \delta \mathbf{W}_{e(\text{body})} + \delta \mathbf{d}^T \mathbf{f} \quad (\text{A.41})$$

or:

$$\delta \mathbf{W}_{e(\text{static})} = \int \int_{sur} \delta \mathbf{u}^T \Phi \, dS + \int \int \int_{vol} \delta \mathbf{u}^T \mathbf{b} \, dV + \delta \mathbf{d}^T \mathbf{f} \quad (\text{A.42})$$

Making the basic finite element relation substitutions, leads to:

$$\delta \mathbf{W}_{\mathbf{e}(\text{static})} = \left[\int \int_{sur} \mathbf{N}^T \boldsymbol{\Phi} dS + \int \int \int_{vol} \mathbf{N}^T \mathbf{b} dV + \mathbf{f} \right] \delta \mathbf{d}^T \quad (\text{A.43})$$

When performing a dynamic analysis, additional terms are needed due to inertial and damping effects. In both cases, resisting forces are generated. Inertial effects will be divided into two components: 1) translational, and 2) rotational. The translational inertia component can be taken as:

$$\delta \mathbf{W}_{\mathbf{e}(\text{inertial-t})} = -\delta \mathbf{u}^T \rho \ddot{\mathbf{u}} \quad (\text{A.44})$$

where: ρ is the mass density, or inertial force per unit acceleration per unit volume of the material, and $\ddot{\mathbf{u}}$ are the element accelerations. Integrating over the volume, we obtain:

$$-\int \int \int_{vol} \delta \mathbf{u}^T \rho \ddot{\mathbf{u}} dV \quad (\text{A.45})$$

The rotational inertia component may need more clarification. Figure A.3 shows a representation of a differential element. Considering the sub-element dA , the force resisting the rotation is $\rho \ddot{x}$, where $x = -w\theta$, and thus $\ddot{x} = -w\ddot{\theta}$. The resisting force can then be written as $-\rho w\ddot{\theta}$. By integrating the moment of the inertial force over the area dA , we obtain the inertial moment per unit length:

$$-\int \int_{area} \rho w \ddot{\theta}(w) dA = -\rho \ddot{\theta} \int \int_{area} w^2 dA = -\rho I \ddot{\theta} \quad (\text{A.46})$$

where: I is the area moment of inertia. Under the virtual rotation $\delta\theta$, the external potential energy per unit area is:

$$-\delta\theta^T \rho I \ddot{\theta} \quad (\text{A.47})$$

Integrating over the length of the element results in the general formulation:

$$\delta \mathbf{W}_{\mathbf{e}(\text{inertial-r})} = - \int_{\text{length}} \delta \theta^T \rho I \ddot{\theta} dl \quad (\text{A.48})$$

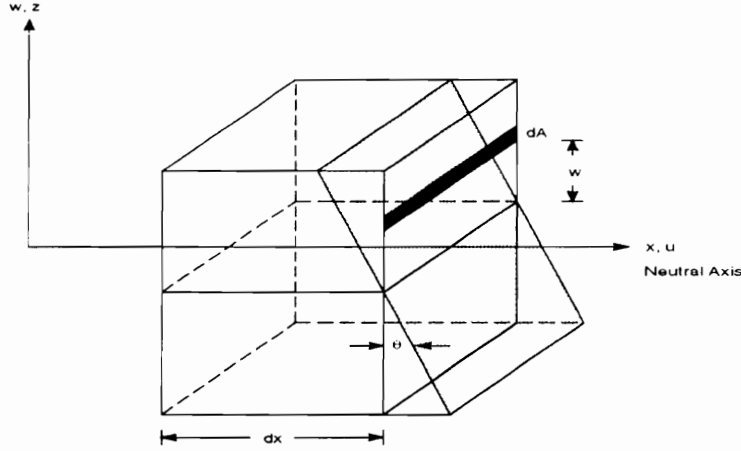


Figure A.3 Differential Element Rotation.

With respect to damping effects, although several forms of damping exist, we will assume viscous damping where a resisting force is generated:

$$\delta \mathbf{W}_{\mathbf{e}(\text{viscous})} = -\delta \mathbf{u}^T \mathbf{c} \dot{\mathbf{u}} \quad (\text{A.49})$$

which leads to:

$$- \int \int \int_{\text{vol}} \delta \mathbf{u}^T \mathbf{c} \dot{\mathbf{u}} dV \quad (\text{A.50})$$

where: c is the coefficient of viscous damping, and $\dot{\mathbf{u}}$ are the element velocities.

In summary, the external virtual work associated with a dynamic analysis that includes the effects of inertia and viscous damping may be expressed as:

$$\delta \mathbf{W}_e = \delta \mathbf{W}_{e(\text{static})} + \delta \mathbf{W}_{e(\text{dynamic})} \quad (\text{A.51})$$

where:

$$\delta \mathbf{W}_{e(\text{dynamic})} = \delta \mathbf{W}_{e(\text{inertial-t})} + \delta \mathbf{W}_{e(\text{inertial-r})} + \delta \mathbf{W}_{e(\text{viscous})} \quad (\text{A.52})$$

which is equal to:

$$\delta \mathbf{W}_{e(\text{dynamic})} = - \int \int \int_{vol} \delta \mathbf{u}^T \rho \ddot{\mathbf{u}} dV - \int_{length} \delta \theta^T \rho I \ddot{\theta} dl - \int \int \int_{vol} \delta \mathbf{u}^T c \dot{\mathbf{u}} dV \quad (\text{A.53})$$

Using the basic finite element relations, along with:

$$\theta = \frac{d\mathbf{u}}{dl} \quad (\text{A.54})$$

$\delta \mathbf{W}_{e(\text{dynamic})}$ can be re-written as:

$$\begin{aligned} \delta \mathbf{W}_{e(\text{dynamic})} = & \left[- \left(\int \int \int_{vol} \mathbf{N}^T \rho \mathbf{N} dV \right) \ddot{\mathbf{d}} - \left(\int_{length} \frac{d}{dl} \mathbf{N}^T \rho I \frac{d}{dl} \mathbf{N} dl \right) \ddot{\mathbf{d}} \right. \\ & \left. - \left(\int \int \int_{vol} \mathbf{N}^T c \mathbf{N} dV \right) \dot{\mathbf{d}} \right] \delta \mathbf{d}^T \quad (\text{A.55}) \end{aligned}$$

For convenience, let:

$$\delta \mathbf{W}_{e(\text{dynamic})} = -(\mathbf{M}\ddot{\mathbf{d}} + \mathbf{C}\dot{\mathbf{d}})\delta \mathbf{d}^T \quad (\text{A.56})$$

where:

$$\mathbf{M} = \int \int \int_{vol} \mathbf{N}^T \rho \mathbf{N} dV + \int_{length} \frac{d}{dl} \mathbf{N}^T \rho I \frac{d}{dl} \mathbf{N} dl \quad (\text{A.57})$$

and:

$$\mathbf{C} = \int \int \int_{vol} \mathbf{N}^T c \mathbf{N} dV \quad (\text{A.58})$$

Recalling that $\delta \mathbf{W}_{\mathbf{e}(\text{static})}$ is:

$$\delta \mathbf{W}_{\mathbf{e}(\text{static})} = \left[\int \int_{sur} \mathbf{N}^T \boldsymbol{\Phi} dS + \int \int \int_{vol} \mathbf{N}^T \mathbf{b} dV + \mathbf{f} \right] \delta \mathbf{d}^T \quad (\text{A.59})$$

The total external virtual work can be expressed as:

$$\delta \mathbf{W}_{\mathbf{e}} = \left[\int \int_{sur} \mathbf{N}^T \boldsymbol{\Phi} dS + \int \int \int_{vol} \mathbf{N}^T \mathbf{b} dV + \mathbf{f} - \mathbf{M}\ddot{\mathbf{d}} - \mathbf{C}\dot{\mathbf{d}} \right] \delta \mathbf{d}^T \quad (\text{A.60})$$

From the basic work and energy relations, we know:

$$\delta \mathbf{W}_{\mathbf{e}} = -\delta \mathbf{U}_{\mathbf{e}}^* \quad (\text{A.61})$$

so that the first variation of external potential energy can be taken as:

$$\delta \mathbf{U}_{\mathbf{e}}^* = \left[- \int \int_{sur} \mathbf{N}^T \boldsymbol{\Phi} dS - \int \int \int_{vol} \mathbf{N}^T \mathbf{b} dV - \mathbf{f} + \mathbf{M}\ddot{\mathbf{d}} + \mathbf{C}\dot{\mathbf{d}} \right] \delta \mathbf{d}^T \quad (\text{A.62})$$

A.4.4 Principle of Stationary Potential Energy

By invoking the principle of stationary potential energy, we have:

$$\delta(\mathbf{U}_i + \mathbf{U}_{\mathbf{e}}^*) = 0 \quad (\text{A.63})$$

or:

$$\left[\mathbf{M}\ddot{\mathbf{d}} + \mathbf{C}\dot{\mathbf{d}} + \mathbf{K}\mathbf{d} - \int \int_{sur} \mathbf{N}^T \boldsymbol{\Phi} dS - \int \int \int_{vol} \mathbf{N}^T \mathbf{b} dV - \mathbf{f} \right] \delta \mathbf{d}^T = 0 \quad (\text{A.64})$$

Since the virtual displacements are non-zero, equality can only be achieved if the quantity within the brackets is zero. Thus, element equations of motion can be written:

$$\mathbf{M}\ddot{\mathbf{d}} + \mathbf{C}\dot{\mathbf{d}} + \mathbf{K}\mathbf{d} = \mathbf{F} \quad (\text{A.65})$$

where:

$$\mathbf{M} = \int \int \int_{vol} \mathbf{N}^T \rho \mathbf{N} dV + \int_{length} \frac{d}{dl} \mathbf{N}^T \rho I \frac{d}{dl} \mathbf{N} dl \quad (\text{A.66})$$

$$\mathbf{C} = \int \int \int_{vol} \mathbf{N}^T c \mathbf{N} dV \quad (\text{A.67})$$

$$\mathbf{K} = \int \int \int_{vol} \mathbf{B}^T \mathbf{D} \mathbf{B} dV + \int \int \int_{vol} \mathbf{B}_s^T \mathbf{D}_s \mathbf{B}_s dV \quad (\text{A.68})$$

$$\mathbf{F} = \int \int_{sur} \mathbf{N}^T \Phi dS + \int \int \int_{vol} \mathbf{N}^T \mathbf{b} dV + \mathbf{f} \quad (\text{A.69})$$

A.5 System Construction

Similar to the element equations of motion, the system equations of motion can be expressed symbolically as:

$$\mathbf{M}\ddot{\mathbf{d}} + \mathbf{C}\dot{\mathbf{d}} + \mathbf{K}\mathbf{d} = \mathbf{F} \quad (\text{A.70})$$

where: \mathbf{M} is the system mass matrix, \mathbf{C} is the system damping matrix, \mathbf{K} is the system stiffness matrix, and \mathbf{F} is the system loading vector. Each system matrix can be constructed from a single element matrix by using what is sometimes called the direct stiffness method. This method simply provides the element coordinates and properties in a form that can be mapped globally. By utilizing this method, the entire element system can be constructed from a single element type. When more than one element type is included in the analysis, a single element of each type is needed to construct the entire element system. An informative discussion concerning the direct stiffness method can be found in Pilkey and Wunderlich (1994).

Appendix B

Finite Element Development

A displacement-based, Rayleigh-Ritz finite element model has been developed to investigate the vibratory response of stiffened plates (e.g. wood floors). The model is comprised of plate and beam elements that have been combined through appropriate coordinate transformations. Although not essential, the interested reader is referred to Appendix A for a short introduction regarding the general theory of displacement based finite elements, and how they can be used to represent dynamic motion.

B.1 Preliminaries

Two types of elements have been included in the analysis: 1) beam elements, and 2) plate elements. It will be shown that a combined element can be constructed through appropriate coordinate transformations. The combined element is advantageous in that the system can be represented by the plate degrees-of-freedom only (thus significantly reducing the size of the system). However, before discussing these issues, the preliminary topics of shape function selection, completeness, continuity, and element matrix evaluation will be discussed.

B.1.1 Shape Functions

An important consideration in the formulation of displacement-based finite elements is the choice of shape functions. For our purposes, each can be generated using a Lagrangian approach. Lagrange interpolation approximates a function, say $f(\zeta)$ by a polynomial of degree $n-1$:

$$p(\zeta) = \sum_{i=1}^n l_i(\zeta) f(\zeta_i) \quad \zeta_1 < \zeta_2 < \zeta_3 \dots < \zeta_n \quad (\text{B.1})$$

where:

$$l_i(\zeta) = \frac{(\zeta - \zeta_1) \dots (\zeta - \zeta_{i-1})(\zeta - \zeta_{i+1}) \dots (\zeta - \zeta_n)}{(\zeta_i - \zeta_1) \dots (\zeta_i - \zeta_{i-1})(\zeta_i - \zeta_{i+1}) \dots (\zeta_i - \zeta_n)} \quad (\text{B.2})$$

In dealing with phenomena such as axial deformation, torsion, and beam bending with shear effects, this form of Lagrange interpolation is satisfactory, and we take $N_i(\zeta) = l_i(\zeta)$, where $N_i(\zeta)$ represent the shape functions.

In situations where a function and its consecutive derivatives must be approximated, a generalized Lagrange interpolation known as Hermite interpolation can be used. In the case of bending without shear effects, we are concerned with the translation and rotation at each interpolation point; thus, an approximating polynomial of degree $2n-1$ can be expressed as:

$$p(\zeta) = \sum_{i=1}^n [\phi_i(\zeta) f(\zeta_i) + \Psi_i(\zeta) f'(\zeta_i)] \quad (\text{B.3})$$

where:

$$\phi_i(\zeta) = [1 - 2l_i'(\zeta)(\zeta - \zeta_i)] l_i^2(\zeta) \quad (\text{B.4})$$

$$\Psi_i(\zeta) = (\zeta - \zeta_i) l_i^2(\zeta) \quad (\text{B.5})$$

$$l_i(\zeta) = \frac{(\zeta - \zeta_1) \dots (\zeta - \zeta_{i-1})(\zeta - \zeta_{i+1}) \dots (\zeta - \zeta_n)}{(\zeta_i - \zeta_1) \dots (\zeta_i - \zeta_{i-1})(\zeta_i - \zeta_{i+1}) \dots (\zeta_i - \zeta_n)} \quad (\text{B.6})$$

$$l'_i(\zeta) = \frac{dl_i(\zeta)}{d\zeta} \quad (\text{B.7})$$

$$f'(\zeta_i) = \frac{df(\zeta_i)}{d\zeta} \quad (\text{B.8})$$

The shape functions $N_i(\zeta)$ can now be cast in terms of $\phi_i(\zeta)$ and $\Psi_i(\zeta)$. In mapping between two coordinate systems, appropriate rotational transformations are needed.

Two-dimensional interpolation functions can be constructed as the product of an appropriate pair of one-dimensional interpolation functions (either Lagrange or Hermite). For example, in Lagrange interpolation, with the introduction of a second dimension η , a shape function could take the form: $N_1 = l_1(\zeta)l_1(\eta)$.

B.1.2 Completeness and Continuity

In applying a Rayleigh-Ritz method to finite elements, two conditions related to shape functions are required. First, the displacement field, \mathbf{u} must be a complete polynomial of degree m . Recalling that $\mathbf{u} = \mathbf{N}\mathbf{d}$, the degree of the polynomial is taken as the degree of the shape function. Second, the element must have C^{m-1} continuity along inter-element boundaries. C^{m-1} continuity implies that \mathbf{u} and its derivatives up to the order of $m - 1$ are continuous. If both of these conditions are satisfied, monotonic convergence in energy is guaranteed.

B.1.3 Evaluation of Element Matrices

Once the appropriate shape functions have been selected, the element matrices can be evaluated (assuming that the elasticity matrices are known). Explicit evaluation of the element matrices is very time consuming and prone to error. An alternative is to evaluate the integral expressions numerically. Although several numerical integration methods exist, Gauss quadrature can be used effectively. An advantage of Gauss quadrature is that it has been optimized for both position and weight. Furthermore, a polynomial of order $(2n - 1)$ is integrated exactly with only n function evaluations. If a given function is not a polynomial, Gauss quadrature is inexact, although accuracy can be increased as more evaluations are used. In a one-dimensional normalized space, Gauss quadrature takes the general form:

$$I = \int_{-1}^1 f(\zeta) d\zeta \cong \sum_{i=1}^n W_i f(\zeta_i) \quad (\text{B.9})$$

where: $f(\zeta)$ is the function being evaluated over the normalized interval of $(-1,1)$, W_i is the optimized weight factor, and $f(\zeta_i)$ is the value of the function evaluated at the optimized sample point ζ_i . Both optimized weight factors and optimized sample point locations can be found in any standard numerical analysis or finite element textbook. In two dimensions, Gauss quadrature is formed by successive applications of the one-dimensional general form:

$$I = \int_{-1}^1 \int_{-1}^1 f(\zeta, \eta) d\zeta d\eta \cong \sum_{i=1}^n \sum_{j=1}^n W_i W_j f(\zeta_i, \eta_j) \quad (\text{B.10})$$

B.2 Beam Element Formulation

Joists in wood floor systems are subjected to bending, shear, axial, and torsional deformations. Bending and shear deformations arise from the direct application of load. While axial deformations result from the joists acting as eccentric stiffeners to the sheathing, torsional deformations result from the rotations of the sheathing. It is the purpose of this section to formulate a beam element that will sufficiently model these deformations.

B.2.1 Models and Element Selection

To begin, we will consider a continuous beam as shown in Figure B.1. By analyzing the shaded (differential) region, it is possible to determine the strain-displacement relations for all deformations other than those due to torsion. If for now, we neglect shear, Figure B.2 shows a physical interpretation of the deformed shape in two-dimensions, where: θ is the beam rotation due to bending, w is the height above the neutral axis, and $u(x,w)$ and $u(x,0)$ are deformations in the axial direction. This idealization corresponds to the Bernoulli–Euler theory where normals remain straight, undeformed, and normal to the neutral axis; thus, the theory models pure bending.

When shear effects are included, a different deformed shape results as seen in Figure B.3, where: γ is the rotation and consequently strain due to the shear deformation. In this case, while normals remain straight and undeformed, they do not necessarily remain normal to the neutral axis. This model is referred to as a Mindlin–Timoshenko beam where the effects of warping due to the shear deformation have been neglected. Based on the Mindlin–Timoshenko model, the following

strain-displacement equations can be written:

$$\epsilon(x, w) = \frac{du(x, 0)}{dx} - u' \frac{d\theta}{dx} \quad (\text{B.11})$$

and:

$$\gamma(x, w) = \frac{dz}{dx} - \theta \quad (\text{B.12})$$

where it is noted that the strains are coupled through the θ term. The corresponding stress-strain relations are:

$$\sigma = E\epsilon \quad (\text{B.13})$$

and:

$$\tau = \frac{1}{K}G\gamma \quad (\text{B.14})$$

where: E is the modulus of elasticity, G is the modulus of rigidity, and K is a section based shear correction factor. This factor equates an assumed uniformly distributed shear with the actual distribution. Based on the strain-displacement and stress-strain relations, a finite element representation can be formed where the unknown displacement fields are: z , θ , and u .

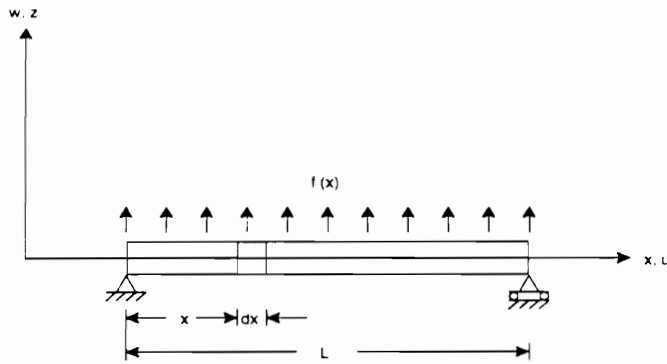


Figure B.1 Continuous Beam Model.

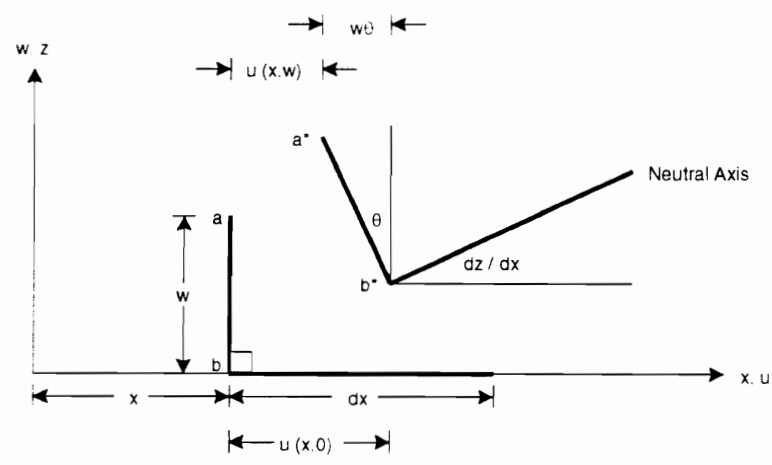


Figure B.2 Beam Deformation Model Excluding Shear and Torsion.

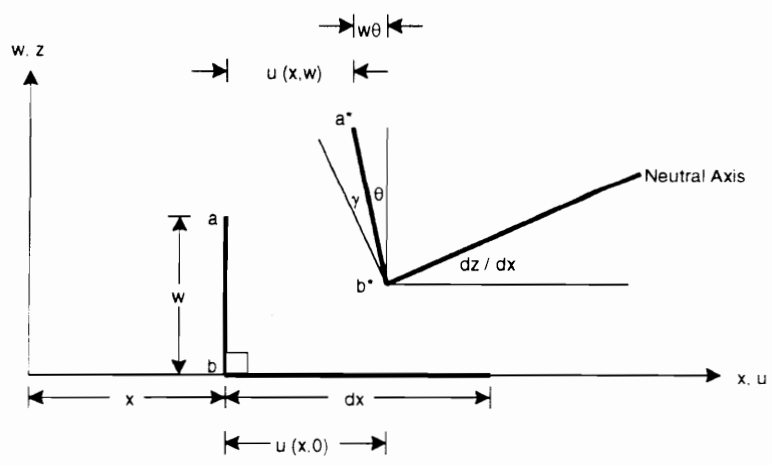


Figure B.3 Beam Deformation Model Including Shear and Excluding Torsion.

In determining the beam shape functions, we will consider the bending (z, θ) and axial displacement fields (u) separately. In bending, consideration is given to both ordinate (z) and rotation (θ); thus, Lagrange interpolation is used. For a standard two-node element, Lagrange interpolation results in linear shape functions. Unfortunately, for beams that include shear deformation, shallow two-node beam elements have the tendency to exhibit exaggerated stiffness that causes element “locking” (deformations close to zero).

To understand the phenomena of element “locking”, consider a static system of equations where a unique solution is obtainable only when the stiffness matrix is non-singular (i.e. has an inverse). To ensure a non-singular matrix, numerical integration requires that the number of independent relations at the integration points be greater than or equal to the number of unknowns (active degrees-of-freedom). For beams that include shear deformation, the coupled stiffness matrix is composed of true bending and shear components:

$$\mathbf{K} = \mathbf{K}_b + \mathbf{K}_s \quad (\text{B.15})$$

where:

$$\mathbf{K}_b = EI[\] \quad (\text{B.16})$$

and:

$$\mathbf{K}_s = \frac{GA}{K}[\] \quad (\text{B.17})$$

where: A is the element area, and the closed brackets refer to matrices that for now, can be considered arbitrary. Observing these three equations, when a beam becomes shallow, \mathbf{K}_s can become large in comparison to \mathbf{K}_b . In an uncoupled (physical) system, this implies that the shear deformation is low, and that the majority of

the deformation comes from the true bending component. However, in the coupled system, the coupling admits high shear stiffness to the coupled stiffness so that exaggerated stiffness values result and the element “locks”. What should happen, is that a constraint should be placed on the shear deformation so that for shallow beams, the shear stiffness is zero. A singular \mathbf{K}_s can enforce this constraint without “locking” the element. To ensure a singular matrix, numerical integration requires that the number of independent relations at the integration points be less than the number of unknowns (active degrees-of-freedom). For two-dimensional analysis, Cook et al. (1989) explains that the near optimal ratio of active degrees-of-freedom to shear constraints is 2-to-1.

Two ways to obtain a singular matrix are to use reduced integration, or a higher order element. One disadvantage of reduced integration is that convergence in energy is lost. In addition, element instability may occur. On the other hand, reduced integration tends to soften elements so that a more accurate element stiffness is achieved. When using higher order elements, full integration is possible so that the convergence in energy is maintained; however, the ratio of active degrees-of-freedom to shear constraints may be lower than the optimal 2-to-1. Based on these considerations, it is apparent that a three-node beam element with either full or reduced integration will suffice in modelling the beam bending. Having chosen a three-node beam element, the interpolation functions in z , and θ will be quadratic. It follows from the choice of a three-node element, that in considering axial deformation, the interpolation functions in u will also be quadratic.

In considering torsion, Figure B.4 shows a differential element and deformation model excluding the effects of warp, where: ϕ is the rotation due to torsion, and γ

is the shear strain due to torsion. From Figure B.4, the strain-displacement relation can be written:

$$\gamma = w \frac{d\phi}{dx} \quad (\text{B.18})$$

where the stress-strain relation is:

$$\tau = G\gamma \quad (\text{B.19})$$

As with the bending and axial deformation interpolation functions, the interpolation functions in the torsional deformation field ϕ will be taken as quadratic.

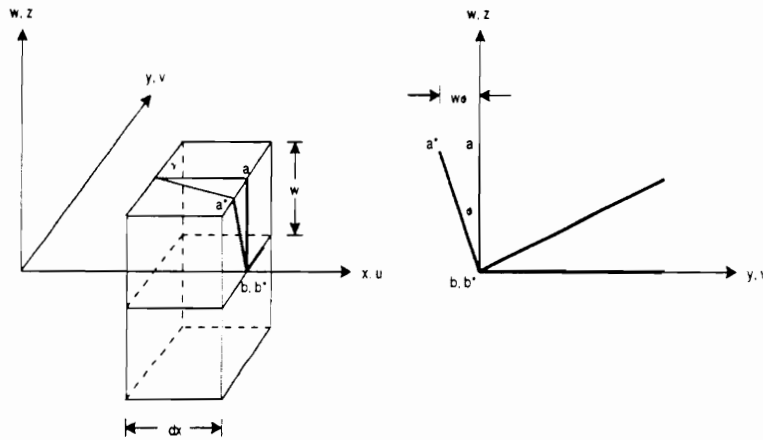


Figure B.4 Torsion Differential Element and Deformation Model Excluding Warp.

In summary, a three-node element has been chosen to model the response of wood floor joists. The element chosen takes into account pure bending deformations, shear deformations, axial deformations, and torsional deformations. In all cases, quadratic

shape functions will be used to approximate the displacement fields. It is noted that the element provides completeness and continuity.

B.2.2 Beam Stiffness Matrix

Performing the required substitutions, the beam element stiffness matrix will have the final form:

$$\mathbf{K} = \{\mathbf{K}_{pb} + \mathbf{K}_s\} + \mathbf{K}_a + \mathbf{K}_{tor} \quad (\text{B.20})$$

where: \mathbf{K}_{pb} is the beam pure bending stiffness, \mathbf{K}_s is the beam shear stiffness, \mathbf{K}_a is the beam axial stiffness, and \mathbf{K}_{tor} is the beam torsional stiffness. The curly brackets refer to the fact that \mathbf{K}_{pb} and \mathbf{K}_s are coupled, thus \mathbf{K} is coupled through these terms. Each expression can be expanded so that:

$$\mathbf{K}_{pb} = EI[] \quad (\text{B.21})$$

$$\mathbf{K}_s = \frac{GA}{K}[] \quad (\text{B.22})$$

$$\mathbf{K}_a = EA[] \quad (\text{B.23})$$

$$\mathbf{K}_t = GJ[] \quad (\text{B.24})$$

where: the only new term is J , the torsional constant. The closed brackets $[]$ refer to matrices obtained by numerical integration. As described, each element stiffness matrix will contain twelve degrees-of-freedom, thus a 12×12 matrix will result.

Although the torsional deformation model excludes the effects of warp, in calculating the torsional constant, warp must be considered. For a rectangular cross-section, J may be taken as:

$$J = \frac{(2a)^3(2b)}{3} \left[1 - \frac{192}{\pi^5} \left(\frac{a}{b} \right) \sum_{n=1,3,5,\dots}^{\infty} \frac{1}{n^5} \tanh \frac{n\pi b}{2a} \right] \quad (\text{B.25})$$

where: a is half the beam width, and b is half the beam depth (Boresi and Chong, 1987). For beam cross-sectional shapes such as I-Joists, J can be taken as a superposition of equivalent rectangular sections (Pilkey and Wunderlich, 1994).

B.2.3 Beam Mass Matrix

In a similar substituting fashion, the beam element mass matrix will also contain twelve degrees-of-freedom where:

$$\mathbf{M} = \mathbf{M}_t + \mathbf{M}_r + \mathbf{M}_a + \mathbf{M}_{tor} \quad (\text{B.26})$$

where: \mathbf{M}_t is the beam mass associated with bending translation (z), \mathbf{M}_r is the beam mass associated with the bending rotation (θ), \mathbf{M}_a is the beam mass associated with axial translation (u), and \mathbf{M}_{tor} is the beam mass associated with torsional rotation (ϕ). Each expression can be expanded so that:

$$\mathbf{M}_t = \rho A [\quad] \quad (\text{B.27})$$

$$\mathbf{M}_r = \rho I [\quad] \quad (\text{B.28})$$

$$\mathbf{M}_a = \rho A [\quad] \quad (\text{B.29})$$

$$\mathbf{M}_{tor} = \rho J [\quad] \quad (\text{B.30})$$

where: ρ is the mass density. The closed brackets $[\quad]$ refer to matrices obtained by numerical integration.

B.3 Basic Plate Element Formulation

In the formulation of a suitable plate element, consideration will be given to pure bending deformations, shear deformations, and in-plane deformations. By including in-plane deformations, it will be possible to obtain system solutions based only on the plate degrees-of-freedom. Orthotropic stress-strain relations will be used in the formulation.

B.3.1 Models and Element Selection

Figure B.5 shows a representation of a continuous plate. As with a continuous beam, by analyzing the shaded differential regions, the deformed shapes can be envisioned. Figure B.6 shows the plate deformed shape in the x - w plane, and Figure B.7 shows the plate deformed shape in the y - w plane.

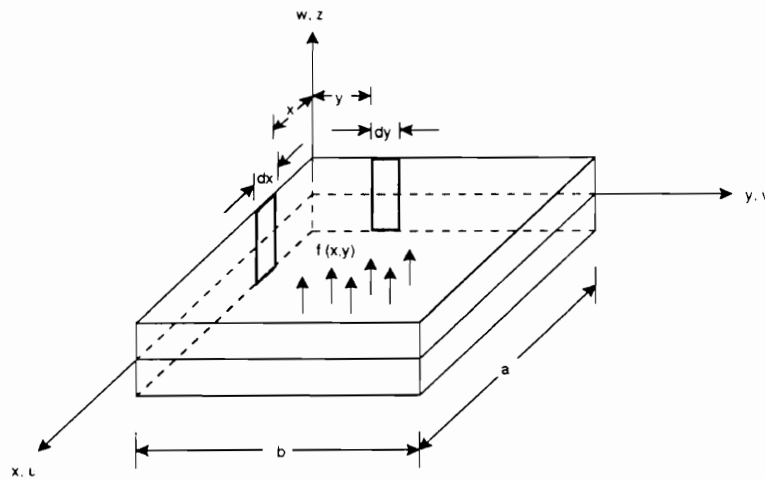


Figure B.5 Continuous Plate Model.

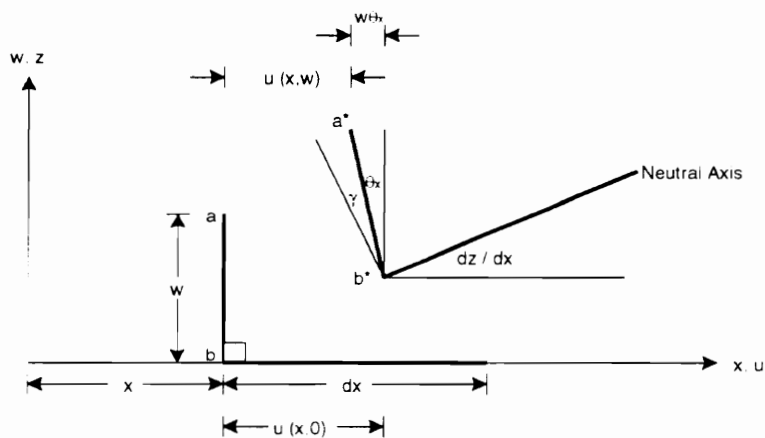


Figure B.6 Plate Deformation Model. x - w Plane.

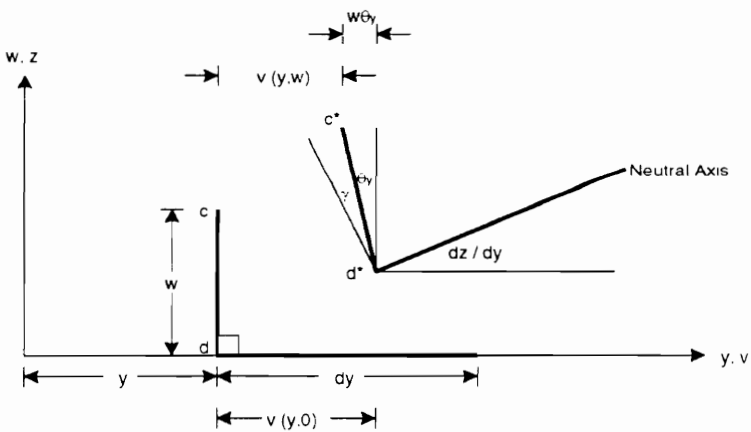


Figure B.7 Plate Deformation Model. y - w Plane.

It follows from Figures B.6 and B.7 that the strain-displacement relations can be written:

$$\epsilon(x, w) = \frac{\partial u(x, 0)}{\partial x} - w \frac{\partial \theta_x}{\partial x} \quad (\text{B.31})$$

$$\gamma(x, w) = \frac{\partial z}{\partial x} - \theta_x \quad (\text{B.32})$$

$$\epsilon(y, w) = \frac{\partial v(y, 0)}{\partial y} - w \frac{\partial \theta_y}{\partial y} \quad (\text{B.33})$$

$$\gamma(y, w) = \frac{\partial z}{\partial y} - \theta_y \quad (\text{B.34})$$

In addition to the bending strains and transverse shear strains just described, shear strains develop in the x-y plane of the plate. Figure B.8 shows a representative model where it is assumed for clarity that u is equal to $u(x, y)$, and v is equal to $v(x, y)$. From Figure B.8, the shear deformation can be expressed as:

$$\gamma(x, y) = \frac{\partial u(x, y)}{\partial y} + \frac{\partial v(x, y)}{\partial x} \quad (\text{B.35})$$

By making the necessary substitutions, the strain-displacement relation in the x-y plane is written:

$$\gamma(x, y) = \frac{\partial u(x, 0)}{\partial y} - w \frac{\partial \theta_x}{\partial y} + \frac{\partial v(y, 0)}{\partial x} - w \frac{\partial \theta_y}{\partial x} \quad (\text{B.36})$$

The stress-strain relations for orthotropic plates have the form:

$$\sigma_x = \frac{E_x}{1 - \nu_x \nu_y} (\epsilon_x + \nu_y \epsilon_y) \quad (\text{B.37})$$

$$\tau_{xw} = \frac{1}{K} G \gamma_{xw} \quad (\text{B.38})$$

$$\sigma_y = \frac{E_y}{1 - \nu_x \nu_y} (\epsilon_y + \nu_x \epsilon_x) \quad (\text{B.39})$$

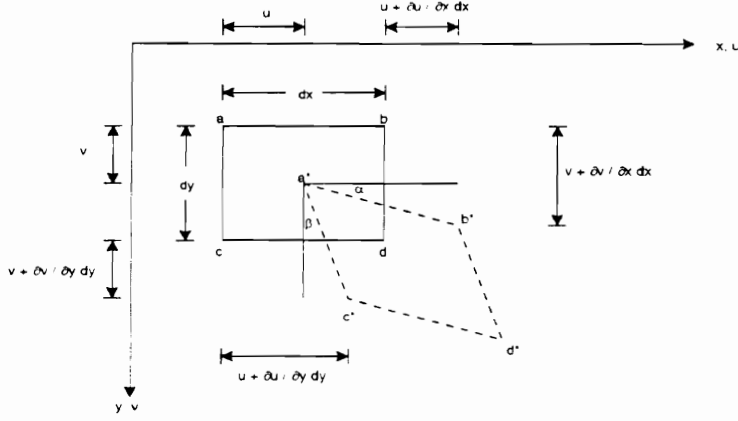


Figure B.8 Model For x-y Plane Shear Deformation.

$$\tau_{yw} = \frac{1}{K} G \gamma_{yw} \quad (\text{B.40})$$

and:

$$\tau_{xy} = G \gamma_{xy} \quad (\text{B.41})$$

where: E_x , E_y and ν_x , ν_y are the effective moduli of elasticity and poisson's ratios in the x and y directions respectively. For clarity, a symbol such as ϵ_x refers to $\epsilon(x, w)$, and a symbol such as τ_{xy} refers to $\tau(x, y)$.

More conveniently, the stress-strain relations can be written:

$$\begin{bmatrix} \sigma_x \\ \sigma_y \\ \tau_{xy} \\ \tau_{xu} \\ \tau_{yu} \end{bmatrix} = \begin{bmatrix} \frac{E_x}{1-\nu_x\nu_y} & \frac{\nu_y E_x}{1-\nu_x\nu_y} & 0 & 0 & 0 \\ \frac{\nu_x E_y}{1-\nu_x\nu_y} & \frac{E_y}{1-\nu_x\nu_y} & 0 & 0 & 0 \\ 0 & 0 & G & 0 & 0 \\ 0 & 0 & 0 & \frac{1}{k}G & 0 \\ 0 & 0 & 0 & 0 & \frac{1}{k}G \end{bmatrix} \begin{bmatrix} \epsilon_x \\ \epsilon_y \\ \gamma_{xy} \\ \gamma_{xu} \\ \gamma_{yu} \end{bmatrix} \quad (\text{B.42})$$

or:

$$\sigma = \mathbf{D} \epsilon \quad (\text{B.43})$$

where ϵ is equivalent to:

$$\begin{bmatrix} \epsilon_x \\ \epsilon_y \\ \gamma_{xy} \\ \gamma_{xu} \\ \gamma_{yu} \end{bmatrix} = \begin{bmatrix} 0 & -u' \frac{\partial}{\partial x} & 0 & \frac{\partial}{\partial x} & 0 \\ 0 & 0 & -u' \frac{\partial}{\partial y} & 0 & \frac{\partial}{\partial y} \\ 0 & -u' \frac{\partial}{\partial y} & -u' \frac{\partial}{\partial x} & \frac{\partial}{\partial y} & \frac{\partial}{\partial x} \\ \frac{\partial}{\partial x} & -1 & 0 & 0 & 0 \\ \frac{\partial}{\partial y} & 0 & -1 & 0 & 0 \end{bmatrix} \begin{bmatrix} z \\ \theta_x \\ \theta_y \\ u \\ v \end{bmatrix} \quad (\text{B.44})$$

or:

$$\epsilon = \mathbf{L} \mathbf{u} \quad (\text{B.45})$$

As in the beam element formulation, caution to avoid shear locking is essential when determining the plate element shape functions. Using the beam element rationale, a nine-node plate element will be used that can either be fully integrated, or selectively integrated. It follows, that for each plate displacement field ($z, \theta_x, \theta_y, u, v$), the shape functions (\mathbf{N}) will be quadratic. With nine-nodes, each plate element will contain 45 degrees-of-freedom where completeness and continuity are provided.

B.3.2 Plate Stiffness Matrix

Performing the required substitutions, the plate element stiffness matrix will have the final form:

$$\mathbf{K} = \{\mathbf{K}_{pb} + \mathbf{K}_{ts}\} + \mathbf{K}_{ip} \quad (\text{B.46})$$

where: \mathbf{K}_{pb} is the plate pure bending stiffness, \mathbf{K}_{ts} is the plate transverse shear stiffness, and \mathbf{K}_{ip} is the plate in-plane stiffness. The curly brackets refer to the fact that \mathbf{K}_{pb} and \mathbf{K}_s are coupled, thus \mathbf{K} is coupled through these terms. Each expression can be expanded so that:

$$\mathbf{K}_{pb} = \frac{h^3}{12} [\quad] \quad (\text{B.47})$$

$$\mathbf{K}_{ts} = \frac{hG}{K} [\quad] \quad (\text{B.48})$$

$$\mathbf{K}_{ip} = h [\quad] \quad (\text{B.49})$$

where: h is the plate thickness. The closed brackets $[\quad]$ refer to matrices obtained by numerical integration. As described, each element stiffness matrix will contain forty-five degrees-of-freedom, thus a 45×45 matrix will result.

B.3.3 Plate Mass Matrix

In a similar substituting fashion, the plate element mass matrix will also contain forty-five degrees-of-freedom where:

$$\mathbf{M} = \mathbf{M}_t + \mathbf{M}_r + \mathbf{M}_{ip} \quad (\text{B.50})$$

where: \mathbf{M}_t is the plate mass associated with bending translation (z), \mathbf{M}_r is the plate mass associated with the bending rotations (θ_x) and (θ_y), and \mathbf{M}_{ip} is the plate mass associated with the in-plane translations (u) and (v). Each expression can be expanded so that:

$$\mathbf{M}_t = \rho h [\quad] \quad (\text{B.51})$$

$$\mathbf{M}_r = \rho \frac{h^3}{12} [\quad] \quad (\text{B.52})$$

$$\mathbf{M}_{ip} = \rho h [\quad] \quad (\text{B.53})$$

where: the closed brackets $[\quad]$ refer to matrices obtained by numerical integration.

B.4 Combined Plate-Beam Element Formulation

In formulating the combined plate-beam element, we will seek to represent the system degrees-of-freedom by those of the plate only. To begin, consider Figure B.9, a typical representation of a floor system. For clarity, further consider only the shaded region where the beam acts as an eccentric stiffener. In two-dimensions, the shaded region, extending along the x -axis, can be envisioned as a combined system (Figure B.10) where further magnification shows the interior geometry of the combined system (Figure B.11). The L-slash symbol denotes the element length.

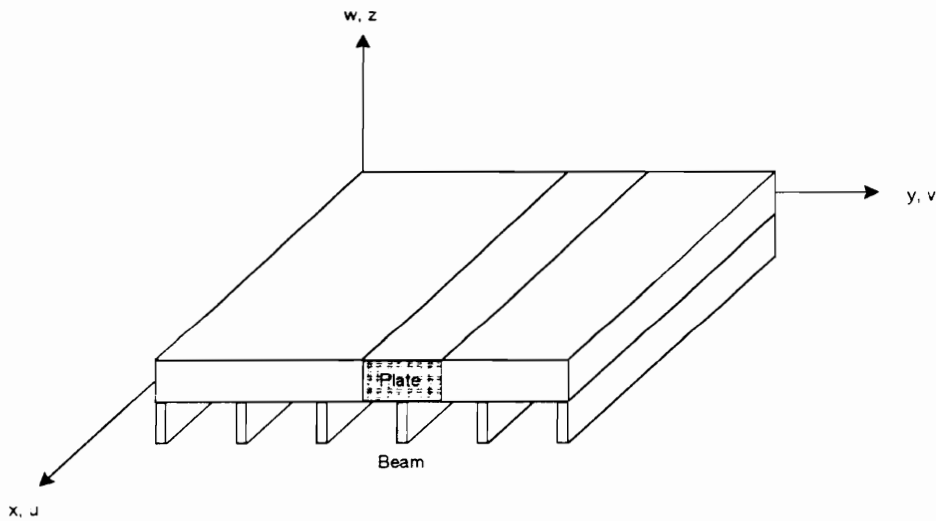


Figure B.9 Representation of Typical Floor System.

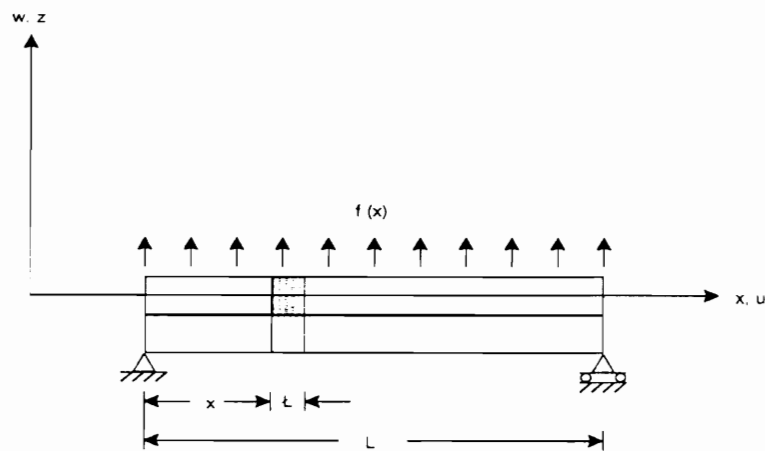


Figure B.10 Combined System Model.

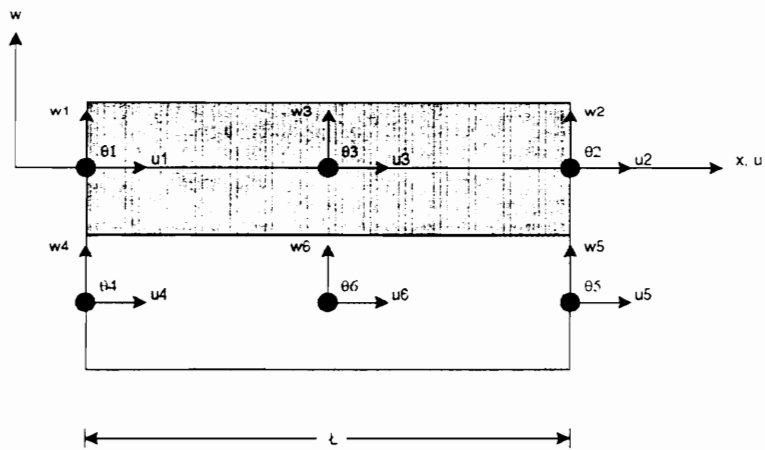


Figure B.11 Combined System Geometry.

Considering only the left end of the combined system in Figure B.11, the deformation model can be represented by Figure B.12:

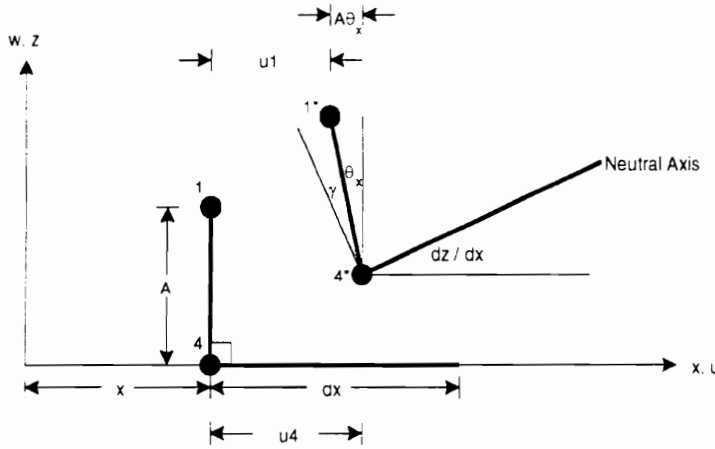


Figure B.12 Combined System Deformation Model.

From the combined system deformation model, it follows that a coordinate transformation equation may be written that will allow the plate to include the beam properties and degrees-of-freedom:

$$\begin{bmatrix} u_4 \\ w_4 \\ \theta_{4_x} \end{bmatrix} = \begin{bmatrix} 1 & 0 & A \\ 0 & 1 & 0 \\ 0 & 0 & 1 \end{bmatrix} \begin{bmatrix} u_1 \\ w_1 \\ \theta_{1_x} \end{bmatrix} \quad (\text{B.54})$$

where it is assumed that there are no vertical gaps between elements and that both elements experience the same rotation.

With regard to the stiffness matrix, denoting the three \times three matrix as the coordinate transformation matrix $[\mathbf{T}]$, and the beam stiffness matrix as $[\mathbf{K}]_{beam}$, the

additional plate stiffness resulting from the beam is:

$$[\mathbf{K}]_{plate+} = [\mathbf{T}]^T [\mathbf{K}]_{beam} [\mathbf{T}] \quad (\text{B.55})$$

where the total plate stiffness is obtained by adding the basic plate stiffness and $[\mathbf{K}]_{plate+}$. In a similar manner, the additional plate stiffness in the y-direction can be obtained. The transformation matrix $[\mathbf{T}]$ is similar to that described by Gupta and Ma (1977) and Miller (1980). In all, the coordinate transformation equations allow the plate-beam system to be represented by the plate degrees-of-freedom only, thus significantly reducing the number of unknown equations and solution time.

B.5 Summary

A combined plate-beam element has been constructed to model the response of stiffened plates. Since both plate and beam elements use quadratic shape functions, completeness and continuity are maintained. The combined element accounts for bending, transverse shear, in-plane, and torsional deformations.

Appendix C

Solution Procedures

In order to obtain useful information from the finite element model, we need to extract the unknown quantities of interest by implementing appropriate solution procedures. Although our primary interest concerns obtaining the dynamic response, the static response can also easily be generated along the way. Static response results will be useful for model verification. In the following discussion, bold letters will refer to non-scalar quantities. In some instances, for clarity, the non-scalar quantities will be expressed by bracket enclosure (for matrices), and by curly bracket enclosure (for vectors).

C.1 Full System

C.1.1 Natural Frequencies

In obtaining values for the system natural frequencies, undamped free-vibration will be assumed. This is a reasonable assumption since the damping factors in wood floors are generally less than 5 percent of critical. Having already assembled the system mass and stiffness matrices, which in our case are known to be symmetric and

positive definite, the characterizing equations of the conservative system are:

$$\mathbf{M}\ddot{\mathbf{d}} + \mathbf{K}\mathbf{d} = 0 \quad (\text{C.1})$$

where: $\ddot{\mathbf{d}}$ are known as the generalized accelerations, and \mathbf{d} are known as the generalized displacements. If we assume synchronous motion, that is, motion where all coordinates exhibit the same time dependence, the following solution may be used:

$$\mathbf{d} = e^{\omega t} \mathbf{u} \quad (\text{C.2})$$

so that upon substitution, an eigenvalue problem results:

$$\mathbf{K}\mathbf{u} = \omega^2 \mathbf{M}\mathbf{u} \quad (\text{C.3})$$

or equivalently:

$$[\mathbf{K} - \omega^2 \mathbf{M}]\mathbf{u} = 0 \quad (\text{C.4})$$

where: ω are the system natural frequencies, ω^2 are the system eigenvalues, \mathbf{u} are the system eigenvectors (natural modes/mode shapes). In order for non-trivial solutions to exist, the determinant of the coefficients must be zero, so that:

$$|\mathbf{K} - \omega^2 \mathbf{M}| = 0 \quad (\text{C.5})$$

Expanding this determinant results in a polynomial known as the characteristic equation whose roots numbering ($i = 1, 2, \dots, n$) can be directly solved for. Unfortunately, for large systems of equations, using the characteristic equation is prohibitive and efficient eigensolutions are alternatively obtained by expressing the eigenvalue problem in terms of a single matrix:

$$[\mathbf{A} - \lambda \mathbf{I}]\mathbf{U} = 0 \quad (\text{C.6})$$

where: \mathbf{I} is the identity matrix, and \mathbf{U} are the eigenvectors of the alternative problem.

The \mathbf{A} matrix and associated eigenvalue problem can be constructed in the following way. First, Cholesky decomposition can be used to factor the system stiffness matrix which is known to be both symmetric and positive definite. The decomposition can be stated:

$$\mathbf{K} = \mathbf{L}\mathbf{L}^T \quad (\text{C.7})$$

where: \mathbf{L} is a lower triangular matrix. Note that the static solution can be obtained from the factored matrix and static load vector using backsubstitution:

$$\mathbf{L}\mathbf{x} = \mathbf{f} \quad (\text{C.8})$$

where: \mathbf{x} represents the static solution, and \mathbf{f} represents the static load vector.

Recognizing the ($i = 1, 2, \dots, n$) roots individually, substituting (C.7) into (C.4) yields:

$$[\mathbf{L}\mathbf{L}^T - \omega_i^2 \mathbf{M}]\mathbf{u}_i = 0 \quad (\text{C.9})$$

By premultiplying this equation by \mathbf{L}^{-1} , and recognizing that \mathbf{I} can be taken as $\mathbf{L}^{-T}\mathbf{L}^T$ we obtain:

$$[\mathbf{L}^{-1}\mathbf{L}\mathbf{L}^T - \omega_i^2 \mathbf{L}^{-1}\mathbf{M}\mathbf{L}^{-T}\mathbf{L}^T]\mathbf{u}_i = 0 \quad (\text{C.10})$$

which can be re-written as:

$$[\mathbf{I} - \omega_i^2 \mathbf{L}^{-1}\mathbf{M}\mathbf{L}^{-T}]\mathbf{L}^T \mathbf{u}_i = 0 \quad (\text{C.11})$$

and finally:

$$[\mathbf{A} - \lambda_i \mathbf{I}]\mathbf{U}_i = 0 \quad (\text{C.12})$$

where:

$$\mathbf{A} = \mathbf{L}^{-1}\mathbf{M}\mathbf{L}^{-T} \quad (\text{C.13})$$

$$\lambda_i = \frac{1}{\omega_i^2} \quad (\text{C.14})$$

and:

$$\mathbf{U}_i = \mathbf{L}^T \mathbf{u}_i \quad (\text{C.15})$$

Now that the eigenvalue problem is in standard form, we can obtain the eigenvalues λ_i and eigenvectors \mathbf{U}_i (natural modes) of the system by any standard method. Unless repeated eigenvalues occur, the eigenvalues are unique without further modification. In the case of the eigenvectors, uniqueness comes only from the ratio of vector elements, where the scale is arbitrary. In other words, while the shape of the natural modes is unique, the amplitude is not. Fortunately, the natural modes can be adjusted so that the amplitudes are unique by implementing some type of normalization procedure. The following normalization procedure has been used:

$$\mathbf{U}_i^T \mathbf{M} \mathbf{U}_i = 1 \quad (\text{C.16})$$

where it can be shown that these normalized eigenvectors, known as normal modes or orthonormal vectors, provide the following:

$$\mathbf{U}_i^T \mathbf{K} \mathbf{U}_i = \lambda_i \quad (\text{C.17})$$

C.1.2 Time History

In obtaining the time history, a superposition method known as modal analysis has been used. This method sets out to describe the motion as a set n -independent, single degree-of-freedom analogous equations. For our system of equations, which exhibit both elastic and inertial coupling, we seek to find an alternate set of generalized

coordinates that render both the stiffness and mass matrices diagonal: thus, the equations uncouple. As will be explained later, the assumption of modal damping allows us to disregard the formation of the damping matrix so that the system of equations becomes:

$$[M]\{\ddot{d}(t)\} + [K]\{d(t)\} = \{F(t)\} \quad (\text{C.18})$$

In obtaining an alternate set of generalized coordinates, properties of the system eigenvectors can be exploited. One property of the system eigenvectors is that they are orthogonal: that is:

$$\{U_i\}^T [M] \{U_j\} = 0 \quad (\text{C.19})$$

and:

$$\{U_i\}^T [K] \{U_j\} = 0 \quad (\text{C.20})$$

where: $i, j = 1, 2, \dots, n$ and $i \neq j$. If we utilize a linear transformation to generate a new set of generalized coordinates, then the matrix of normal modes $[U]$ can be used to diagonalize both the stiffness and mass matrices in terms of the new generalized (normal) coordinates $\eta(t)$:

$$\{d(t)\} = [U]\{\eta(t)\} \quad (\text{C.21})$$

In addition to orthogonality, the system eigenvectors form a linearly independent set. Thus, the motion of the system can be obtained as a superposition of natural modes and appropriate constants:

$$\{d(t)\} = c_1(t)\{U_1\} + c_2(t)\{U_2\} + \dots + c_n(t)\{U_n\} = \sum_{i=1}^n c_i(t)\{U_i\} \quad (\text{C.22})$$

Using the concepts of orthogonality, linear transformation, and linear independence, the following relationship can be used to uncouple the system equations of

motion and provide a time-history:

$$\{d(t)\} = \sum_{i=1}^n \eta_i(t) \{U_i\} = [U] \{\eta(t)\} \quad (\text{C.23})$$

where $\{\eta(t)\}$ are normal coordinates.

In applying the linear transformation, the original set of equations:

$$[M]\{\ddot{d}(t)\} + [K]\{d(t)\} = \{F(t)\} \quad (\text{C.24})$$

can be rewritten as:

$$[M][U]\{\ddot{\eta}(t)\} + [K][U]\{\eta(t)\} = \{F(t)\} \quad (\text{C.25})$$

where $[U]$ are the normalized eigenvectors. Premultiplying by $[U]^T$ yields:

$$[U]^T[M][U]\{\ddot{\eta}(t)\} + [U]^T[K][U]\{\eta(t)\} = [U]^T F(t) \quad (\text{C.26})$$

which due to the use of the normalized eigenvectors, is equivalent to:

$$\ddot{\eta}_i(t) + \omega_i^2 \eta_i(t) = N_i(t) \quad (\text{C.27})$$

where:

$$N_i(t) = \{U_i\}^T F(t) \quad (\text{C.28})$$

The resulting set of uncoupled equations have single degree-of-freedom forms. Thus, it is possible to represent each individual mode as an independent single degree-of-freedom system, such that the summation of modal responses will yield the total response. In considering a general single degree-of-freedom system of the form:

$$m\ddot{\eta}(t) + c\dot{\eta}(t) + k\eta(t) = N(t) \quad (\text{C.29})$$

or equivalently:

$$\ddot{\eta}(t) + 2\zeta\omega\dot{\eta}(t) + \omega^2\eta(t) = \frac{N(t)}{m} \quad (\text{C.30})$$

it can be shown that the response of each mode in the uncoupled system may be expressed in normal coordinates as:

$$\begin{aligned} \eta_i(t) = & \frac{1}{m\omega_{di}} \int_0^t N_i(\tau) e^{-\zeta_i\omega_i(t-\tau)} \sin\omega_{di}(t-\tau) d\tau + \\ & \eta_i(0) e^{-\zeta_i\omega_i t} \left[\cos\omega_{di}t + \frac{\zeta_i\omega_i}{\omega_{di}} \sin\omega_{di}t \right] + \frac{\dot{\eta}_i(0)}{\omega_{di}} e^{-\zeta_i\omega_i t} \sin\omega_{di}t \end{aligned} \quad (\text{C.31})$$

where: ω_i is the i^{th} undamped natural frequency, ω_{di} is the i^{th} damped natural frequency which is equal to $\omega_i (1 - \zeta_i^2)^{\frac{1}{2}}$, ζ_i is the i^{th} viscous damping factor, $\eta_i(0)$ is the initial displacement, and $\dot{\eta}_i(0)$ is the initial velocity. The initial displacement, $\eta_i(0)$, and initial velocity, $\dot{\eta}_i(0)$, can be further expressed as:

$$\eta_i(0) = \{U_i\}^T [M] \{d(0)\} \quad (\text{C.32})$$

and:

$$\dot{\eta}_i(0) = \{U_i\}^T [M] \{\dot{d}(0)\} \quad (\text{C.33})$$

Once the modal responses have been obtained in normal coordinates, nodal coordinate responses can be obtained by summing the products of the normal coordinate responses and appropriate normal modes.

The contribution due to the applied load in (C.31) is seen to be in the form of a convolution integral. For applied loads that are characterized by simple geometries, such as step functions, the convolution integral can be evaluated closed form and a continuous time representation may be utilized. However, for more complex loadings, a closed form solution is difficult if not impossible to obtain. In these instances,

numerical evaluation of the convolution integral is required that represents the loading in discrete time. The discrete time counterpart to the convolution integral is the convolution sum. In general, if the convolution integral has the form:

$$x(t) = \int_0^t F(t - \tau)h(\tau)d\tau \quad (\text{C.34})$$

then the convolution sum can be expressed:

$$x_k = T \sum_{j=0}^{k-1} F_{k-j-1}h_j \quad (\text{C.35})$$

where: T is the reciprocal of the sample rate.

As previously mentioned, since we will be assuming modal damping, the damping matrix need not be explicitly constructed in determining the time-history. This is because modal damping allows a damping factor to be assigned to each mode independently: thus if we have obtained modal damping factors a-priori, damping can be accounted for strictly in the single degree-of-freedom calculations.

C.1.3 Summary

Both the natural frequencies and time history can be obtained without construction of the viscous damping matrix. In the case of natural frequencies, damping effects should be minimal due to the small viscous damping factors associated with floor systems. In the time history analysis, the assumption of modal damping allows the system of equations to uncouple using modal analysis so that the damping effects can be taken into account in the single degree-of-freedom calculations.

In obtaining the system natural frequencies, an eigenvalue problem results that can be solved in standard form by any particular method. The resulting normal modes can be used in a coordinate transformation that allows the system equations

to uncouple in normal coordinates: thus a set of independent single degree-of-freedom equations can be used to represent the response in normal coordinates. The response in nodal coordinates can then be obtained by multiplying the normal coordinate responses by the appropriate normal modes.

C.2 Reduced System

In finite element analysis, system equations are so numerous that solution procedures working on the full system are unreasonable from a performance standpoint. Furthermore, since in most structures only a limited number of modes contribute appreciably to the response, a reduced system of equations is sought so that solution time will be minimized, and accuracy maximized. To this end, Ritz vectors, as described by Wilson et al. (1982), have been used to reduce the size of the system to one that is more manageable and acceptably accurate. The same eigenvalue procedures and modal analysis procedures used for the full system can be used for the reduced system.

In describing the generation of Ritz vectors, we will begin with the general equations of motion:

$$[M]\{\ddot{d}(t)\} + [K]\{d(t)\} = \{F(t)\} \quad (\text{C.36})$$

Since $\{F(t)\}$ implies $\{F(s, t)\}$, that is, a time-varying load composed of space vectors and time functions, the following can be written:

$$\{F(t)\} = \{F(s, t)\} = \sum_k \{f_k(s)\} g_k(t) \quad (\text{C.37})$$

where: k is the number of vectors needed to describe the loading, $\{f_k(s)\}$ is the k^{th} load vector, and $g_k(t)$ is the k^{th} time function. Assuming a single load, the first vector

can be generated from:

$$[K]\{u_1^*\} = \{f(s)\} \quad (\text{C.38})$$

where the first Ritz vector $\{u_1\}$ is found by normalizing the vector $\{u_1^*\}$ with respect to the system mass matrix so that:

$$\{u_1\}^T M \{u_1\} = 1 \quad (\text{C.39})$$

Additional $i = 2, 3, \dots, N$ Ritz vectors are generated by solving:

$$[K]\{u_i^*\} = [M]\{u_{i-1}\} \quad (\text{C.40})$$

where the resulting vectors are orthogonalized with respect to the mass matrix:

$$\{u_i^{**}\} = \{u_i^*\} - \sum_{j=1}^{i-1} c_j \{u_j\} \quad (\text{C.41})$$

where:

$$c_j = \{u_j\}^T [M] \{u_i^*\} \quad (\text{C.42})$$

and normalized with respect to the mass matrix:

$$\{u_i\}^T M \{u_i\} = 1 \quad (\text{C.43})$$

From a physical standpoint, the first Ritz vector represents the static response due to the load vector $\{f(s)\}$. The dynamic forces neglected in this first step can be considered as an error vector, which is accounted for in the loading term used for the generation of the second Ritz vector. Similarly, the error vector associated with the second Ritz vector can be used in the third Ritz vector generating equation, and so on. From this description, it is evident that the Ritz vectors are load dependent. Thus, vectors that are not excited by the given loading will not be included in the analysis.

Once the N Ritz vectors have been calculated, the equations of motion can be written:

$$[M_1]\{\ddot{d}(t)\} + [K_1]\{d(t)\} = \{f_1(s)\} g(t) \quad (C.44)$$

where the reduced $N \times N$ system matrices are:

$$[M_1] = [U]^T [M] [U] \quad (C.45)$$

$$[K_1] = [U]^T [K] [U] \quad (C.46)$$

and the N dimensional load vector is:

$$\{f_1(s)\} = [U]^T \{f(s)\} \quad (C.47)$$

Solving the eigenvalue problem associated with the reduced system will provide approximate full system natural frequencies. In evaluating the reduced system, it is noted that while a diagonal mass matrix results, a non-diagonal stiffness matrix results. This is important since in using modal analysis, the stiffness matrix must be diagonal. Using the exact eigenvectors of the reduced system in a coordinate transformation will allow the stiffness matrix to become diagonal in the usual way while allowing the terms in the mass matrix to be scaled accordingly. Thus, solving:

$$[K_1 - \omega_i^2 M_1] z_i = 0 \quad (C.48)$$

where the eigenvectors are consequently normalized, the final set of Ritz vectors for the reduced system can be taken as:

$$[U_R] = [U][Z] \quad (C.49)$$

where the set of vectors $[U_R]$ are now orthogonal with respect to the system mass and stiffness matrices and may be good approximations of the exact system mode shapes.

Appendix D

Series Solutions

This Appendix provides the series solutions representing the exact solutions in the Model Validation chapter. Unless otherwise noted, the results provide center-point displacements (w) of simply supported plates under the action of a center-point load (p).

D.1 Static Response

D.1.1 Isotropic

$$w = \frac{4p}{\pi^4 Dab} \sum_{m=1,3,5,\dots}^{\infty} \sum_{n=1,3,5,\dots}^{\infty} \frac{\sin\left(\frac{m\pi}{2}\right)^2 \sin\left(\frac{n\pi}{2}\right)^2}{\left[\left(\frac{m}{a}\right)^2 + \left(\frac{n}{b}\right)^2\right]^2} \quad (\text{D.1})$$

where:

$$D = \frac{Eh^3}{12(1 - \nu^2)} \quad (\text{D.2})$$

where: a = Plate length, b = Plate width, E = Plate modulus of elasticity, h = Plate thickness, and ν = Plate Poisson's ratio.

D.1.2 Orthotropic

$$w = \frac{4p}{\pi^4 ab} \sum_{m=1,3,5,\dots}^{\infty} \sum_{n=1,3,5,\dots}^{\infty} \frac{\sin\left(\frac{m\pi}{2}\right)^2 \sin\left(\frac{n\pi}{2}\right)^2}{\left[\left(\frac{m^4}{a^4}\right) D_x + 2\left(\frac{m^2 n^2}{a^2 b^2}\right) D + \left(\frac{n^4}{b^4}\right) D_y\right]} \quad (\text{D.3})$$

where:

$$D_x = \frac{h^3 E_x}{12(1 - \nu_x \nu_y)} \quad (\text{D.4})$$

$$D_y = \frac{h^3 E_y}{12(1 - \nu_x \nu_y)} \quad (\text{D.5})$$

$$D = D_{xy} + 2G_{xy} \quad (\text{D.6})$$

$$D_{xy} = \frac{h^3 E_x \nu_y}{12(1 - \nu_x \nu_y)} = \frac{h^3 E_y \nu_x}{12(1 - \nu_x \nu_y)} \quad (\text{D.7})$$

$$G_{xy} = \frac{h^3 G}{12} \quad (\text{D.8})$$

where: a = Plate length, b = Plate width, E_x = Plate modulus of elasticity in the local x-direction. E_y = Plate modulus of elasticity in the local y-direction. G = Plate modulus of rigidity in the local x-y plane. ν_x = Plate Poisson's ratio in the local x-direction. and ν_y = Plate Poisson's ratio in the local y-direction.

D.1.3 Isotropic (Transverse Shear Flexible)

$$\begin{bmatrix} a_{11} & a_{12} & a_{13} \\ a_{21} & a_{22} & a_{23} \\ a_{31} & a_{32} & a_{33} \end{bmatrix} \begin{Bmatrix} w \\ \psi_1 \\ \psi_2 \end{Bmatrix} = \begin{Bmatrix} P \\ 0 \\ 0 \end{Bmatrix} \quad (\text{D.9})$$

where:

$$a_{11} = kGh \left[\left(\frac{m\pi}{a} \right)^2 + \left(\frac{n\pi}{b} \right)^2 \right] \quad (\text{D.10})$$

$$a_{22} = D \left[\left(\frac{m\pi}{a} \right)^2 + \frac{1-\nu}{2} \left(\frac{n\pi}{b} \right)^2 \right] + kGh \quad (\text{D.11})$$

$$a_{33} = D \left[\frac{1-\nu}{2} \left(\frac{m\pi}{a} \right)^2 + \left(\frac{n\pi}{b} \right)^2 \right] + kGh \quad (\text{D.12})$$

$$a_{12} = a_{21} = kGh \frac{m\pi}{a} \quad (\text{D.13})$$

$$a_{13} = a_{31} = kGh \frac{n\pi}{b} \quad (\text{D.14})$$

$$a_{23} = a_{32} = D \left(\frac{1+\nu}{2} \right) \frac{m\pi}{a} \frac{n\pi}{b} \quad (\text{D.15})$$

$$P = \frac{4p}{ab} \sin \left(\frac{m\pi}{2} \right) \sin \left(\frac{n\pi}{2} \right) \quad (\text{D.16})$$

where: a = Plate length, b = Plate width, ψ_1, ψ_2 = Shear rotations, k = Shear form factor, G = Plate modulus of rigidity, h = Plate thickness, and D = Plate Bending Stiffness (See D.1.1).

D.1.4 Isotropic (Equidistant Stiffeners)

$$u' = \frac{4p}{\pi^4 ab} \sum_{m=1,3,5,\dots}^{\infty} \sum_{n=1,3,5,\dots}^{\infty} \frac{\sin\left(\frac{m\pi}{2}\right)^2 \sin\left(\frac{n\pi}{2}\right)^2}{\left[\left(\frac{m^4}{a^4}\right) D_x + 2\left(\frac{m^2 n^2}{a^2 b^2}\right) D + \left(\frac{n^4}{b^4}\right) D_y\right]} \quad (\text{D.17})$$

where:

$$D_x = \frac{E s t^3}{12 \left[s - h + h \left(\frac{t}{t_1} \right)^3 \right]} \quad (\text{D.18})$$

$$D_y = \frac{EI}{s} \quad (\text{D.19})$$

$$D = 2G'_{xy} + \frac{C}{s} \quad (\text{D.20})$$

where: a = Plate length, b = Plate width, E = Plate modulus of elasticity, s = Stiffener spacing, h = Stiffener width, t = Plate thickness, t_1 = Combined depth of plate and stiffener, I = Area moment of inertia about the neutral axis of a T-section, G'_{xy} = Plate torsional rigidity, and C = Stiffener torsional rigidity. See Timoshenko and Woinowsky-Krieger (1959) or Ugural (1981) for more details. It is important to note that this solution provides a rough estimate, more exact theories are available.

D.1.5 Isotropic (Dual Span)

$$w = \frac{b^2}{4\pi^2 D} \sum_{m=1,3,5,\dots}^{\infty} \frac{A}{m^2} (-1)^{\left(\frac{m-1}{2}\right)} \left(\frac{\beta_m \tanh(\beta_m)}{\cosh(\beta_m)} \right) \quad (\text{D.21})$$

where:

$$A = \frac{-p}{m\pi} (-1)^{\frac{m-1}{2}} \left[\frac{\beta_m \tanh(\beta_m)}{\cosh(\beta_m) \left(\tanh(\beta_m) + \coth(\beta_m) + \frac{\beta_m}{\cosh(\beta_m)^2} - \frac{\beta_m}{\sinh(\beta_m)^2} \right)} \right] \quad (\text{D.22})$$

$$\beta_m = \frac{m\pi a}{2b} \quad (\text{D.23})$$

where: a = Plate length. b = Plate width. D = Plate Bending Stiffness (See D.1.1). For the solution described, the plate spans are assumed to have equal length and width. Furthermore, w represents the displacement at the center of the right span, while the location of the concentrated load p is at the center of the left span.

D.2 Dynamic Response

D.2.1 Isotropic

The natural frequencies can be expressed as:

$$\omega_{m,n} = \pi^2 \left[\left(\frac{m}{a} \right)^2 + \left(\frac{n}{b} \right)^2 \right] \sqrt{\frac{D}{\rho}} \quad (\text{D.24})$$

where:

$$D = \frac{Eh^3}{12(1 - \nu^2)} \quad (\text{D.25})$$

where: $\omega_{m,n}$ = Plate natural frequencies (radians/second), a = Plate length, b = Plate width, E = Plate modulus of elasticity, h = Plate thickness, ν = Plate Poisson's ratio, and ρ = Plate mass density. Plate natural frequencies can alternatively be expressed in terms of Hertz as:

$$f_{m,n} = \frac{\omega_{m,n}}{2\pi} \quad (\text{D.26})$$

where: $f_{m,n}$ = Plate natural frequencies (Hertz).

Time-history expressions have been constructed to take into account a time-zero step function input force (Figure D.1). In each of the following expressions: a = Plate length, b = Plate width, ρ = Plate mass density, $\zeta_{m,n}$ = Plate viscous damping factors as percent of critical, and:

$$\omega_{dm,n} = \omega_{m,n} \sqrt{1 - \zeta_{m,n}^2} \quad (\text{D.27})$$

where: $\omega_{dm,n}$ = Plate damped natural frequencies (radians/second).

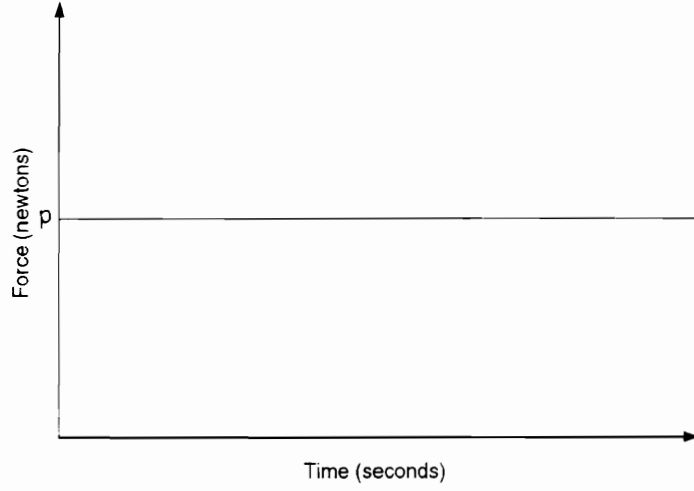


Figure D.1 Graphical Representation of Time-Zero Step Function.

Displacement time-history can be expressed:

$$u = \frac{4p}{\rho ab} \sum_{m=1,2,3,\dots}^{\infty} \sum_{n=1,2,3,\dots}^{\infty} A \left[1 - e^{-\zeta_{m,n}\omega_{m,n}t} \left(\cos(\omega_{dm,n}t) + \frac{\zeta_{m,n}\omega_{m,n}}{\omega_{dm,n}} \sin(\omega_{dm,n}t) \right) \right] \quad (D.28)$$

where:

$$A = \frac{1}{\omega_{m,n}^2} \left[\sin\left(\frac{m\pi}{2}\right)^2 \sin\left(\frac{n\pi}{2}\right)^2 \right] \quad (D.29)$$

Velocity time history can be expressed:

$$\dot{u} = \frac{4p}{\rho ab} \sum_{m=1,2,3,\dots}^{\infty} \sum_{n=1,2,3,\dots}^{\infty} A \left[\left[\frac{\omega_{dm,n}}{\omega_{m,n}^2} + \frac{\zeta_{m,n}^2}{\omega_{dm,n}} \right] e^{-\zeta_{m,n}\omega_{m,n}t} \sin(\omega_{dm,n}t) \right] \quad (D.30)$$

where:

$$A = \left[\sin \left(\frac{m\pi}{2} \right)^2 \sin \left(\frac{n\pi}{2} \right)^2 \right] \quad (\text{D.31})$$

Acceleration time-history can be expressed:

$$\ddot{u} = \frac{4p}{\rho ab} \sum_{m=1,2,3,\dots}^{\infty} \sum_{n=1,2,3,\dots}^{\infty} A \left[e^{-\zeta_{m,n}\omega_{m,n}t} \{ B \cos(\omega_{dm,n}t) - C \sin(\omega_{dm,n}t) \} \right] \quad (\text{D.32})$$

where:

$$A = \left[\sin \left(\frac{m\pi}{2} \right)^2 \sin \left(\frac{n\pi}{2} \right)^2 \right] \quad (\text{D.33})$$

$$B = \left[\frac{\omega_{dm,n}^2}{\omega_{m,n}^2} + \zeta_{m,n}^2 \right] \quad (\text{D.34})$$

$$C = \zeta_{m,n} \left[\frac{\omega_{dm,n}}{\omega_{m,n}} + \frac{\zeta_{m,n}^2 \omega_{m,n}}{\omega_{dm,n}} \right] \quad (\text{D.35})$$

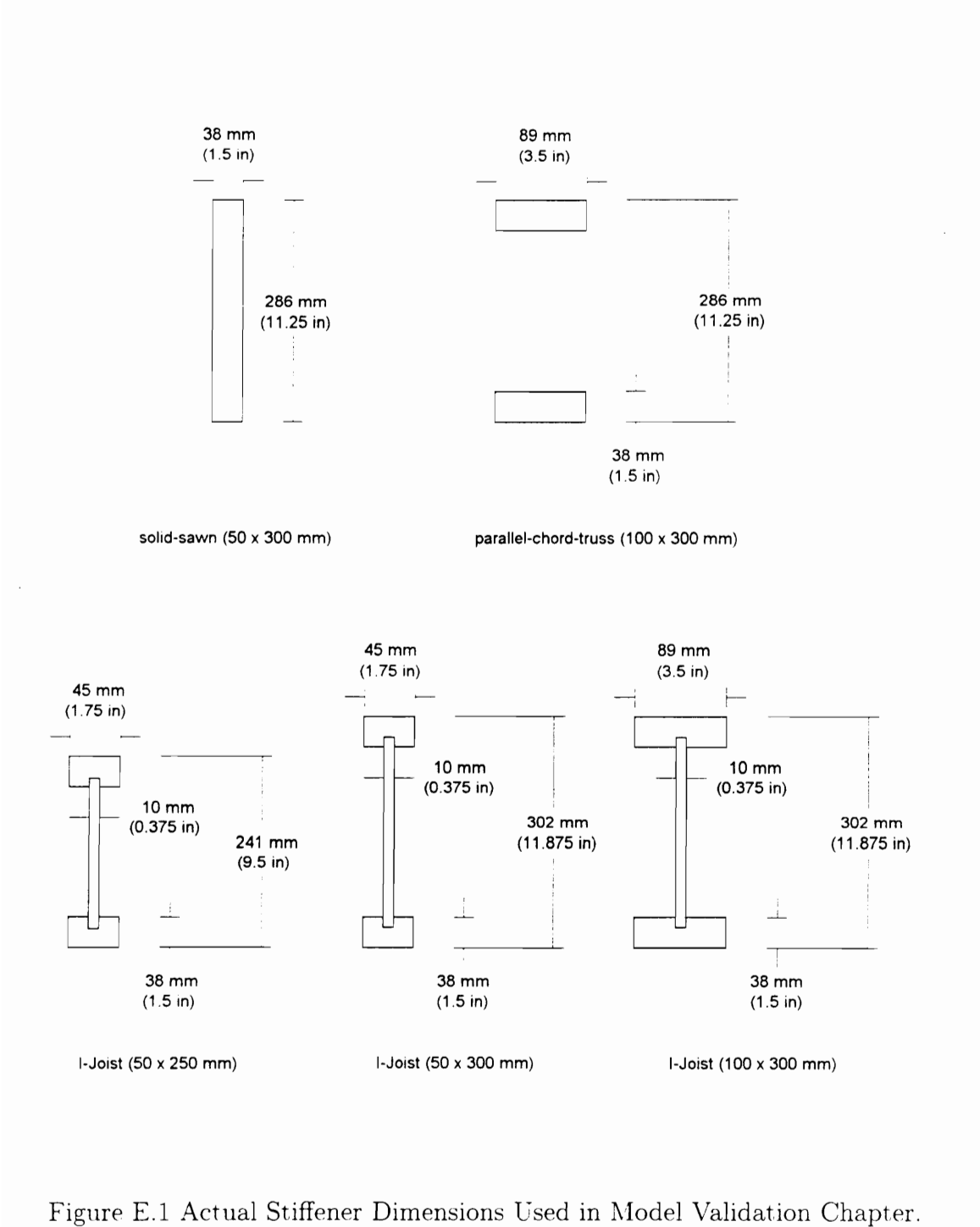
Appendix E

Quick Reference

This appendix was constructed to provide a central repository of information regarding the material properties, structural geometry, and mesh geometry associated with the analyses found in this dissertation.

E.1 Model Validation

Actual stiffener dimensions used in the Model Validation chapter are shown in Figure E.1. Following Figure E.1, material properties and mesh geometry are considered for each individual floor.



Floor a

Floor Specifics:

	FLOOR LENGTH:	4.88 m
	FLOOR WIDTH:	4.88 m
NUMBER OF STIFFENERS SPANNING IN THE GLOBAL X-DIRECTION:		9
SPACING OF STIFFENERS SPANNING IN THE GLOBAL X-DIRECTION:		600. mm

Sheathing Specifics:

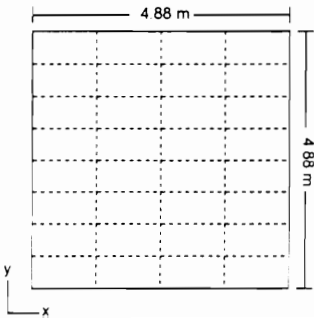
	THICKNESS:	18. mm
MODULUS OF ELASTICITY IN THE GLOBAL X-DIRECTION:		3018. N/mm ²
MODULUS OF ELASTICITY IN THE GLOBAL Y-DIRECTION:		5133. N/mm ²
POISSON RATIO IN THE GLOBAL X-DIRECTION:		.235
POISSON RATIO IN THE GLOBAL Y-DIRECTION:		.400
SHEAR MODULUS IN THE GLOBAL X-Y PLANE:		621. N/mm ²
SHEAR MODULUS IN THE GLOBAL X-Z AND Y-Z PLANES:		621. N/mm ²
SHEAR MODULUS FORM FACTOR:		1.20
	DENSITY:	5498. N/m ³

Stiffener Specifics:

STIFFENERS SPANNING IN THE GLOBAL X-DIRECTION

STIFFENER	E (N/mm ²)	I (mm ⁴)	J (mm ⁴)	A (mm ²)	G (N/mm ²)	K	DENSITY (N/m ³)
1	10611.	7.40D7	4.82D6	10890.	663.	1.20	6283.
2	9853.	7.40D7	4.82D6	10890.	616.	1.20	6283.
3	10611.	7.40D7	4.82D6	10890.	663.	1.20	6283.
4	11231.	7.40D7	4.82D6	10890.	702.	1.20	6283.
5	9026.	7.40D7	4.82D6	10890.	564.	1.20	6283.
6	11162.	7.40D7	4.82D6	10890.	698.	1.20	6283.
7	10748.	7.40D7	4.82D6	10890.	672.	1.20	6283.
8	10197.	7.40D7	4.82D6	10890.	637.	1.20	6283.
9	8544.	7.40D7	4.82D6	10890.	534.	1.20	6283.

Mesh Layout:



Floor b

Floor Specifics:

	FLOOR LENGTH:	4.88 m
	FLOOR WIDTH:	4.88 m
NUMBER OF STIFFENERS SPANNING IN THE GLOBAL X-DIRECTION:		9
SPACING OF STIFFENERS SPANNING IN THE GLOBAL X-DIRECTION:		600. mm

Sheathing Specifics:

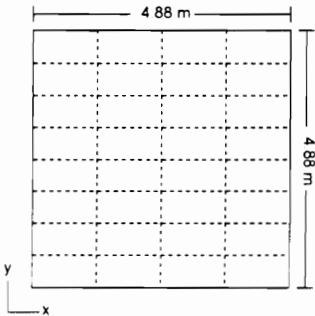
	THICKNESS:	18. mm
MODULUS OF ELASTICITY IN THE GLOBAL X-DIRECTION:		3218. N/mm ²
MODULUS OF ELASTICITY IN THE GLOBAL Y-DIRECTION:		3459. N/mm ²
POISSON RATIO IN THE GLOBAL X-DIRECTION:		.279
POISSON RATIO IN THE GLOBAL Y-DIRECTION:		.300
SHEAR MODULUS IN THE GLOBAL X-Y PLANE:		621. N/mm ²
SHEAR MODULUS IN THE GLOBAL X-Z AND Y-Z PLANES:		621. N/mm ²
SHEAR MODULUS FORM FACTOR:		1.20
	DENSITY:	5498. N/m ³

Stiffener Specifics:

STIFFENERS SPANNING IN THE GLOBAL X-DIRECTION

STIFFENER	E (N/mm ²)	I (mm ⁴)	J (mm ⁴)	A (mm ²)	G (N/mm ²)	K	DENSITY (N/m ³)
1	10611.	7.40D7	4.82D6	10890.	663.	1.20	6283.
2	9784.	7.40D7	4.82D6	10890.	611.	1.20	6283.
3	10611.	7.40D7	4.82D6	10890.	663.	1.20	6283.
4	11162.	7.40D7	4.82D6	10890.	698.	1.20	6283.
5	9026.	7.40D7	4.82D6	10890.	564.	1.20	6283.
6	11093.	7.40D7	4.82D6	10890.	693.	1.20	6283.
7	10680.	7.40D7	4.82D6	10890.	667.	1.20	6283.
8	10128.	7.40D7	4.82D6	10890.	633.	1.20	6283.
9	8613.	7.40D7	4.82D6	10890.	538.	1.20	6283.

Mesh Layout:



Floor c

Floor Specifics:

	FLOOR LENGTH:	4.88 m
	FLOOR WIDTH:	4.88 m
NUMBER OF STIFFENERS SPANNING IN THE GLOBAL X-DIRECTION:		9
SPACING OF STIFFENERS SPANNING IN THE GLOBAL X-DIRECTION:		600. mm

Sheathing Specifics:

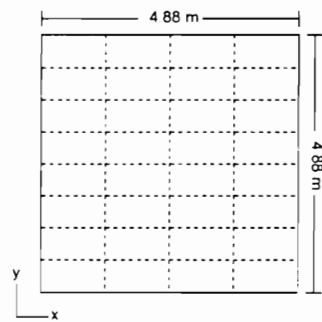
	THICKNESS:	18. mm
MODULUS OF ELASTICITY IN THE GLOBAL X-DIRECTION:		4086. N/mm ²
MODULUS OF ELASTICITY IN THE GLOBAL Y-DIRECTION:		4097. N/mm ²
POISSON RATIO IN THE GLOBAL X-DIRECTION:		.299
POISSON RATIO IN THE GLOBAL Y-DIRECTION:		.300
SHEAR MODULUS IN THE GLOBAL X-Y PLANE:		621. N/mm ²
SHEAR MODULUS IN THE GLOBAL X-Z AND Y-Z PLANES:		621. N/mm ²
SHEAR MODULUS FORM FACTOR:		1.20
	DENSITY:	5498. N/m ³

Stiffener Specifics:

STIFFENERS SPANNING IN THE GLOBAL X-DIRECTION

STIFFENER	E (N/mm ²)	I (mm ⁴)	J (mm ⁴)	A (mm ²)	G (N/mm ²)	K	DENSITY (N/m ³)
1	7303.	1.08D8	2.39D6	6774.	276.	1.20	9425.
2	8337.	1.08D8	2.39D6	6774.	276.	1.20	9425.
3	7235.	1.08D8	2.39D6	6774.	276.	1.20	9425.
4	7372.	1.08D8	2.39D6	6774.	276.	1.20	9425.
5	7510.	1.08D8	2.39D6	6774.	276.	1.20	9425.
6	7235.	1.08D8	2.39D6	6774.	276.	1.20	9425.
7	6959.	1.08D8	2.39D6	6774.	276.	1.20	9425.
8	7510.	1.08D8	2.39D6	6774.	276.	1.20	9425.
9	8406.	1.08D8	2.39D6	6774.	276.	1.20	9425.

Mesh Lavout:



Floor d

Floor Specifics:

	FLOOR LENGTH:	4.88 m
	FLOOR WIDTH:	4.88 m
NUMBER OF STIFFENERS SPANNING IN THE GLOBAL X-DIRECTION:		9
SPACING OF STIFFENERS SPANNING IN THE GLOBAL X-DIRECTION:		600. mm

Sheathing Specifics:

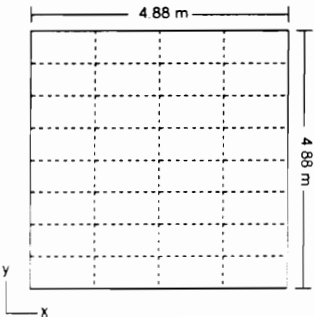
	THICKNESS:	18. mm
MODULUS OF ELASTICITY IN THE GLOBAL X-DIRECTION:		3845. N/mm ²
MODULUS OF ELASTICITY IN THE GLOBAL Y-DIRECTION:		3480. N/mm ²
POISSON RATIO IN THE GLOBAL X-DIRECTION:		.332
POISSON RATIO IN THE GLOBAL Y-DIRECTION:		.300
SHEAR MODULUS IN THE GLOBAL X-Y PLANE:		621. N/mm ²
SHEAR MODULUS IN THE GLOBAL X-Z AND Y-Z PLANES:		621. N/mm ²
SHEAR MODULUS FORM FACTOR:		1.20
	DENSITY:	5498. N/m ³

Stiffener Specifics:

STIFFENERS SPANNING IN THE GLOBAL X-DIRECTION

STIFFENER	E (N/mm ²)	I (mm ⁴)	J (mm ⁴)	A (mm ²)	G (N/mm ²)	K	DENSITY (N/m ³)
1	8130.	1.08D8	2.39D6	6774.	276.	1.20	9425.
2	8406.	1.08D8	2.39D6	6774.	276.	1.20	9425.
3	7786.	1.08D8	2.39D6	6774.	276.	1.20	9425.
4	7717.	1.08D8	2.39D6	6774.	276.	1.20	9425.
5	7786.	1.08D8	2.39D6	6774.	276.	1.20	9425.
6	8199.	1.08D8	2.39D6	6774.	276.	1.20	9425.
7	6821.	1.08D8	2.39D6	6774.	276.	1.20	9425.
8	7166.	1.08D8	2.39D6	6774.	276.	1.20	9425.
9	8544.	1.08D8	2.39D6	6774.	276.	1.20	9425.

Mesh Layout:



Floor e

Floor Specifics:

	FLOOR LENGTH:	4.88 m
	FLOOR WIDTH:	4.88 m
NUMBER OF STIFFENERS SPANNING IN THE GLOBAL X-DIRECTION:		9
SPACING OF STIFFENERS SPANNING IN THE GLOBAL X-DIRECTION:		600. mm

Sheathing Specifics:

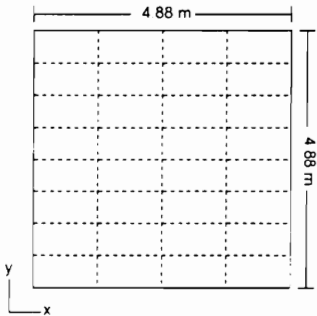
	THICKNESS:	18. mm
MODULUS OF ELASTICITY IN THE GLOBAL X-DIRECTION:		3542. N/mm ²
MODULUS OF ELASTICITY IN THE GLOBAL Y-DIRECTION:		3824. N/mm ²
POISSON RATIO IN THE GLOBAL X-DIRECTION:		.278
POISSON RATIO IN THE GLOBAL Y-DIRECTION:		.300
SHEAR MODULUS IN THE GLOBAL X-Y PLANE:		621. N/mm ²
SHEAR MODULUS IN THE GLOBAL X-Z AND Y-Z PLANES:		621. N/mm ²
SHEAR MODULUS FORM FACTOR:		1.20
DENSITY:		5498. N/m ³

Stiffener Specifics:

STIFFENERS SPANNING IN THE GLOBAL X-DIRECTION

STIFFENER	E (N/mm ²)	I (mm ⁴)	J (mm ⁴)	A (mm ²)	G (N/mm ²)	K	DENSITY (N/m ³)
1	6339.	1.08D8	2.39D6	6774.	276.	1.20	9425.
2	8130.	1.08D8	2.39D6	6774.	276.	1.20	9425.
3	8268.	1.08D8	2.39D6	6774.	276.	1.20	9425.
4	8681.	1.08D8	2.39D6	6774.	276.	1.20	9425.
5	5650.	1.08D8	2.39D6	6774.	276.	1.20	9425.
6	5857.	1.08D8	2.39D6	6774.	276.	1.20	9425.
7	8681.	1.08D8	2.39D6	6774.	276.	1.20	9425.
8	8130.	1.08D8	2.39D6	6774.	276.	1.20	9425.
9	8199.	1.08D8	2.39D6	6774.	276.	1.20	9425.

Mesh Layout:



Floor f

Floor Specifics:

	FLOOR LENGTH:	4.88 m
	FLOOR WIDTH:	4.88 m
NUMBER OF STIFFENERS SPANNING IN THE GLOBAL X-DIRECTION:		9
SPACING OF STIFFENERS SPANNING IN THE GLOBAL X-DIRECTION:		600. mm

Sheathing Specifics:

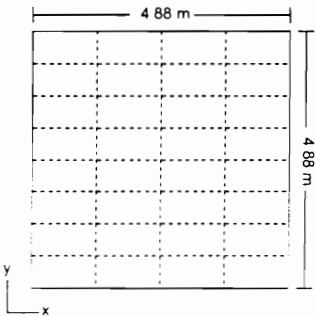
	THICKNESS:	18. mm
MODULUS OF ELASTICITY IN THE GLOBAL X-DIRECTION:		3941. N/mm ²
MODULUS OF ELASTICITY IN THE GLOBAL Y-DIRECTION:		3707. N/mm ²
POISSON RATIO IN THE GLOBAL X-DIRECTION:		.319
POISSON RATIO IN THE GLOBAL Y-DIRECTION:		.300
SHEAR MODULUS IN THE GLOBAL X-Y PLANE:		621. N/mm ²
SHEAR MODULUS IN THE GLOBAL X-Z AND Y-Z PLANES:		621. N/mm ²
SHEAR MODULUS FORM FACTOR:		1.20
	DENSITY:	5498. N/m ³

Stiffener Specifics:

STIFFENERS SPANNING IN THE GLOBAL X-DIRECTION

STIFFENER	E (N/mm ²)	I (mm ⁴)	J (mm ⁴)	A (mm ²)	G (N/mm ²)	K	DENSITY (N/m ³)
1	11506.	3.89D7	8.45D5	4961.	621.	3.15	7069.
2	15020.	3.89D7	8.45D5	4961.	621.	3.15	7069.
3	12540.	3.89D7	8.45D5	4961.	621.	3.15	7069.
4	12264.	3.89D7	8.45D5	4961.	621.	3.15	7069.
5	12884.	3.89D7	8.45D5	4961.	621.	3.15	7069.
6	16398.	3.89D7	8.45D5	4961.	621.	3.15	7069.
7	11231.	3.89D7	8.45D5	4961.	621.	3.15	7069.
8	10197.	3.89D7	8.45D5	4961.	621.	3.15	7069.
9	12884.	3.89D7	8.45D5	4961.	621.	3.15	7069.

Mesh Layout:



Floor g

Floor Specifics:

	FLOOR LENGTH:	4.88 m
	FLOOR WIDTH:	4.88 m
NUMBER OF STIFFENERS SPANNING IN THE GLOBAL X-DIRECTION:		9
SPACING OF STIFFENERS SPANNING IN THE GLOBAL X-DIRECTION:		600. mm

Sheathing Specifics:

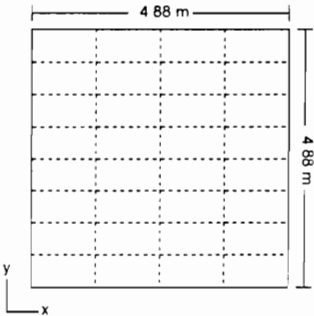
	THICKNESS:	18. mm
MODULUS OF ELASTICITY IN THE GLOBAL X-DIRECTION:		3645. N/mm ²
MODULUS OF ELASTICITY IN THE GLOBAL Y-DIRECTION:		3865. N/mm ²
POISSON RATIO IN THE GLOBAL X-DIRECTION:		.283
POISSON RATIO IN THE GLOBAL Y-DIRECTION:		.300
SHEAR MODULUS IN THE GLOBAL X-Y PLANE:		621. N/mm ²
SHEAR MODULUS IN THE GLOBAL X-Z AND Y-Z PLANES:		621. N/mm ²
SHEAR MODULUS FORM FACTOR:		1.20
	DENSITY:	5498. N/m ³

Stiffener Specifics:

STIFFENERS SPANNING IN THE GLOBAL X-DIRECTION

STIFFENER	E (N/mm ²)	I (mm ⁴)	J (mm ⁴)	A (mm ²)	G (N/mm ²)	K	DENSITY (N/m ³)
1	12540.	3.89D7	8.45D5	4961.	621.	3.15	7069.
2	8475.	3.89D7	8.45D5	4961.	621.	3.15	7069.
3	10611.	3.89D7	8.45D5	4961.	621.	3.15	7069.
4	13160.	3.89D7	8.45D5	4961.	621.	3.15	7069.
5	13160.	3.89D7	8.45D5	4961.	621.	3.15	7069.
6	14193.	3.89D7	8.45D5	4961.	621.	3.15	7069.
7	12540.	3.89D7	8.45D5	4961.	621.	3.15	7069.
8	10197.	3.89D7	8.45D5	4961.	621.	3.15	7069.
9	11231.	3.89D7	8.45D5	4961.	621.	3.15	7069.

Mesh Layout:



Floor h

Floor Specifics:

	FLOOR LENGTH:	4.88 m
	FLOOR WIDTH:	4.88 m
NUMBER OF STIFFENERS SPANNING IN THE GLOBAL X-DIRECTION:		9
SPACING OF STIFFENERS SPANNING IN THE GLOBAL X-DIRECTION:		600. mm

Sheathing Specifics:

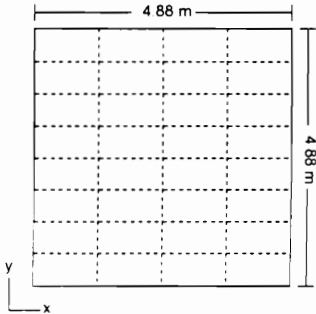
	THICKNESS:	18. mm
MODULUS OF ELASTICITY IN THE GLOBAL X-DIRECTION:		3783. N/mm ²
MODULUS OF ELASTICITY IN THE GLOBAL Y-DIRECTION:		3914. N/mm ²
POISSON RATIO IN THE GLOBAL X-DIRECTION:		.290
POISSON RATIO IN THE GLOBAL Y-DIRECTION:		.300
SHEAR MODULUS IN THE GLOBAL X-Y PLANE:		621. N/mm ²
SHEAR MODULUS IN THE GLOBAL X-Z AND Y-Z PLANES:		621. N/mm ²
SHEAR MODULUS FORM FACTOR:		1.20
	DENSITY:	5498. N/m ³

Stiffeners Specifics:

STIFFENERS SPANNING IN THE GLOBAL X-DIRECTION

STIFFENER	E (N/mm ²)	I (mm ⁴)	J (mm ⁴)	A (mm ²)	G (N/mm ²)	K	DENSITY (N/m ³)
1	6270.	6.83D7	8.62D5	5535.	621.	2.58	7069.
2	11851.	6.83D7	8.62D5	5535.	621.	2.58	7069.
3	13367.	6.83D7	8.62D5	5535.	621.	2.58	7069.
4	12815.	6.83D7	8.62D5	5535.	621.	2.58	7069.
5	12333.	6.83D7	8.62D5	5535.	621.	2.58	7069.
6	18121.	6.83D7	8.62D5	5535.	621.	2.58	7069.
7	12815.	6.83D7	8.62D5	5535.	621.	2.58	7069.
8	11851.	6.83D7	8.62D5	5535.	621.	2.58	7069.
9	12815.	6.83D7	8.62D5	5535.	621.	2.58	7069.

Mesh Layout:



Floor i

Floor Specifics:

	FLOOR LENGTH:	4.88 m
	FLOOR WIDTH:	4.88 m
NUMBER OF STIFFENERS SPANNING IN THE GLOBAL X-DIRECTION:		9
SPACING OF STIFFENERS SPANNING IN THE GLOBAL X-DIRECTION:		600. mm

Sheathing Specifics:

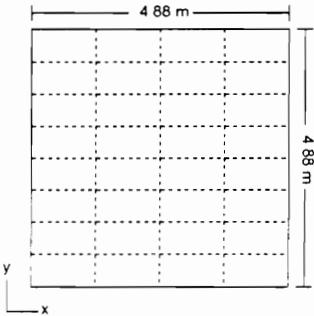
	THICKNESS:	18. mm
MODULUS OF ELASTICITY IN THE GLOBAL X-DIRECTION:		3803. N/mm ²
MODULUS OF ELASTICITY IN THE GLOBAL Y-DIRECTION:		4265. N/mm ²
POISSON RATIO IN THE GLOBAL X-DIRECTION:		.268
POISSON RATIO IN THE GLOBAL Y-DIRECTION:		.300
SHEAR MODULUS IN THE GLOBAL X-Y PLANE:		621. N/mm ²
SHEAR MODULUS IN THE GLOBAL X-Z AND Y-Z PLANES:		621. N/mm ²
SHEAR MODULUS FORM FACTOR:		1.20
	DENSITY:	5498. N/m ³

Stiffener Specifics:

STIFFENERS SPANNING IN THE GLOBAL X-DIRECTION

STIFFENER	E (N/mm ²)	I (mm ⁴)	J (mm ⁴)	A (mm ²)	G (N/mm ²)	K	DENSITY (N/m ³)
1	12333.	6.83D7	8.62D5	5535.	621.	2.58	7069.
2	12884.	6.83D7	8.62D5	5535.	621.	2.58	7069.
3	11024.	6.83D7	8.62D5	5535.	621.	2.58	7069.
4	11437.	6.83D7	8.62D5	5535.	621.	2.58	7069.
5	11437.	6.83D7	8.62D5	5535.	621.	2.58	7069.
6	15434.	6.83D7	8.62D5	5535.	621.	2.58	7069.
7	12333.	6.83D7	8.62D5	5535.	621.	2.58	7069.
8	11024.	6.83D7	8.62D5	5535.	621.	2.58	7069.
9	12333.	6.83D7	8.62D5	5535.	621.	2.58	7069.

Mesh Lavout:



Floor j

Floor Specifics:

	FLOOR LENGTH:	4.88 m
	FLOOR WIDTH:	4.88 m
NUMBER OF STIFFENERS SPANNING IN THE GLOBAL X-DIRECTION:		9
SPACING OF STIFFENERS SPANNING IN THE GLOBAL X-DIRECTION:		600. mm

Sheathing Specifics:

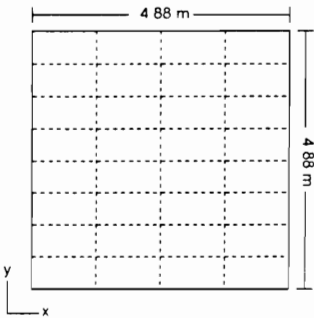
	THICKNESS:	18. mm
MODULUS OF ELASTICITY IN THE GLOBAL X-DIRECTION:		4417. N/mm ²
MODULUS OF ELASTICITY IN THE GLOBAL Y-DIRECTION:		4596. N/mm ²
POISSON RATIO IN THE GLOBAL X-DIRECTION:		.288
POISSON RATIO IN THE GLOBAL Y-DIRECTION:		.300
SHEAR MODULUS IN THE GLOBAL X-Y PLANE:		621. N/mm ²
SHEAR MODULUS IN THE GLOBAL X-Z AND Y-Z PLANES:		621. N/mm ²
SHEAR MODULUS FORM FACTOR:		1.20
	DENSITY:	5498. N/m ³

Stiffener Specifics:

STIFFENERS SPANNING IN THE GLOBAL X-DIRECTION

STIFFENER	E (N/mm ²)	I (mm ⁴)	J (mm ⁴)	A (mm ²)	G (N/mm ²)	K	DENSITY (N/m ³)
1	9922.	1.28D8	2.46D6	8923.	621.	4.16	7069.
2	8337.	1.28D8	2.46D6	8923.	621.	4.16	7069.
3	9922.	1.28D8	2.46D6	8923.	621.	4.16	7069.
4	11300.	1.28D8	2.46D6	8923.	621.	4.16	7069.
5	10611.	1.28D8	2.46D6	8923.	621.	4.16	7069.
6	11369.	1.28D8	2.46D6	8923.	621.	4.16	7069.
7	9302.	1.28D8	2.46D6	8923.	621.	4.16	7069.
8	10611.	1.28D8	2.46D6	8923.	621.	4.16	7069.
9	9922.	1.28D8	2.46D6	8923.	621.	4.16	7069.

Mesh Layout:



Floor *k*

Floor Specifics:

	FLOOR LENGTH:	4.88 m
	FLOOR WIDTH:	4.88 m
NUMBER OF STIFFENERS SPANNING IN THE GLOBAL X-DIRECTION:		9
SPACING OF STIFFENERS SPANNING IN THE GLOBAL X-DIRECTION:		600. mm

Sheathing Specifics:

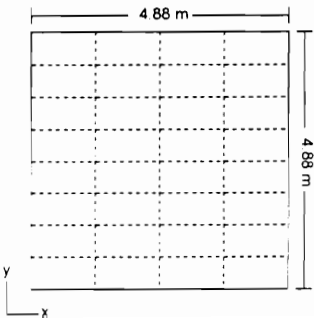
	THICKNESS:	18. mm
MODULUS OF ELASTICITY IN THE GLOBAL X-DIRECTION:		3631. N/mm ²
MODULUS OF ELASTICITY IN THE GLOBAL Y-DIRECTION:		4479. N/mm ²
POISSON RATIO IN THE GLOBAL X-DIRECTION:		.243
POISSON RATIO IN THE GLOBAL Y-DIRECTION:		.300
SHEAR MODULUS IN THE GLOBAL X-Y PLANE:		621. N/mm ²
SHEAR MODULUS IN THE GLOBAL X-Z AND Y-Z PLANES:		621. N/mm ²
	SHEAR MODULUS FORM FACTOR:	1.20
	DENSITY:	5498. N/m ³

Stiffener Specifics:

STIFFENERS SPANNING IN THE GLOBAL X-DIRECTION

STIFFENER	E (N/mm ²)	I (mm ⁴)	J (mm ⁴)	A (mm ²)	G (N/mm ²)	K	DENSITY (N/m ³)
1	10748.	1.28D8	2.46D6	8923.	621.	4.16	7069.
2	10404.	1.28D8	2.46D6	8923.	621.	4.16	7069.
3	9577.	1.28D8	2.46D6	8923.	621.	4.16	7069.
4	9646.	1.28D8	2.46D6	8923.	621.	4.16	7069.
5	9233.	1.28D8	2.46D6	8923.	621.	4.16	7069.
6	9853.	1.28D8	2.46D6	8923.	621.	4.16	7069.
7	10680.	1.28D8	2.46D6	8923.	621.	4.16	7069.
8	10680.	1.28D8	2.46D6	8923.	621.	4.16	7069.
9	10955.	1.28D8	2.46D6	8923.	621.	4.16	7069.

Mesh Layout:



E.2 Performance Improvement Investigation

The actual stiffener dimensions used in the Performance Improvement Investigation chapter are shown in Figures E.2a and E.2b. Following Figures E.2a and E.2b, material properties and mesh geometry are considered for each individual, unmodified floor.



Figure E.2a Actual Stiffener Dimensions Used in Performance Improvement Investigation Chapter.

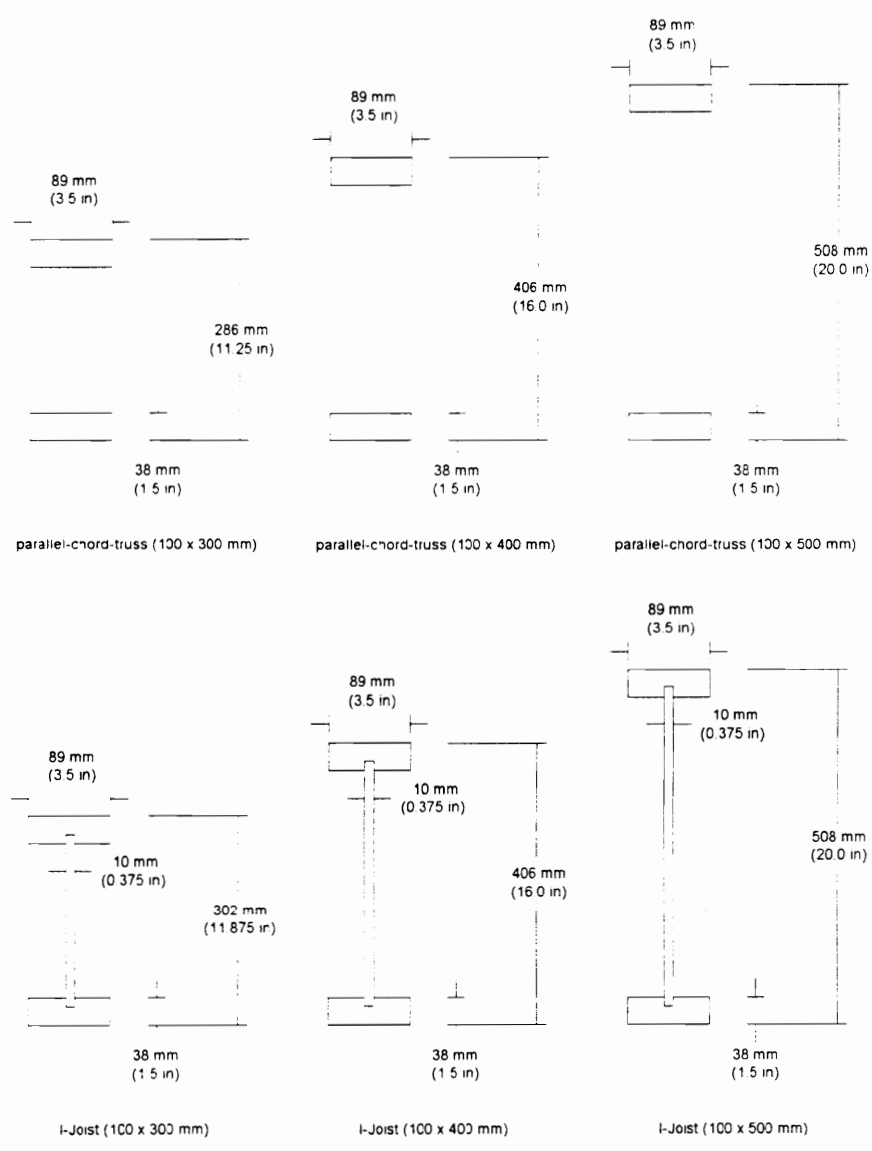


Figure E.2b Actual Stiffener Dimensions Used in Performance Improvement Investigation Chapter.

Floor A

Floor Specifics:

	FLOOR LENGTH:	4.88 m
	FLOOR WIDTH:	4.88 m
NUMBER OF STIFFENERS SPANNING IN THE GLOBAL X-DIRECTION:		9
SPACING OF STIFFENERS SPANNING IN THE GLOBAL X-DIRECTION:		600. mm

Sheathing Specifics:

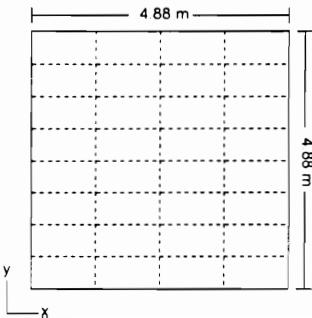
	THICKNESS:	18. mm
MODULUS OF ELASTICITY IN THE GLOBAL X-DIRECTION:		3721. N/mm ²
MODULUS OF ELASTICITY IN THE GLOBAL Y-DIRECTION:		4072. N/mm ²
POISSON RATIO IN THE GLOBAL X-DIRECTION:		.274
POISSON RATIO IN THE GLOBAL Y-DIRECTION:		.300
SHEAR MODULUS IN THE GLOBAL X-Y PLANE:		621. N/mm ²
SHEAR MODULUS IN THE GLOBAL X-Z AND Y-Z PLANES:		621. N/mm ²
SHEAR MODULUS FORM FACTOR:		1.20
	DENSITY:	5498. N/m ³

Stiffener Specifics:

STIFFENERS SPANNING IN THE GLOBAL X-DIRECTION

STIFFENER	E (N/mm ²)	I (mm ⁴)	J (mm ⁴)	A (mm ²)	G (N/mm ²)	K	DENSITY (N/m ³)
1	11024.	7.40D7	4.82D6	10890.	689.	1.20	6283.
2	11024.	7.40D7	4.82D6	10890.	689.	1.20	6283.
3	11024.	7.40D7	4.82D6	10890.	689.	1.20	6283.
4	11024.	7.40D7	4.82D6	10890.	689.	1.20	6283.
5	11024.	7.40D7	4.82D6	10890.	689.	1.20	6283.
6	11024.	7.40D7	4.82D6	10890.	689.	1.20	6283.
7	11024.	7.40D7	4.82D6	10890.	689.	1.20	6283.
8	11024.	7.40D7	4.82D6	10890.	689.	1.20	6283.
9	11024.	7.40D7	4.82D6	10890.	689.	1.20	6283.

Mesh Lavout:



Floor B

Floor Specifics:

	FLOOR LENGTH:	4.88 m
	FLOOR WIDTH:	4.88 m
NUMBER OF STIFFENERS SPANNING IN THE GLOBAL X-DIRECTION:		9
SPACING OF STIFFENERS SPANNING IN THE GLOBAL X-DIRECTION:		600. mm

Sheathing Specifics:

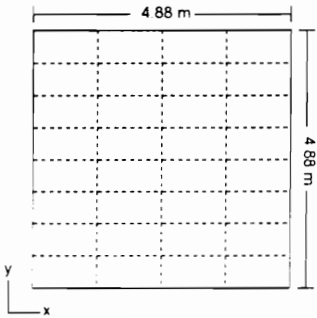
	THICKNESS:	18. mm
MODULUS OF ELASTICITY IN THE GLOBAL X-DIRECTION:		3721. N/mm ²
MODULUS OF ELASTICITY IN THE GLOBAL Y-DIRECTION:		4072. N/mm ²
POISSON RATIO IN THE GLOBAL X-DIRECTION:		.274
POISSON RATIO IN THE GLOBAL Y-DIRECTION:		.300
SHEAR MODULUS IN THE GLOBAL X-Y PLANE:		621. N/mm ²
SHEAR MODULUS IN THE GLOBAL X-Z AND Y-Z PLANES:		621. N/mm ²
SHEAR MODULUS FORM FACTOR:		1.20
	DENSITY:	5498. N/m ³

Stiffener Specifics:

STIFFENERS SPANNING IN THE GLOBAL X-DIRECTION

STIFFENER	E (N/mm ²)	I (mm ⁴)	J (mm ⁴)	A (mm ²)	G (N/mm ²)	K	DENSITY (N/m ³)
1	11024.	1.08D8	2.39D6	6774.	276.	1.20	9425.
2	11024.	1.08D8	2.39D6	6774.	276.	1.20	9425.
3	11024.	1.08D8	2.39D6	6774.	276.	1.20	9425.
4	11024.	1.08D8	2.39D6	6774.	276.	1.20	9425.
5	11024.	1.08D8	2.39D6	6774.	276.	1.20	9425.
6	11024.	1.08D8	2.39D6	6774.	276.	1.20	9425.
7	11024.	1.08D8	2.39D6	6774.	276.	1.20	9425.
8	11024.	1.08D8	2.39D6	6774.	276.	1.20	9425.
9	11024.	1.08D8	2.39D6	6774.	276.	1.20	9425.

Mesh Layout:



Floor C

Floor Specifics:

	FLOOR LENGTH:	7.32 m
	FLOOR WIDTH:	4.88 m
NUMBER OF STIFFENERS SPANNING IN THE GLOBAL X-DIRECTION:		9
SPACING OF STIFFENERS SPANNING IN THE GLOBAL X-DIRECTION:		600. mm

Sheathing Specifics:

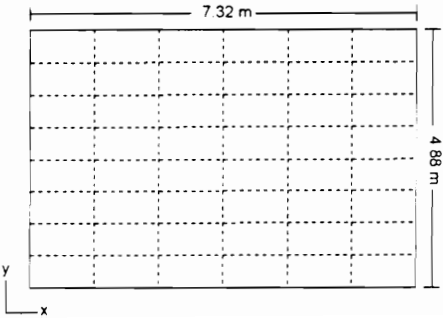
	THICKNESS:	18. mm
MODULUS OF ELASTICITY IN THE GLOBAL X-DIRECTION:		3721. N/mm ²
MODULUS OF ELASTICITY IN THE GLOBAL Y-DIRECTION:		4072. N/mm ²
POISSON RATIO IN THE GLOBAL X-DIRECTION:		.274
POISSON RATIO IN THE GLOBAL Y-DIRECTION:		.300
SHEAR MODULUS IN THE GLOBAL X-Y PLANE:		621. N/mm ²
SHEAR MODULUS IN THE GLOBAL X-Z AND Y-Z PLANES:		621. N/mm ²
SHEAR MODULUS FORM FACTOR:		1.20
	DENSITY:	5498. N/m ³

Stiffener Specifics:

STIFFENERS SPANNING IN THE GLOBAL X-DIRECTION

STIFFENER	E (N/mm ²)	I (mm ⁴)	J (mm ⁴)	A (mm ²)	G (N/mm ²)	K	DENSITY (N/m ³)
1	11024.	2.34D8	2.39D6	6774.	276.	1.20	9425.
2	11024.	2.34D8	2.39D6	6774.	276.	1.20	9425.
3	11024.	2.34D8	2.39D6	6774.	276.	1.20	9425.
4	11024.	2.34D8	2.39D6	6774.	276.	1.20	9425.
5	11024.	2.34D8	2.39D6	6774.	276.	1.20	9425.
6	11024.	2.34D8	2.39D6	6774.	276.	1.20	9425.
7	11024.	2.34D8	2.39D6	6774.	276.	1.20	9425.
8	11024.	2.34D8	2.39D6	6774.	276.	1.20	9425.
9	11024.	2.34D8	2.39D6	6774.	276.	1.20	9425.

Mesh Layout:



Floor D

Floor Specifics:

	FLOOR LENGTH:	9.15 m
	FLOOR WIDTH:	4.88 m
NUMBER OF STIFFENERS SPANNING IN THE GLOBAL X-DIRECTION:		9
SPACING OF STIFFENERS SPANNING IN THE GLOBAL X-DIRECTION:		600. mm

Sheathing Specifics:

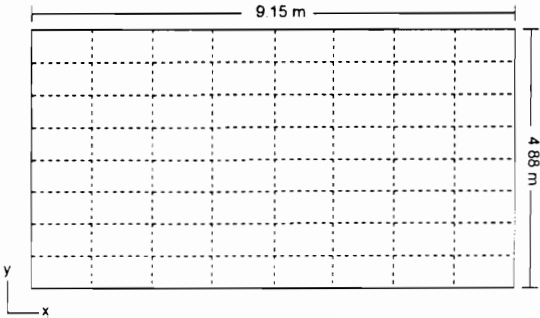
	THICKNESS:	18. mm
MODULUS OF ELASTICITY IN THE GLOBAL X-DIRECTION:		3721. N/mm ²
MODULUS OF ELASTICITY IN THE GLOBAL Y-DIRECTION:		4072. N/mm ²
POISSON RATIO IN THE GLOBAL X-DIRECTION:		.274
POISSON RATIO IN THE GLOBAL Y-DIRECTION:		.300
SHEAR MODULUS IN THE GLOBAL X-Y PLANE:		621. N/mm ²
SHEAR MODULUS IN THE GLOBAL X-Z AND Y-Z PLANES:		621. N/mm ²
SHEAR MODULUS FORM FACTOR:		1.20
	DENSITY:	5498. N/m ³

Stiffener Specifics:

STIFFENERS SPANNING IN THE GLOBAL X-DIRECTION

STIFFENER	E (N/mm ²)	I (mm ⁴)	J (mm ⁴)	A (mm ²)	G (N/mm ²)	K	DENSITY (N/m ³)
1	11024.	3.78D8	2.39D6	6774.	276.	1.20	9425.
2	11024.	3.78D8	2.39D6	6774.	276.	1.20	9425.
3	11024.	3.78D8	2.39D6	6774.	276.	1.20	9425.
4	11024.	3.78D8	2.39D6	6774.	276.	1.20	9425.
5	11024.	3.78D8	2.39D6	6774.	276.	1.20	9425.
6	11024.	3.78D8	2.39D6	6774.	276.	1.20	9425.
7	11024.	3.78D8	2.39D6	6774.	276.	1.20	9425.
8	11024.	3.78D8	2.39D6	6774.	276.	1.20	9425.
9	11024.	3.78D8	2.39D6	6774.	276.	1.20	9425.

Mesh Layout:



Floor E

Floor Specifics:

	FLOOR LENGTH:	4.88 m
	FLOOR WIDTH:	4.88 m
NUMBER OF STIFFENERS SPANNING IN THE GLOBAL X-DIRECTION:		9
SPACING OF STIFFENERS SPANNING IN THE GLOBAL X-DIRECTION:		600. mm

Sheathing Specifics:

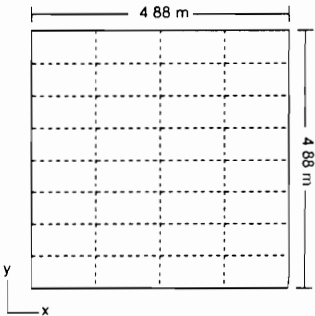
	THICKNESS:	18. mm
MODULUS OF ELASTICITY IN THE GLOBAL X-DIRECTION:		3721. N/mm ²
MODULUS OF ELASTICITY IN THE GLOBAL Y-DIRECTION:		4072. N/mm ²
POISSON RATIO IN THE GLOBAL X-DIRECTION:		.274
POISSON RATIO IN THE GLOBAL Y-DIRECTION:		.300
SHEAR MODULUS IN THE GLOBAL X-Y PLANE:		621. N/mm ²
SHEAR MODULUS IN THE GLOBAL X-Z AND Y-Z PLANES:		621. N/mm ²
SHEAR MODULUS FORM FACTOR:		1.20
	DENSITY:	5498. N/m ³

Stiffener Specifics:

STIFFENERS SPANNING IN THE GLOBAL X-DIRECTION

STIFFENER	E (N/mm ²)	I (mm ⁴)	J (mm ⁴)	A (mm ²)	G (N/mm ²)	K	DENSITY (N/m ³)
1	13780.	1.28D8	2.46D6	8923.	621.	4.16	7069.
2	13780.	1.28D8	2.46D6	8923.	621.	4.16	7069.
3	13780.	1.28D8	2.46D6	8923.	621.	4.16	7069.
4	13780.	1.28D8	2.46D6	8923.	621.	4.16	7069.
5	13780.	1.28D8	2.46D6	8923.	621.	4.16	7069.
6	13780.	1.28D8	2.46D6	8923.	621.	4.16	7069.
7	13780.	1.28D8	2.46D6	8923.	621.	4.16	7069.
8	13780.	1.28D8	2.46D6	8923.	621.	4.16	7069.
9	13780.	1.28D8	2.46D6	8923.	621.	4.16	7069.

Mesh Layout:



Floor F

Floor Specifics:

	FLOOR LENGTH:	7.32 m
	FLOOR WIDTH:	4.88 m
NUMBER OF STIFFENERS SPANNING IN THE GLOBAL X-DIRECTION:		9
SPACING OF STIFFENERS SPANNING IN THE GLOBAL X-DIRECTION:		600. mm

Sheathing Specifics:

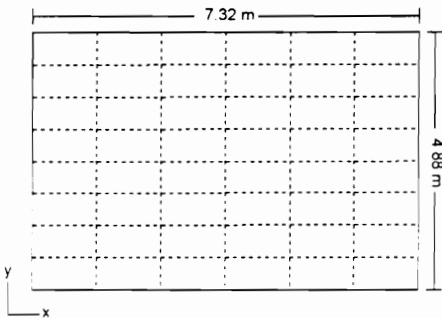
	THICKNESS:	18. mm
MODULUS OF ELASTICITY IN THE GLOBAL X-DIRECTION:		3721. N/mm ²
MODULUS OF ELASTICITY IN THE GLOBAL Y-DIRECTION:		4072. N/mm ²
POISSON RATIO IN THE GLOBAL X-DIRECTION:		.274
POISSON RATIO IN THE GLOBAL Y-DIRECTION:		.300
SHEAR MODULUS IN THE GLOBAL X-Y PLANE:		621. N/mm ²
SHEAR MODULUS IN THE GLOBAL X-Z AND Y-Z PLANES:		621. N/mm ²
SHEAR MODULUS FORM FACTOR:		1.20
	DENSITY:	5498. N/m ³

Stiffener Specifics:

STIFFENERS SPANNING IN THE GLOBAL X-DIRECTION

STIFFENER	E (N/mm ²)	I (mm ⁴)	J (mm ⁴)	A (mm ²)	G (N/mm ²)	K	DENSITY (N/m ³)
1	13780.	2.59D8	2.49D6	9923.	621.	3.15	7069.
2	13780.	2.59D8	2.49D6	9923.	621.	3.15	7069.
3	13780.	2.59D8	2.49D6	9923.	621.	3.15	7069.
4	13780.	2.59D8	2.49D6	9923.	621.	3.15	7069.
5	13780.	2.59D8	2.49D6	9923.	621.	3.15	7069.
6	13780.	2.59D8	2.49D6	9923.	621.	3.15	7069.
7	13780.	2.59D8	2.49D6	9923.	621.	3.15	7069.
8	13780.	2.59D8	2.49D6	9923.	621.	3.15	7069.
9	13780.	2.59D8	2.49D6	9923.	621.	3.15	7069.

Mesh Layout:



Floor G

Floor Specifics:

FLOOR LENGTH: 9.15 m

FLOOR WIDTH: 4.88 m

NUMBER OF STIFFENERS SPANNING IN THE GLOBAL X-DIRECTION: 9

SPACING OF STIFFENERS SPANNING IN THE GLOBAL X-DIRECTION: 600. mm

Sheathing Specifics:

THICKNESS: 18. mm

MODULUS OF ELASTICITY IN THE GLOBAL X-DIRECTION: 3721. N/mm²

MODULUS OF ELASTICITY IN THE GLOBAL Y-DIRECTION: 4072. N/mm²

POISSON RATIO IN THE GLOBAL X-DIRECTION: .274

POISSON RATIO IN THE GLOBAL Y-DIRECTION: .300

SHEAR MODULUS IN THE GLOBAL X-Y PLANE: 621. N/mm²

SHEAR MODULUS IN THE GLOBAL X-Z AND Y-Z PLANES: 621. N/mm²

SHEAR MODULUS FORM FACTOR: 1.20

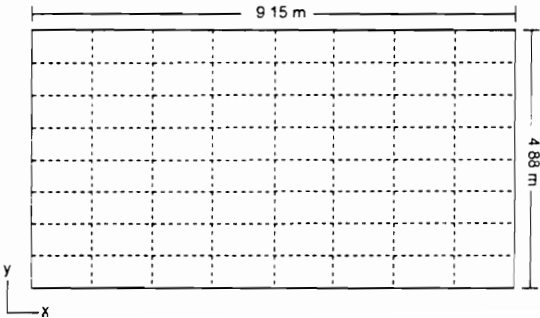
DENSITY: 5498. N/m³

Stiffener Specifics:

STIFFENERS SPANNING IN THE GLOBAL X-DIRECTION

STIFFENER	E (N/mm ²)	I (mm ⁴)	J (mm ⁴)	A (mm ²)	G (N/mm ²)	K	DENSITY (N/m ³)
1	13780.	4.39D8	2.52D6	10890.	621.	2.65	7069.
2	13780.	4.39D8	2.52D6	10890.	621.	2.65	7069.
3	13780.	4.39D8	2.52D6	10890.	621.	2.65	7069.
4	13780.	4.39D8	2.52D6	10890.	621.	2.65	7069.
5	13780.	4.39D8	2.52D6	10890.	621.	2.65	7069.
6	13780.	4.39D8	2.52D6	10890.	621.	2.65	7069.
7	13780.	4.39D8	2.52D6	10890.	621.	2.65	7069.
8	13780.	4.39D8	2.52D6	10890.	621.	2.65	7069.
9	13780.	4.39D8	2.52D6	10890.	621.	2.65	7069.

Mesh Lavout:



Vita

Robert E. Kalkert was born in Norwood, Massachusetts, on May 20, 1968. After graduating from the University of Massachusetts, Amherst in 1991, the author enrolled at the Virginia Polytechnic Institute and State University.